Application of Multi-Port Mixing for Passive Suppression of Thermo-Acoustic Instabilities in Premixed Combustors

Jordan Thomas Farina

Dissertation submitted to the faculty of the Virginia Polytechnic Institute and State University in partial fulfillment of the requirements for the degree of

Doctor of Philosophy
In
Mechanical Engineering

Uri Vandsburger, Chair
Brian Y. Lattimer
Walter F. O'Brien
Joseph A. Ranalli
Robert L. West

Feb. 18, 2013
Blacksburg, Virginia

Keywords: lean premixed, gas turbines, combustion, thermo-acoustic instabilities, passive control

Application of Multi-Port Mixing for Passive Suppression of Thermo-Acoustic Instabilities in Premixed Combustors

Jordan Thomas Farina

ABSTRACT

The utilization of lean premixed combustors has become attractive to designers of industrial gas turbines as a means of meeting strict emissions standards without compromising efficiency. Mixing the fuel and air prior to combustion allows for lower temperature flame zones, creating the potential for drastically reduced nitrous oxide emissions. While effective, these systems are commonly plagued by combustion driven instabilities. These instabilities produce large pressure and heat release rate fluctuations due to a resonant interaction between the combustor acoustics and the flame. A primary feedback mechanism responsible for driving these systems is the propagation of Fuel/Air Ratio (FAR) fluctuations into the flame zone. These fluctuations are formed inside of the premixing chamber when fuel is injected into and mixed with an oscillating air flow.

The research presented here aimed to develop new technology for premixer designs, along with an application strategy, to avoid resonant thermo-acoustic events driven by FAR fluctuations. A passive fuel control technique was selected for investigation and implementation. The selected technique utilized fuel injections at multiple, strategically placed axial locations to target and inhibit FAR fluctuations at the dominant resonant mode of the combustor. The goal of this research was to provide an understanding of the mixing response inside a realistic premixer geometry and investigate the effectiveness of the proposed suppression technique.

The mixing response was investigated under non-reacting flow conditions using a unique modular premixer. The premixer incorporated variable axial fuel injection locations, as well as interchangeable mixing chamber geometries. Two different chamber designs were tested: a simple annular chamber and one incorporating an axial swirler. The mixing response of the simple annular geometry was well characterized, and it was found that multiple injections could be effectively configured to suppress the onset of an unstable event at very lean conditions. Energy dense flame zones produced at higher equivalence ratios, however, were found to be uncontrollable using this technique. Additionally, the mixing response of the swirl geometry was difficult to predict. This was found to be the result of large spatial gradients formed in the dynamic velocity field as acoustic waves passed through the swirl vanes.

Acknowledgements

During the course of a long and complex project, there are people that without whose assistance and guidance, you would have never finished. Some of these people you chose to work with, and others you are just lucky to meet and know along the way. I wish I could list the contributions from everyone that deserves acknowledgement, but I fear that the list would grow too long and this document is due any day now. So, I will do my best to at least name everyone.

I would like to begin by thanking Bruce Cambata and Joe Garst of Electric Jet, LLC. for providing both financial support and an invaluable work experience. I have had the privilege of working with them since 2007. Their willingness to dream big has allowed me to have amazing opportunities working on projects that I, along with them, believe are very important. Their original vision of using hydrogen as a clean energy solution motivated this work. I hope that the work performed here will one day prove to further enhance their success.

I would like to thank my advisor, Dr. Uri Vandsburger, and my committee members Dr. Walter O'Brien, Dr. Robert West, Dr. Joe Ranalli, and Dr. Brian Lattimer. Their knowledge and constant willingness to help, along with their words of encouragement and excitement, were greatly beneficial to the completion of this research. I would especially like to thank and single out Joe Ranalli from this list. He has been a colleague, mentor, and friend starting from the day he recruited me to the lab. His expertise in the field and extensive knowledge of the lab and experimental techniques were instrumental in completing this research.

I would also like to thank another friend, colleague, and mentor, Dr. Chris Martin. His wealth of knowledge and patience to teach me were the only reasons this project ever got off the ground.

I would also like to thank my fellow lab mates, both past and present. Their daily contributions of ideas or assistance in working though problems provided me with invaluable help getting through this project. Anyone that has worked in this type of experimental setting knows that it is critical to have people you can count on. I would first like to thank Sam Shiver from this group. Sam was always ready to lend a hand, despite having a heavy workload of his own, to help me battle through any problem. Trust me, I had a few. I would also like to thank Craig English, Jason Dress, Matt Perry, and Steve LePera for all of the advice, knowledge, assistance, or well needed distractions during my tenure in the lab. I am fortunate to have had the opportunity to work with all of these guys, and I am proud to call them my friends.

I would also like to thank my family. They were always supportive and believed in me, even when my own faith would waver. Their words of encouragement always seemed to come when I needed them the most, and I cannot express how thankful I was and will always be for having their support.

Finally, I would like to thank my soon to be wife, Emily. I really do not know how to put into words how thankful I am for having Emily in my life. Her constant support, patience, and understanding throughout this process will never be forgotten, and I look forward to starting our new life together.

Table of Contents

List of Figures

List of Tables

Nomenclature

BTU	British Thermal Unit
NO_x	Oxides of nitrogen
FAR	Fuel/Air Ratio
φ	Equivalence Ratio
R	Rayleigh Index
p'	Pressure fluctuation, Pa
u'	Axial velocity fluctuation, m/s
φ'	Equivalence ratio fluctuation
q'	Fluctuating heat release rate, kW
FTF	Flame Transfer Function
ATF	Acoustic Transfer Function
U_{mix}	Average mixture velocity
τ	Convective time delay, s
x_{inj}	Axial distance between fuel injection and premixer exit, m
f	Frequency, Hz
T	Acoustic period, s
Phase delay	Linear phase delay, deg/Hz
MTF	Mixing Transfer Function
FFT	Fast Fourier Transform
Target Frequency	Location of maximum FAR damping, Hz
v	Turbulent velocity, m/s
x_0	Location of premixer dump plane, m
H	Height of mixing channel, m
$C(x_0, t)$	Impulse response of fuel concentration at dump plane as function of time
ν_T	Turbulent viscosity, m^2/s
D_{AB}	Molecular diffusion, m^2/s

Sc	Turbulent Schmidt Number
SCFM	Standard cubic feet per minute
SLPM	Standard liters per minute
U_θ	Tangential velocity, m/s
r	Radial coordinate, m
SN	Swirl Number
$SN_{geometric}$	Swirl number approximated by device geometry
D_{hub}	Hub diameter of axial swirler, m
$D_{centerbody}$	Centerbody diameter of premixer, m
D_{sw}	Axial swirler outer diameter, m
θ	Swirler vane angle, degrees
No Swirl Premixer	Premixer assembled without axial swirler
Swirl Premixer	Premixer assembled with axial swirler
10-30S	Gen 1 fuel injector (10 jets – 0.030"dia "S"traight Radial injection)
8-18T	Gen 2 fuel injector (8 jets – 0.018"dia "T"angential injection)
12-18T	Gen 2 fuel injector (12 jets – 0.018"dia "T"angential injection)
TL	Transmission loss
Ma	Mach number
k	Specific heat ratio
p_0	Total pressure, psi
p	Static pressure, psi
I/I_0	Incident to Transmitted intensity
c	Molar concentration, mol^3/m
ε	Molar absorption coefficient
l	Laser path length through test volume, m
PMT	Photo Multiplier Tube
ND	Nondimensional neutral density filter number

LHV	Lower Heating Value of fuel, kJ/kg
$\dot{m}$	Mass flow rate, kg/s
$\dot{Q}$	Total power of flame, kW
E	Voltage, V
A,B,n	Constants in King's Law
Δp	Differential pressure, psi
ρ	Gas density, kg/m^3
SPL	Sound pressure level, dB
G_{XX}, G_{YY}	Auto Spectrums of input and output signals
G_{XY}, G_{YX}	Cross Spectrums
FRF	Frequency Response Function
γ^2	Coherence
rms	Root mean square of signal
Q	Air flow rate, SCFM
Str	Strouhal Number

Chapter 1: Introduction

This chapter begins by identifying the motivation and need for a passive control strategy to suppress thermo-acoustic instabilities in lean premixed combustors. The chapter proceeds to develop the necessary background information supporting the use of multiple fuel injections as a valid passive control strategy. The chapter concludes by outlining the specific objectives for each phase of this research leading to the application of the passive control concept in an experimental lean premixed combustor.

1.1 Motivation and Identification of Need

As the demand for clean energy continually increases, so does the need for developing new solutions to utilize existing and future energy sources. These include both alternative and fossil fuels. Recently, combustion turbine plants have been an attractive means of producing both clean and efficient power. These plants can be powered by a large range of fuels, from liquid fuels such as fuel oil or kerosene, to gaseous fuels such as natural gas, low BTU biomass gas, coal derived syngas, or hydrogen [1]. Fuel flexibility allows these power plants to produce energy with the most economical and available sources. When combined with waste heat recovery systems (combined cycle plants), these plants can achieve excellent thermal efficiencies. However, increasingly stringent pollution standards have forced these plants to provide additional measures to clean up their emissions.

Many techniques exist, and are currently in place, to deal with the harmful emissions that can be produced during combustion. The most harmful potential bi-products of combustion are the oxides of sulfur (SO_x) and nitrogen (NO_x). SO_x is dealt with in two primary ways: the use of low sulfur fuels and/or scrubbers in the exhaust stacks. NO_x poses a tougher challenge. Unlike sulfur, the nitrogen needed to form NO_x is present in the air, which is the most common oxidizer in combustion systems. Common techniques to deal with NO_x include: Selective Catalytic Reduction (SCR), Selective Non-Catalytic Reduction (SNCR), Exhaust Gas Recirculation (EGR), Water or Steam Injection, and Oxy/Fuel Combustion [2]. Without expanding further on the detailed procedures involved for each technique, note that all of these processes require additional systems that can add to the cost, complexity, or energy requirements that reduce the

overall efficiency of the power plant. Another NO_x control strategy, which requires no additional system and does not threaten loss of combustion efficiency, is the use of lean premixed combustion. For these reasons, lean premixed has become an attractive alternative to the aforementioned processes. In lean premixed combustion (or prevaporized when used with liquid fuels) the fuel is mixed with excess air before entering the flame zone. The lean fuel mixture produces a lower temperature flame zone, and thus avoids the conditions that produce high levels of NO_x [3]. However, lean premixed systems are commonly susceptible to combustion driven instabilities. These instabilities produce large pressure and heat release rate fluctuations due to the resonant interaction between the flame and acoustics of the combustion chamber. Due to this interaction, they are often referred to as Thermo-Acoustic instabilities [4]. These events can decrease the operational limits of the engine and cause severe damage to critical engine components.

Techniques exist to mitigate the severity of thermo-acoustic instabilities associated with lean premixed combustion. Methods for dealing with these instabilities are classified as either active or passive control. Active control methods continually monitor the conditions inside the combustor and modulate either the fuel or air to suppress or prevent the onset of an instability [5-7]. While effective, these systems are met with resistance due to the complexity of the sensors required to accurately monitor the engine, the actuators necessary to modulate the air or fuel delivery, and the control algorithms needed to successfully suppress the events.

Passive control refers to measures which require no operational monitoring [8]. The techniques or devices involved are designed into the engine to provide stable operation at a range of conditions. One of the simplest, yet effective, control strategies has been the installation of acoustic energy absorbers, such as Helmholtz or quarter-wave resonators, into the combustor [9]. Other researchers have found success by modifying the air or fuel delivery system to inhibit mass flow fluctuations at dominant resonant frequencies [10]. Others have demonstrated that altering the flame zone can decrease the susceptibility of combustors to unstable events. Two different approaches have been applied to achieve this effect. One, fuel additives such as hydrogen have been used to strengthen and stabilize the flame zone, which typically results in a more compact flame [11-16]. Alternatively, modifications to the injector/burner design have

been used to distribute the available energy over a larger volume by increasing the flame size and reaction zone [17, 18].

Over the past years, our group at Virginia Tech, in collaboration with Electric Jet LLC., has focused on expanding the role of hydrogen as a clean alternative to fossil fuels in gas turbine engines. During this time, the group developed a lean premixed hydrogen combustor and integrated it into an existing Jet-A fueled turboprop engine [19-21]. The engine was successfully operated with pure gaseous hydrogen, while producing sub ppm NO_x levels. These ultra-low emissions are the product of extremely lean operating conditions that are only achievable due to the high flame speeds of hydrogen[22]. However, due to flame propagation into the premixing chamber (flashback), the operational range of the engine was limited to only 30% of its rated power. As with many lean premixed systems, it was discovered that these flashbacks were the result of combustion instabilities that were driven by equivalence ratio fluctuations produced inside of the premixer.

Motivated by this limitation, the current project aims to develop new premixer technologies, along with an application strategy, capable of preventing fuel/air ratio (FAR) fluctuations from driving the combustor unstable. A passive fuel control strategy was selected for investigation and implementation. The selected control strategy utilizes strategically placed axial fuel injection locations to target and inhibit FAR fluctuations at the dominant resonant mode of the combustor. Manipulation of the mixing response from multiple fuel injections, primarily by adjusting the convective delay between axial injection locations, allows the current research to focus the effective range of FAR damping. This approach allows for a sophisticated investigation of the passive control strategy. The goal of this research was to provide an understanding of the mixing response inside realistic premixer geometries and investigate the effectiveness of the proposed suppression technique. While the proposed strategy is not limited to any specific gaseous fuel, the project's ultimate goal was to achieve stable operation in a lean premixed hydrogen combustor.

1.2 Background

This section begins by detailing how the inherent design of lean premixed combustors, while beneficial to NOx emissions, increases the susceptibility of these systems to be affected by thermo-acoustic instabilities. The section proceeds to investigate the mechanisms responsible for promoting these interactions and introduces common techniques to model and measure these events. Emphasis will be placed on the specific role that FAR fluctuations play in driving these instabilities. The section concludes by presenting the theory behind using multiple axial fuel injections to suppress the onset of a resonant interaction by inhibiting the most commonly observed driving mechanism, FAR fluctuations.

.

1.2.1 Susceptibility of Lean Premixed Combustion to Thermo-Acoustic Instabilities

Lean premixed combustion has become an attractive and efficient means to reduce NO_x in gas turbine combustors by producing lower temperature flame zones. Details on the combustion chemistry and thermal NO_x mechanisms for lean premixed combustion are provided in detail in popular combustion texts by Turns [2], Glassman [3], and Kuo [23]. Lefebvre [24] provides various examples of lean premixed combustor designs that have been put into service by many major gas turbine manufacturers. However, the emission benefits are not without their costs. Lean premixed combustors have been shown to be highly susceptible to combustion driven instabilities. These events have been discovered to result in increased heat transfer to combustor walls and turbine blades, decreased combustion efficiencies, increased NO_x emissions [24], and decreased stability margins due to blowout [25] or flashback [26, 27]. Due to these severe penalties, along with the prevalence of combustion instabilities in lean premixed systems, it has become common to implement a thermo-acoustic analysis into the design process of premixed burners [28]. Engine manufacturers and research institutions, such as General Electric [29], Pratt and Whitney [7], Siemens [17], NASA [7], and ALSTOM [30], have all published design practices and techniques to model and mitigate combustion instabilities. The increased susceptibility of lean premixed systems, compared to their conventional diffusion style counterparts, is a function of the inherent mode of operation and common design practices to achieve the best emissions.

Conventional diffusion style gas turbine combustors introduce all of the air through large dilution and cooling holes in the combustor liner to mix with the fuel and burn at roughly stoichiometric conditions. Alternatively, premixed combustors inject a large portion of the air into a mixing chamber upstream of the combustion chamber. To achieve the appropriate air flow splits, a decreased number of dilution and cooling holes are required in the combustor liner. The result is a more acoustically rigid combustor liner with less acoustic damping than a typical combustor [31, 32]. This lack of energy dissipation allows the acoustics to affect a premixed flame (variations in FAR and heat release rate) much more easily than a diffusion flame [33].

To achieve the greatest NO_x reduction, premixed combustors typically operate near the lean flammability limit of the fuel. At these conditions, small non-uniformities in the fuel mixture reaching the flame zone can cause localized extinctions and re-ignitions of the fuel mixture [34]. This produces large fluctuations in heat release rate, accompanied by strong pressure fluctuations, due to rapid expansion of combustion gases. To avoid these situations, many engines are forced to operate at higher equivalence ratios or incorporate pilot burners to help stabilize the flame [35] and, therefore, accept the increase in NO_x emissions. However, this has not been found to be a general fix-all remedy. Janus, et. al [36] found that richer conditions were also highly susceptible to instabilities. Janus suspected that this effect was due to the overall increase in temperature and available energy in the flame zone. Yet, Huang [33] points out the energy required to produce and sustain pressure fluctuations represents only a very small portion of the total energy available in the fuel.

1.2.2 Mechanisms for Instabilities in Lean Premixed Combustors

Combustion instabilities are not unique to lean premixed systems. In fact, the conditions in which combustion instabilities are sustained exist in most combustion systems, ranging from liquid rockets [37-39] to industrial furnaces [40]. As described by Lord Rayleigh [41], if periodic pressure fluctuations become in phase with the heat release rated from combustion, or any heat source, the strength of the oscillation will amplify. In the same manner, if the heat release rate is out of phase with the pressure oscillation, the amplitude will be attenuated. These conditions are expressed with the well-known Rayleigh Criterion, as shown in eq. 1.1,

$$R = \int_0^T p'(t)q'(t)dt \qquad \begin{matrix} R > 0, \text{ Amplification} \\ R < 0, \text{ Damping} \end{matrix} \tag{1.1}$$

where *p'* and *q'* represent the unsteady quantities of pressure and heat release rate, respectively. While the Rayleigh condition can be met in various types of combustion systems, this section will focus on the mechanisms unique to lean premixed combustors.

Chu [42] shows that pressure waves are created at a flame boundary as the result of local displacements in the flame front, independent from any acoustic coupling. Displacements of the flame can be caused by changes in flame speed, heat release rate rate, mixture concentrations, temperature gradients, or velocities across the flame. Due to the various length scales and turbulent nature of the flame front, the generated pressure waves contain broad band frequency content. This is commonly referred to as "combustion noise" and is illustrated in Figure 1.1

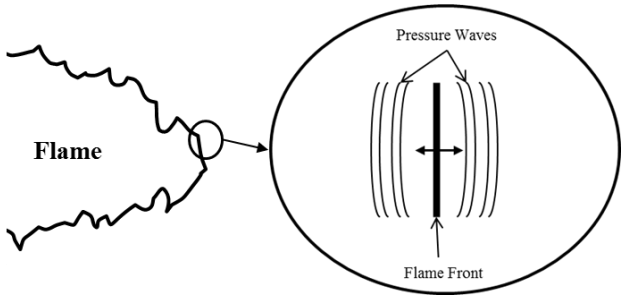

Figure 1.1. Illustration of pressure waves generated at the flame front.

These pressure waves can amplify if enough energy, greater than the viscous losses of the system, is released at the resonant frequencies of the combustor. At these frequencies, standing waves are established in the combustor and mixing chamber, producing periodic pressure and velocity fluctuations. Among other effects, this creates equivalence ratio oscillations due to the interaction of the fuel injection and the unsteady air velocity. These concentration variations are convected to the flame front and, depending on the characteristics of the flame, can produce fluctuations in heat release rate. If the oscillations satisfy the Rayleigh condition, a resonant feedback interaction will amplify the system until the limit cycle of the combustor is reached. A closed loop dynamic system model, as seen in Figure 1.2, is typically used to illustrate this process, where *q'*, *u'*, and *φ'* are the unsteady quantities of heat release rate, velocity, and equivalence ratio, respectively. Thermo-acoustic interactions are generally described using only

the inner loop. However, to account for the effects of mixing, the outer loop is necessary for premixed systems.

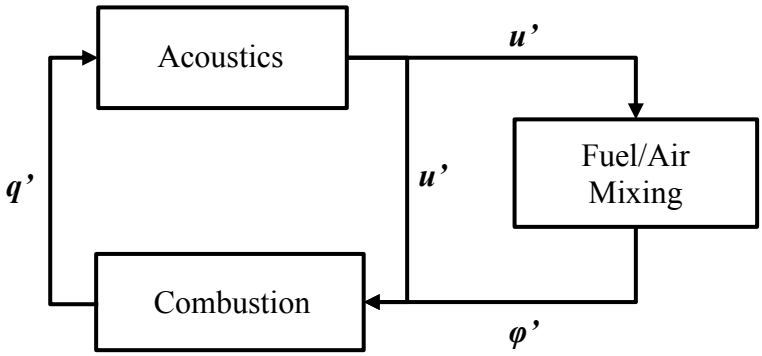

Figure 1.2. Dynamic system model of the thermo-acoustic interaction in a lean premixed combustor.

As mentioned, the fuel/air mixing interaction is not the only mechanism that can drive instabilities. It has been shown that the flame can respond to periodic changes in velocity [43], vortices [44], and flame anchoring [45]. While this study recognizes the multitude of effects that can influence the dynamics of the flame, emphasis has been placed on equivalence ratio fluctuations. Research suggests that this is the dominant instability mechanism plaguing engines operated with lean premixed combustors [10], even if other mechanisms are present. Investigations into combustors with multiple instability mechanisms have shown that the elimination of equivalence ratio oscillations can prevent or decrease the overall magnitude of the instabilities [46].

1.2.3 Closed Loop Dynamic System Description of Thermo-Acoustic Instabilities

Linear control theory has become a common method to characterize and analyze the closed loop coupling between the combustion processes and acoustics in lean premixed combustors. Linearized, or small perturbation, models and experimental measurements have been used to develop transfer functions to describe to the flame, acoustics, and mixing. Closed loop linear stability analyses of these transfer functions, such as Bode Criteria [47] and Nyquist Analysis [48], have proven to be an accurate way of identifying stability boundaries. However, these models cannot be used to predict the magnitude of the instability due to the highly non-linear nature of the system, which is often driven to a limit cycle. The magnitude is defined by an

energy balance between the non-linear viscous dissipation losses and heat release rate of the flame.

This section will briefly review theoretical treatments, and experimental techniques and observations of both the flame and acoustic transfer functions. Development of the mixing models will be covered in greater detail in later sections.

Flame Transfer Functions

In 1956, Merk [49] was one of the early researchers to apply a linear analysis to model the response of a flame in an acoustic cavity. In 1980, Mugridge [25] extended this work by applying Merk's theoretical flame transfer function to an experiment. Mugridge found that the theory was inadequate to define the boundaries of stability, and he suggested that more needed to be known about the flame's response. Since then researchers have performed numerous studies and enhanced the development of these theoretical models. In 2003, Lieuwen [4] provided an excellent review summarizing the modeling efforts of the acoustic-flame interaction in premixed combustors.

The dynamic response of the flame to unsteady perturbations, or Flame Transfer Function (*FTF*), is commonly measured by actively driving the combustor with known periodic perturbations, without allowing any feedback response, and measuring the heat release rate response. This open loop method allows the researcher to isolate each process individually. In premixed systems, the flame is known to respond to both acoustic velocity and equivalence ratio fluctuations, which must be measured separately. The two *FTF*s are shown in eq. 1.2,

$$FTF(f) = \frac{q'(f)}{u'(f)} or \frac{q'(f)}{\varphi'(f)} \qquad 1.2$$

where f is the frequency of the periodic oscillation, and q', u', and φ' are the unsteady quantities of heat release rate, velocity, and equivalence ratio, respectively. Evaluation of the response to equivalence ratio fluctuations is commonly performed by modulating the fuel into the air stream using a high frequency solenoid or piezoelectric stack [50]. Velocity fluctuations are typically produced by an acoustic driver, such as a speaker or siren, mounted in the air stream prior to the combustion zone [43]. However, the flame response to velocity fluctuation must be observed

independently of any fluctuations in equivalence ratio. This is accomplished by mixing the fuel far enough upstream that there can be no concentration gradients at the flame zone [51]. In both situations, it must be ensured that the driving amplitudes be limited to prevent any non-linear effects. This limit is typically determined experimentally by increasing the driving amplitude until the measured response ceases to be linearly related.

The measured flame dynamics, to both velocity and equivalence ratio perturbations, indicate that premixed flames respond like a low-pass filter with a linear phase delay between the response and the disturbance. This suggests that the flame integrates, or dampens out, high frequency oscillations. Ranalli [50] observed that the phase delay was related to the convective time scales associated with both the velocity and equivalence ratio disturbances. Ranalli [47] also found that the bandwidth, or cutoff frequency, of the flame had an inverse relationship to the volume of the flame zone.

Acoustic Transfer Function

The acoustic transfer function (*ATF*) is the dynamic frequency response of acoustic velocity to heat release rate perturbations, shown in eq. 1.3,

$$ATF(f) = \frac{u'(f)}{q'(f)} \tag{1.3}$$

where f is the frequency of the periodic oscillation, and u' and q' represent the unsteady quantities of velocity and heat release rate, respectively. This is commonly modeled using the linearized acoustic wave equation and a plane wave assumption where the flame is represented by a compact source (i.e. the length of the flame is much shorter than the wavelength of the oscillation) [25]. This technique has proven to be an accurate way for modeling the acoustic response in simple combustors with known temperature gradients. While this approach is a common first step for modeling realistic complex combustor geometries, higher order techniques are being developed to enhance and refine predictive capabilities. These techniques include acoustic Finite Element Models (FEM) and Computational Fluid Dynamic (CFD) predictions of the flame's heat release rate [7, 28].

The measurement of the acoustic transfer function, as detailed by Black [52], follows a similar open loop approach as the aforementioned flame transfer function. While the flame transfer function involves a periodic input of known frequency and amplitude, the acoustic transfer function uses heat release rate from the flame as a broad band energy input. Therefore, the response of the system can be acquired over the entire frequency spectrum. Care must be taken such that the flame energy level is high enough to sustain good coherence at the frequency range of interest, yet low enough as to not induce a resonant feedback interaction between the flame and the acoustic response (i.e. singing).

Using the acoustic transfer function measurement technique, Ranalli [47] and Black [52] observed that the response of a simple turbulent combustor rig demonstrates second-order behavior. Specifically, it is characterized by an increase in gain and a phase change at the natural or resonant frequency of the combustor. Black also theoretically verified that this frequency coincided with the lowest order mode, which, for his combustor geometry, was the first longitudinal mode. Dominant combustion instabilities are commonly observed at this lowest order resonant frequency. Higher order resonances are typically attenuated by the low pass characteristics of the flame, thus reducing their severity.

1.2.4 Time Delay Model for Equivalence Ratio Oscillations and Heat Release Rate

The role of equivalence ratio (φ), or Fuel/Air Ratio (FAR), oscillations in the thermo-acoustic interaction of a lean premixed combustor is generally described using a time delay, or time lag model [32]. This type of model is characterized by a linear phase delay and constant gain. Acoustic disturbances created at the flame zone produce periodic velocity oscillations that propagate into the fuel/air mixing chamber. The interaction between the fuel inlet and unsteady velocity produce rich and lean "packets" of fuel. These "packets" are not discrete, but they take the same form as the unsteady velocity, in this case, sinusoidal. The "packets" are then convected by the bulk flow, travelling at a velocity of U_{avg}, towards the flame zone and, upon arrival, create an instantaneous increase in heat release rate. This model is conceptualized for a simple premixed system in Figure 1.3. The characteristic time delay, τ, for this simple system is the convective time from the fuel injector to the flame zone, shown below in eq. 1.4,

$$\tau = \tau_{conv} = \frac{L + L'}{U_{avg}} \quad 1.4$$

where L is the distance from the fuel injector to the combustor chamber, and L' is the flame offset distance. The accompanying linear phase takes the form of eq. 1.5,

$$phase(f) = \tau * 2\pi f \quad 1.5$$

where the phase delay is represented by the slope of the phase verses frequency correlation and has the units of (rad/Hz). For other systems, such as liquid premixed/prevaporized, it may be important to consider delays due to evaporation, mixing, or chemical reactions. For these systems, the characteristic time delay would take the form of eq. 1.6.

$$\tau = \tau_{conv} + \tau_{evap} + \tau_{mix} + \tau_{chem} \quad 1.6$$

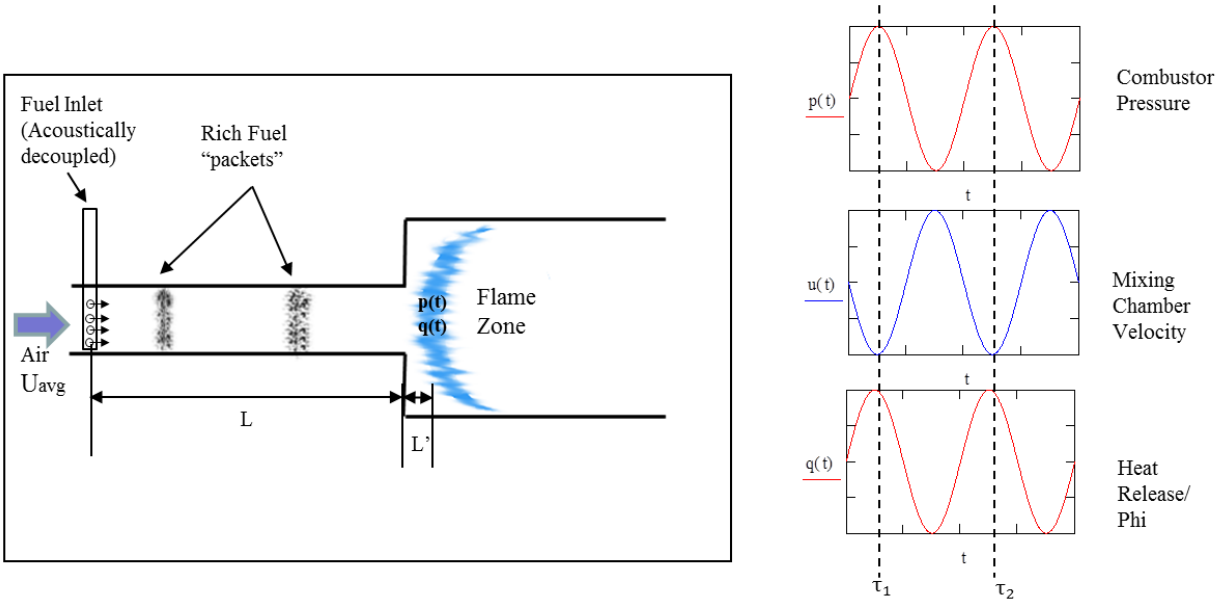

Figure 1.3. Time Delay model of equivalence ratio oscillations in a simplified premixed combustor.

As detailed by Richards et. al [32], the most likely conditions to amplify this system are when the time delay of the fuel injection is an integer multiple of the acoustic period of the oscillation. As Richards points out, this simply is a restatement of the Rayleigh Criterion, due to the previously established relation between fuel concentration and heat release rate. These conditions are presented for both the acoustic period (T) and frequency (f) in eq. 1.7.

$$\frac{\tau}{T} = \tau * f = 1,2,3 \ldots \quad 1.7$$

Putnam observed in industrial systems that it was not necessary for the time lag to be exactly matched to the acoustic period. Putnam suggests that amplification of the system is still possible with discrepancies as high as 25%, as shown in eq. 1.8.

$$\frac{\tau}{T} = n \pm 0.25, n = 1,2,3 \ldots \quad 1.8$$

In practice, the prediction of conditions that produce instabilities is more complicated. For the case that was illustrated, and described by Richards et. al, an increase in pressure at the flame caused a decrease in velocity at the injector, producing a rich "packet" of fuel. Lieuwen [53] details how, depending on the acoustic boundary conditions and fuel injector location, an increase in pressure at the flame could just as easily result in an increase in velocity at the fuel injector, thus producing a lean mixture. This illustrates the importance of knowing the phase relation between the pressure at the flame zone and velocity at the fuel injector. For example, Richards et. al found that the instability boundaries for his test combustor were when the convective time delay was between 0.45 and 0.7 of the acoustic period.

The application of this model is further complicated by the spatial distribution of heat release rate in the flame zone [53]. This results in a distribution of time lags due to the range of convective delays for each fuel particle. Finding the dominant time delay, along with the distribution, commonly requires experimental measurements, but some researchers have found success predicting this using CFD [29].

Two major assumptions were used in the development of this model. First, the fuel injection supply must be decoupled from the air stream. This is commonly achieved with the use of choked or high impedance fuel jets. However, for systems where this is not possible due to design constraints, relations have been developed by Lieuwen [53] and Yi, et. al [54] to include the resulting interactions produced from fuel supply line effects. It is also assumed that the periodic velocity fluctuations inside of the mixing chamber are one-dimensional (1-D) plane waves. No considerations, however, were made to allow for spatial velocity gradients.

The pathway in which equivalence ratio fluctuations are produced and the role of these fluctuations in precipitating and driving thermo-acoustic instabilities are often referred to as the "Richards-Lieuwen" mechanism. This distinction is attributed to the vast amount of experimental (Richards) and theoretical (Lieuwen) work provided by these researchers. Both Nyguen [55] and Mogia et. al [56] experimentally verified that this mechanism was responsible for combustion instabilities in their test combustors. This mechanism is typically observed in the 100-1000Hz range, and it is commonly the dominant unstable mode of operation in lean premixed combustors.

1.2.5 Mixing Model

In the description of the heat release rate response to equivalence ratio oscillations only a brief mention was made of the accompanying response of equivalence ratio to velocity perturbations. This response is referred to as the Mixing Transfer Function (*MTF*), shown in eq. 1.9,

$$MTF(f) = \frac{\varphi'(f)}{u'(f)} \tag{1.9}$$

where f is the periodic frequency of oscillation, and φ' and u' represent the unsteady quantities of equivalence ratio and velocity, respectively. In the previously developed model, the mixing transfer function was approximated with a constant gain and a phase delay proportional to the convective time of the fuel. Constant gain assumes that the concentration gradients produced from the interaction between the unsteady air flow and the fuel injection are preserved throughout the mixing chamber and are independent of frequency.

Refinement of the mixing transfer function to include the effects of turbulent mixing and the corresponding smoothing of concentration gradients were developed by both Martin [57] and Scarinci, et. al [58]. While the two models are similar, the following discussion is focused on Martin's approach with mention to the differences used by Scarinci. Both techniques develop the dynamic mixing model by performing a frequency, or impulse, response analysis on the concentration distribution created from a theoretical impulse of fuel injected at a given distance from the exit of the 1-D mixing chamber.

The concentration distribution, as developed by Martin [57], assumes an impulse of fuel is released at location x_{inj}, referring to Figure 1.4. The pulse of fuel is convected with the mean free stream air velocity, U, towards the dump plane, x_0.

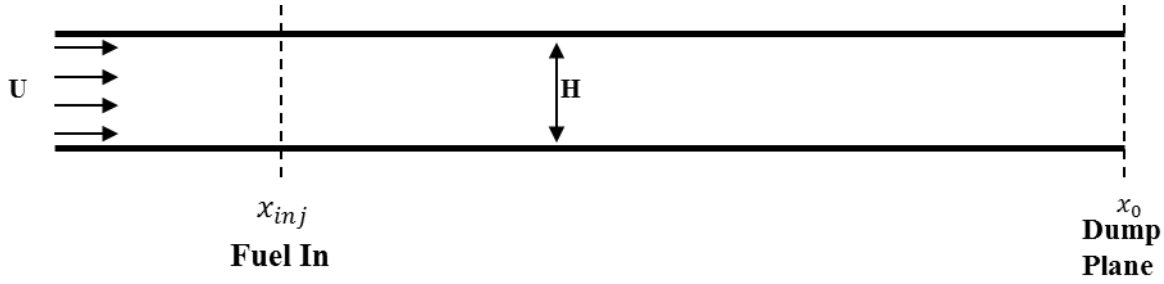

Figure 1.4. Schematic of a 1-D Mixing duct used in the formulation of the impulse response function of the fuel injection.

As the pulse is convected, the fuel is diffused into the air due to turbulent mixing. This turbulent mixing is modeled using a Random Walk Stochastic model with a relative intensity based on the turbulent velocity, $v = \%turbulence*U$ and time scale, $\tau = H/U$, where H is the characteristic turbulent length scale. The resulting concentration distribution at the dump plane derived by Martin [57] is shown in eq. 1.10.

$$C(x_0, t) = \frac{1}{\sqrt{2\pi(2\tau v^2 t)}} e^{\frac{-(x_{inj}-Ut)^2}{2(2\tau v^2 t)}} \qquad 1.10$$

The resulting concentration profiles are slightly right skewed Gaussian distributions, as can be seen in Figure 1.5. The skew is a result of including convection terms in the development of this model. However, Scarinci [58] neglects this effect and assumes that the distribution is purely Gaussian. This represents the only major discrepancy between the two models. This figure also provides an example of the effect of increasing injection distance while holding turbulent intensity and mean air velocity constant. As the injection distance increases, the fuel disperses, causing the concentration distribution to broaden. The rate at which this process occurs is a function of the turbulent intensity, mean velocity, and turbulent time scale.

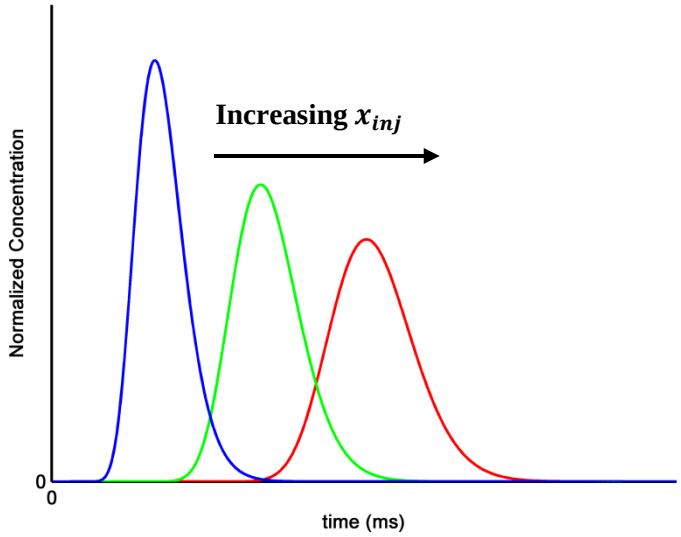

Figure 1.5. Concentration profiles at the dump plane demonstrating the effect of increasing injection distance with turbulent intensity and mean velocity held constant.

The frequency response, or *MTF*, was produced by transforming the time dependent concentration profiles into the frequency domain using a Fourier Transform, shown in eq. 1.11.

$$MTF(f) = \int_{-\infty}^{\infty} C(x_0, t) e^{-i2\pi f t}\, dt \qquad 1.11$$

While the analytical solution for eq. 1.11 would be extremely difficult to formulate, the transfer function can be easily obtained numerically with the use of a Fast Fourier Transform (FFT). Representative magnitude and phase plots are provided for multiple injection distances in Figure 1.6. Similar to the flame, the mixing response behaves as a low pass filter. The higher frequency concentration gradients are smoothed or dampened out due to the turbulent mixing effects, and the bandwidth of the response is directly related to the level of mixing, either due to turbulence intensity or convective time. The response also demonstrates a nearly linear phase delay, where the predicted values are in excellent agreement with the simple convective time delay model. Small deviations from linear are observed, but for this research they are considered negligible.

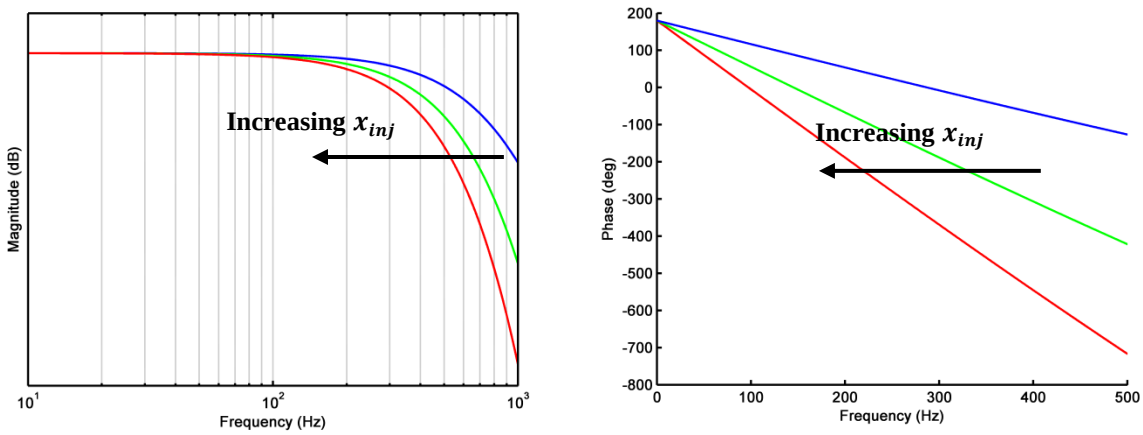

Figure 1.6. Mixing transfer functions (*MTFs*) showing effects of changing injection distances, x_{inj}.

One minor modification was made to the model developed by Martin [57]. Martin originally showed the 0 Hz phase crossing at 0 degrees. Upon examination, it was determined that the phase crossing should, in fact, be 180 degrees. This is based on the characteristics of the physical system and the definition of the mixing transfer function, which is the equivalence ratio response to velocity perturbations. This modification can easily be rationalized by conceptualizing the physical processes in a mixing chamber under quasi-steady state operation (0 Hz). For example, assuming constant fuel flow, if the velocity in the mixing chamber is increased, which corresponds to an increase in air mass flow, the overall equivalence ratio will be decreased. Conversely, if the velocity is decreased, the equivalence ratio will be increased. This simple explanation demonstrates that the velocity (input) and equivalence ratio (output) must always be out of phase under near steady state operation, thus justifying the slight alteration to Martin's model.

As with previous models, the development of the mixing model utilizes a 1-D plane wave assumption. It also assumes that the turbulence is the only factor driving mixing, which neglects any effects from molecular diffusion, making it applicable for any gaseous fuel. Neglecting molecular diffusion is based on examining the magnitude of the nondimensional Turbulent Schmidt Number, *Sc*, shown in eq. 1.12, which relates turbulent viscosity (ν_T) to molecular diffusion (D_{AB}) [59]. Even for modest levels of turbulence, *Sc* is greater than 200

$$Sc = \frac{\nu_T}{D_{AB}} \qquad 1.12$$

This assumption was further validated experimentally by Kelman, et. al [60], who found that turbulence was the only important parameter for mixing high-momentum micro jets in a turbulent cross-flow.

Based on the results obtained from the mixing model, it is suggested that fuel injector designs incorporate extremely long injection distances to dampen out equivalence ratio oscillations produced in premixed combustors. While this is a valid approach, necessary lengths to fully attenuate common instability frequencies are unattainable in engine applications, which are limited by space and weight constraints. For example, consider a gas turbine with a 3% total pressure drop across the combustor, which is in the range of typical designs, and a mean turbulence intensity of 10% (typical assumption). Without the addition of turbulence generators or other mixing devices, the mixing chamber would need to be on the order of several feet to achieve a 10dB drop in magnitude at 300Hz. Other parameters, such as mixing chamber geometry and compressor outlet temperature and pressure, are needed to fully define the system and determine the exact mixing length required. Even so, this quick example illustrates that the required mixing lengths are closer to the overall size of typical engines, instead of the combustor section. One of the more important parameters chosen for this example was the cutoff frequency. This value was selected based on the observed unstable frequency for the current research, but it is representative of frequencies that are commonly observed in these systems. It is important to recognize that higher frequency modes would require shorter mixing distances. However, all necessary lengths for practical combustors far exceed typical design constraints.

1.2.6 Multiple Injections and FAR Oscillation Damping

The strategic placement of multiple fuel injections allows for compact premixer designs that are able to dampen FAR oscillations at designed frequencies [10]. This concept is illustrated in Figure 1.7 by comparing a single injection location to two injection locations in a simple premixing chamber. For this brief discussion, the magnitude is assumed to be constant throughout the entire frequency range, and the fuel flow is evenly split between locations. The effects of mixing will be presented later.

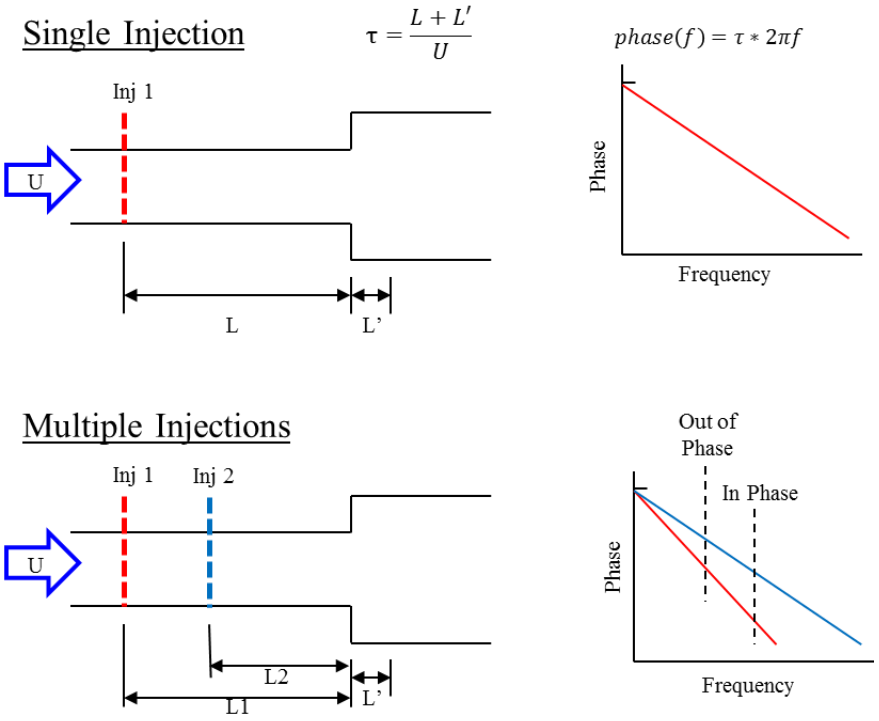

Figure 1.7. Schematic of the application of multiple fuel injection locations in a simplified combustor.

As already established, a single injection produces a fluctuating FAR at the exit, with a phase delay that is linearly related to the convective delay. Depending on conditions, this wave could be either in or out of phase with the driving acoustic pressure. If in phase, the interaction will amplify and drive the system unstable. However, as previously discussed, these conditions are difficult to predict, making the single injection design difficult to successfully implement, although possible. One additional factor must be considered in attempting to design a stable single injection premixer. Many lean premixed combustors demonstrate a frequency switching, or hopping, behavior between discrete unstable modes [48], including the one used in this current research. As the convective delay of the fuel injection is moved to correctly align the phase, the combustor can jump to a different resonant frequency. While the change in frequency is typically less than 100Hz, instead of gaining stability, the phase relationship at the new frequency continues to promote an instability, simply at a different unstable mode.

Instead of attempting to gain stability by adjusting the phase between the FAR and pressure, multiple injections aim to suppress the onset of the instability by damping the resulting FAR wave. Each injection location has a convective delay with an accompanying linear phase

relationship. The multiple waves become superimposed and produce a resultant wave that is related to the amplitude and phase of the injections. As shown in Figure 1.7, at the frequencies when the two waves are out of phase, the resulting wave will have zero temporal fluctuations. However, when in phase, the amplitude will double and, assuming an even distribution of fuel, match the magnitude of the single injection. This interesting result demonstrates that FAR oscillations produced from multiple injections are always less than or equal to the equivalent single injection system.

The goal of multiple injections is to provide the maximum FAR oscillation damping at the known dominant unstable frequency. This "target" frequency can either be determined experimentally or theoretically predicted. Once known, the fuel injection locations can be placed based on this frequency and operating condition. A representative frequency response of a two injection system, including the effects from mixing, is shown in Figure 1.8. Only the magnitude is presented because the damping is the primary factor in the application of this approach.

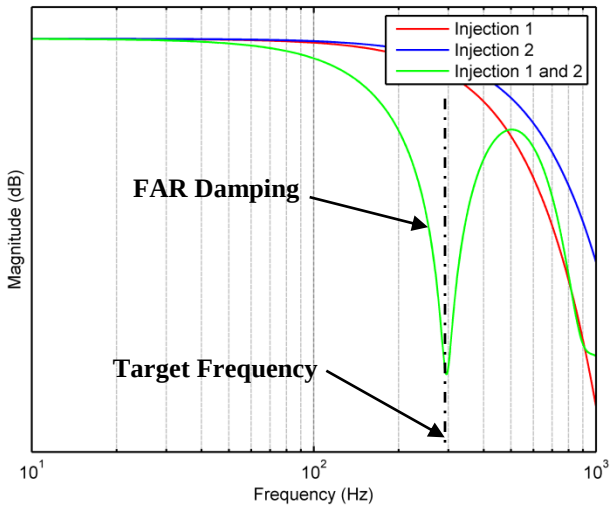

Figure 1.8. Frequency spectrum for the mixing transfer function (*MTF*) with multiple injection locations demonstrating FAR damping at a target frequency. Mixing effects are included.

Only two notable observations can be made when mixing effects are included in the response of multiple injections. First, the minor differences in the magnitude of the two waves limit the damping of the resulting wave. In practical systems where the injections are fairly close together, this effect is minimal. Also, due to the low pass characteristics of the mixing transfer function, no significant improvement is observed at higher frequencies.

Many researchers have explored the use of multiple or staged injection. Most notable was the work performed by Scarinci, et. al [10]. Instead of using multiple fuel injections, Scarinci used numerous air injection locations to suppress FAR oscillations across the entire frequency spectrum. Using this approach, he was able to develop a stable combustor for an existing unstable gas turbine. Similarly, Richards, et. al [8] found that two fuel injection locations were almost always more stable than a single injection. Richards performed this experiment by testing a lean premixed natural gas burner that could be fueled at three separate locations. These successes, along with others [61, 62], have shown that the use of multiple injections is a valid passive control technique for equivalence ratio driven combustion instabilities.

While researchers have demonstrated the validity of using multiple injections, most of the previous work took a more global stability approach. These test rigs and premixer/combustor designs incorporated multiple or staged injection locations aimed to suppress a wide range of frequencies. Numerous conditions were acknowledged that could possibly excite an instability or, to the opposite effect, produce stable combustion. With this in mind, a global approach lacks the detail to conclusively determine if an increase in stability is solely due to FAR damping, or if it results from any one of a number of contributing factors. The current research aims to narrow the effective range of passive control (FAR damping), by manipulating the mixing response from only two injection locations, to provide an in-depth investigation of the proposed control technique as well as the underlying driving mechanisms.

1.3 Project Objectives

The goal of this project was to apply a multi-port fuel injection strategy to passively suppress the onset of a resonant thermo-acoustic interaction by damping FAR fluctuations. The objectives of this work were divided into two phases. The first phase focused on the measurement and characterization of the mixing response in a non-reacting flow. The objective was to provide a model that can be used to accurately predict the response from multiple injections in an operational combustor. Phase two applied the knowledge gained in phase one to construct a premixer with two fuel injection locations specifically targeted to suppress an instability in a lean premixed combustor. The objectives for each phase of this project are listed.

Phase I: Cold Flow Mixing Response

- Design, build, and instrument a prototype modular premixer and atmospheric combustor capable of accurately measuring mixing responses in a non-reacting flow.
- Characterize mixing response for a single injection in a simplified (no swirl) and full (swirl) geometry premixer, examining effects of convective delay, mean flow rate, and equivalence ratio.
- Investigate the application of multiple injections as a FAR damping technique. Validate the use of a single injection model to accurately predict multiple injection responses.

Phase II: Hot Tests and Passive Control

- Design and instrument an experimental rig capable of measuring the heat release rate and pressure fluctuations of an unstable combustor.
- Characterize unstable modes of the combustor operated with the simplified and full geometry premixer. Determine effects of fuel type, convective delay, equivalence ratio, and bulk flow rates.
- Determine dominant unstable modes and identify driving mechanisms.
- Apply a two injection passive control strategy to target and suppress the onset of resonant thermo-acoustic events in an unstable premixed combustor.

Chapter 2: Experimental Methods

This chapter details the experimental apparatus and diagnostics used in this study. Experiments for this research were performed at the Combustion Systems Dynamics Lab (CSDL) in Blacksburg Virginia. The lab is a part of the Mechanical Engineering Department at Virginia Tech with a primary focus on combustion driven instabilities.

2.1 Experimental Combustor

The experiments for this project were conducted using a turbulent combustor with a modular premixing fuel injector. The term combustor, for this study, refers to the entire testing apparatus. The combustor was comprised of an air flow conditioning section, acoustic driver, premixer inlet with instrumentation ports, modular premixer, and variable length combustion chamber. A schematic of the testing rig is shown in Figure 2.1. The combustor was also equipped with an independently controlled fuel and air delivery system and a data acquisition system. Each part of the system will be discussed in the following sections.

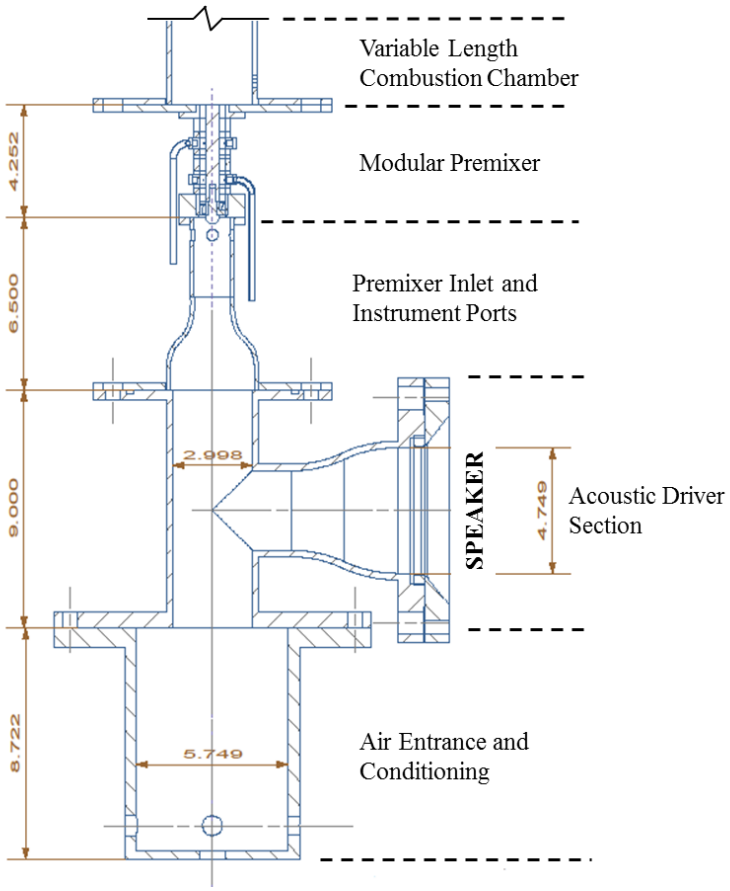

Figure 2.1. Section view of the experimental combustor detailing each component.

2.1.1 Air and Fuel Delivery System

Air System

Compressed air was supplied to the test cell using an Ingersoll Rand (SSR-EP40SE) rotary screw type air compressor. The output of the compressor was held between 100-115psi, while operating in an ON/OFF line mode. This mode of operation is performed using an inlet valve that is opened when the pressure drops to 100psi, and closed when the pressure reaches 115psi. This is the preferred mode of operation for this compressor when the demand on air is low in comparison with the maximum rated output (157 SCFM @ 125psig). The compressed air was then dried to a dew point of 40°F. An accumulator tank was placed in line, after the compressor, to dampen pressure fluctuations created by the compressor. The dried air then proceeded into the test cell, where the pressure was further controlled using a series of two single stage regulators. The discharge pressure of the first and second stage regulators was set to 40 and 20 psig, respectively. The two stage system was installed to help mitigate variations in the mass flow rate due to compressor cycling. The mass flow rate to the experiment was controlled using a manually operated metering valve, in conjunction with a thermal air mass flow meter (Hastings 0-1000 SLPM).

All flow meters, both air and fuel, were calibrated prior to operation. The meters were calibrated using an orifice plate calibration rig, as shown in Figure 2.2. Only a brief overview is presented in this section. Refer to the CSDL calibration rig documentation for a more detailed description and procedure.

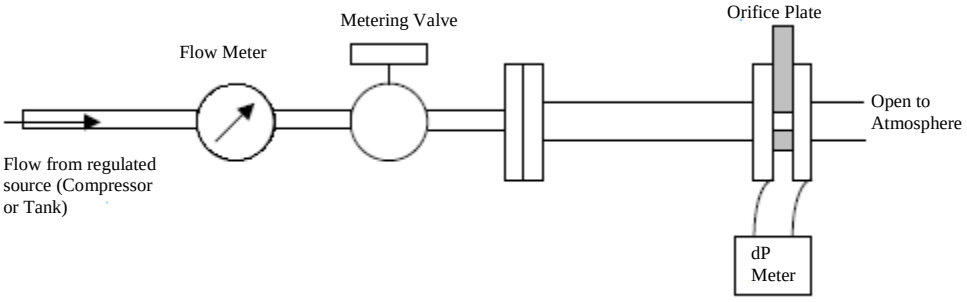

Figure 2.2. Schematic of the orifice plate calibration rig for gaseous fuels and air.

The procedure is as follows: insert the flow meter in series with the calibration rig, select the appropriate orifice and differential pressure transducer(s) for the flow rate range of the meter,

and vary the flow rate using a manual metering valve. The pressure drop across the orifice and the output voltage from the meter were recorded at each flow rate. Using the differential pressure, along with the upstream temperature and atmospheric pressure, the mass flow rate through the orifice is calculated using known relations [63]. This mass flow rate is correlated with the output from the meter to provide a new calibration, or to ensure the current calibration is still satisfactory. To ensure an accurate calibration, the pressure transducer was calibrated prior to testing using a dead weight tester. A sample calibration is shown in Figure 2.3.

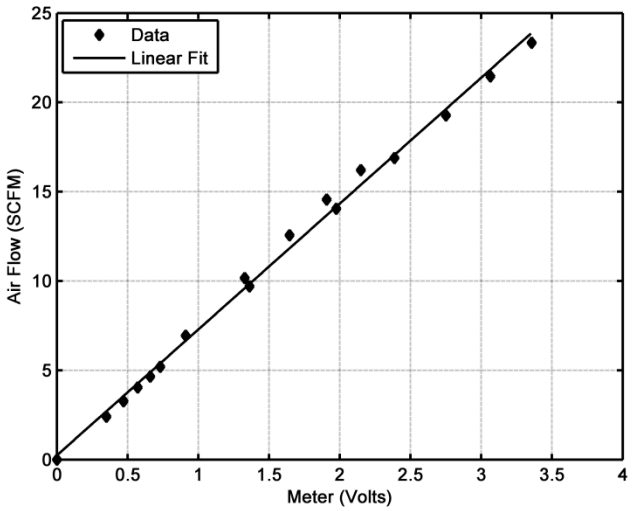

Figure 2.3. Sample air flow meter calibration with a linear best fit.

Fuel System

The fuel supply to the experiment is split into two processes: one for natural gas and another for all other gaseous fuels. Natural gas was compressed on site from a low pressure pipeline, from approximately 5 psig to a maximum of 5500 psig using a 4 stage natural gas compressor (Universal Air Products Corporation 5409 CNG) and dryer. The gas was compressed, dried, and stored in a 40 cubic foot storage tank, rated to 5500 psig. The gas was regulated to an operating pressure of 120 psig using two dome loaded pressure regulators installed in series. The storage tank was heated using a hot water circulation system to prevent freezing of the natural gas due to the rapid expansion through the first regulator. The fuel was then supplied to the experiment using two independently controlled fuel rails. Each rail was equipped with a flow meter, metering valve, and shutoff ball valve. Three different flow meters were interchanged, depending on the fuel type and testing conditions, so that each was operated in the upper range of

their respective limits to ensure the highest level of accuracy. A specific calibration curve was created for each flow meter with natural gas and hydrogen, using the aforementioned process.

Other gaseous fuels, specifically hydrogen for this experiment, were supplied to the test combustor using compressed gas cylinders purchased and delivered from a local gas distributing company. The cylinders were plumbed together in parallel and regulated to 120 psig using a single stage regulator. The fuel was fed into the two fuel rails using a manifold, and the rest of the fuel system was identical to the one described above for natural gas.

2.1.2 Turbulent Combustor

Air Entrance and Conditioning

Air was introduced through four 1/2" diameter air lines mounted evenly spaced around the circumference of the Air Entrance section. Each line was approximately four inches long, and drilled with eight 1/8" holes directed tangentially. The lines connected to a manifold and were supplied by a single source. Two layers of perforated plate along with a 1/2" layer of honeycomb were installed downstream of the entrance pipes. This served two purposes: 1) it acoustically decouples the large air volume from the rest of the experiment, and 2) it provides a well-conditioned uniform flow.

Acoustic Driver

The purpose of the acoustic driver was to drive the periodic velocity oscillations that were required to perform the open loop mixing transfer function measurements. The acoustic driver was installed into the side branch of the combustor using a flanged Tee section, as shown in Figure 2.1. The driver was an 8" JPL Selenium Woofer, model number 8W4P, and was used in conjunction with a Peavy CS 800 X amplifier with a 600W output. The woofer was capable of producing 300W rms continuous and 600W peak. Care was taken to prevent overpowering the driver by monitoring the input voltage. The driver had an 8-ohm resistance and was always operated in a continuous manner; therefore, was limited to approximately 50 Volts of excitation. The linearity of the acoustic driver system was verified at each frequency of interest.

Premixer Inlet and Instrumentation

The premixer inlet was designed to provide a smooth transition from the acoustic driving section to the premixer inlet. This transition is important to prevent the creation of secondary flows due to rapid expansions or contractions. This section was equipped with four instrument taps to provide diagnostic access to the entrance of the premixer. This section housed instrumentation to measure pressure and velocity fluctuations, as well as measure steady state temperature and pressure.

This section was constructed by welding a custom made flange to a 3" to 1-1/4" diameter 304SS reducing pipe bell. The custom flange was constructed out of 1/4" 304SS and followed a standard 4"-150lb flange bolt pattern. The top of the bell was welded to a 4" long section of 1-1/4" schedule 40 pipe with the 4-1/4"NPT tapped holes. A premixer mating flange was welded to the end of the pipe to allow for quick installation and removal of the premixer, which was extremely important due to the large number of tests.

Variable Length Combustion Chamber

The combustion chamber used in this experiment was constructed out of three sections that could easily be installed or removed during operation to vary the overall length between the premixer exit and open atmosphere. This variable length chamber has the flexibility to allow for a self-excited resonant interaction between the combustion and acoustics to either exist, or not. To prevent the resonant interaction and allow for open loop measurements the combustion chamber was removed. Alternatively, the length was extended to promote a resonant interaction during combustion tests. This configuration was used to investigate the dominant unstable modes and effectiveness of the proposed suppression technique. The change in length typically does not change the dominant unstable mode, but it simply allows for the system to become self-excited. Schuller[64] suggests that, on similar systems, this is because the modal response of the system is locked to the upstream plenum, and is independent of the downstream chamber. This was the observed behavior of the utilized combustor.

The three sections of the combustion chamber were constructed out of standard 3" schedule 40 304SS pipe. Lap joints were created by turning down approximately half the wall thickness over

1” lengths on the ends of corresponding sections. It is important to use loose sliding fits to allow for the thermal expansion during operation. This particular design used 10 thousandths of an inch of clearance.

The base section was flanged to the exit of the modular premixer using a custom made adapter flange. The premixer exit was flush mounted to the adapter flange using 4 (¼”-20) bolts, and the combustion chamber was externally flanged following a 4”-150lb flange bolt pattern. The combustor walls were cooled with a removable shower head style cooling block installed around the outside of the chamber approximately two inches downstream of the premixer dump plane. The cooling block was supplied with a single 1/2” air line with a maximum feed pressure of 110psig.

2.1.3 Modular Premixer

This section will describe, in detail, the modular premixer and each of the major components. The premixer’s main function was the independent control of the convective time delay between multiple fuel injection locations and the flame zone. In addition, the premixer was designed to be fuel flexible and have a large operating envelope to allow for a broad range of conditions to be investigated. An exploded and assembled Computer Aided Design (CAD) rendering of the premixer is shown in Figure 2.4.

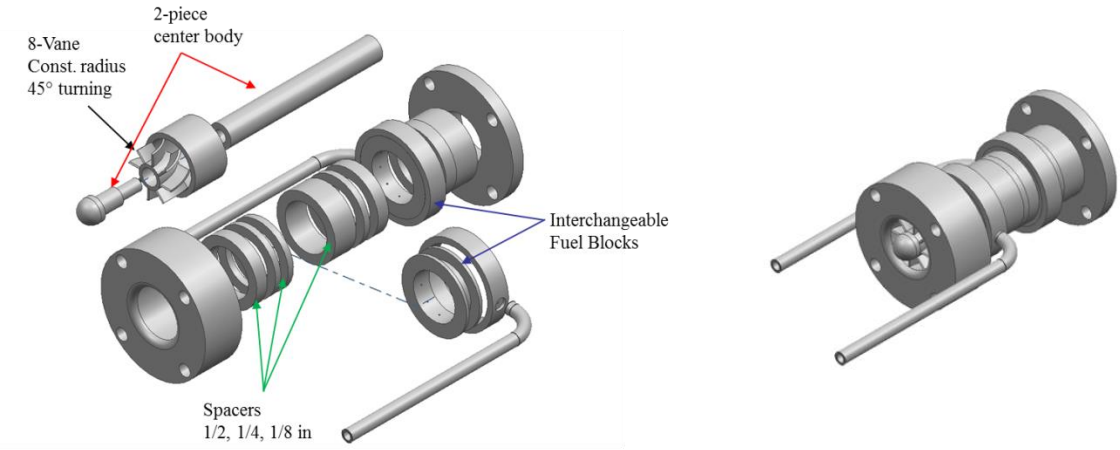

Figure 2.4. CAD rendering of the modular premixer. Exploded view (left), assembled view (right)

Premixer Concept

The premixer concept used in this research evolved from previous designs that were developed at Virginia Tech. Along with making the design modular, the only significant modification was made to the fuel injection strategy. Refer to Farina [19] for detailed explanations of the premixer's design features. Only a brief explanation of the conceptual design, along with some supporting material, is presented in this section.

A swirl and dump plane-stabilized annular premixer was used for this research. A section view of the premixer is provided in Figure 2.5 to highlight the components and flow path. Air is introduced into the mixing channel through a smooth inlet to reduce losses. The mixing channel is 0.25 inches high and is bounded by the centerbody and the outer shell, which have 0.5" and 1" diameters, respectively. Tangential momentum is imparted to the flow using an axial swirler with eight constant radius vanes creating a swirling flow. These swirl vanes can be removed and replaced with a set of vanes with no turning angle. Fuel injection blocks, as seen in Figure 2.4 and Figure 2.5, inject the fuel through multiple fuel jets into the annulus at discrete axial locations to create a uniform distribution of fuel. The design allows for the simultaneous use of up to 6 fuel injection blocks, only two of which are shown, at various axial locations in the premixer. The spacing is set by machined spacers that provide incremental changes of 0.125" between 0.6875" and 3.1875".

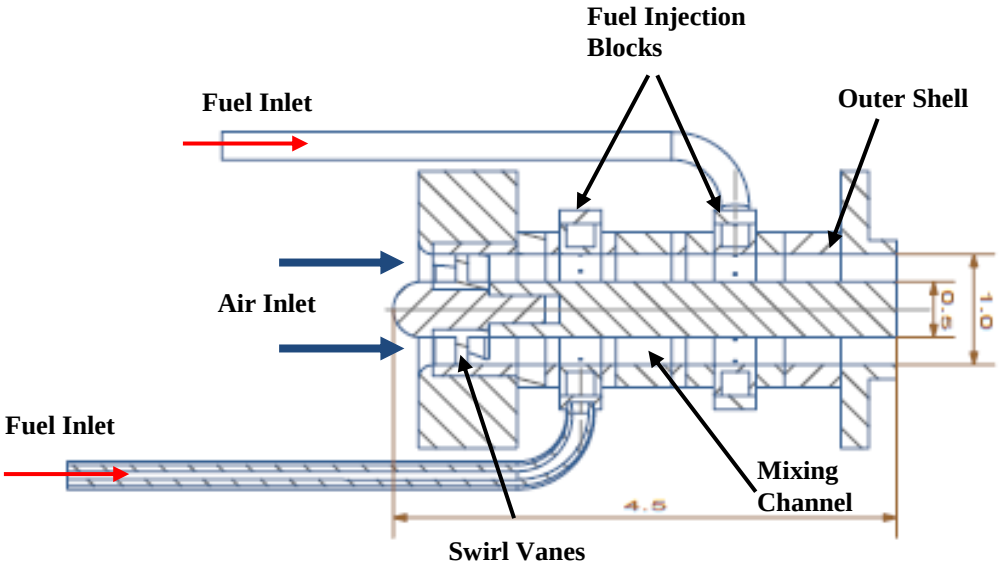

Figure 2.5. Section view of the modular premixer.

Swirl Vanes

Swirl vanes were used in this premixer design for two main purposes. First, the swirling flow enhances the mixing between the air and fuel jets. This enhanced mixing allows for shorter injection distances to achieve a uniform distribution of fuel entering the flame zone. The swirling flow also produces a low pressure recirculation zone at the exit of the premixer. This zone anchors and stabilizes the flame by recirculating hot combustion products into the oncoming fuel mixture. The level of swirl is characterized by a nondimensional Swirl Number (SN), which is defined as the ratio of the axial flux of tangential momentum to the axial flux of axial momentum [31]. This relation is shown in eq. 2.1, where U_x is the axial velocity, U_θ is the tangential velocity, and r is the radial coordinate. Lefebvre [31] suggested a minimal swirl number of 0.6 to create the conditions described above, which is typically classified as high swirl.

$$SN = \frac{\int U_x U_\theta r^2 dr}{r \int U_x^2 r dr} \tag{2.1}$$

As previously mentioned, the axial swirler was constructed out of eight constant radius vanes. A CAD rendering of the design is shown in Figure 2.6. The vanes had 45 degrees of turning (θ) between the leading and trailing edge. The vanes were 0.5" long with a 0.7" mean radius of curvature. The diameter of the hub (D_{hub}) and swirler (D_{sw}) were 0.5" and 1", respectively. The vanes had a constant thickness throughout the entire chord, along with rounded leading and trailing edges for smooth flow transitions. This swirler had an SN of 0.72 based on a geometric approximation for axial vanes provided by Lefebvre [31], shown in eq. 2.2.

$$SN_{geometric} = \frac{2}{3} \frac{1 - \left(\frac{D_{hub}}{D_{sw}}\right)^3}{1 - \left(\frac{D_{hub}}{D_{sw}}\right)^2} \tan(\theta) \tag{2.2}$$

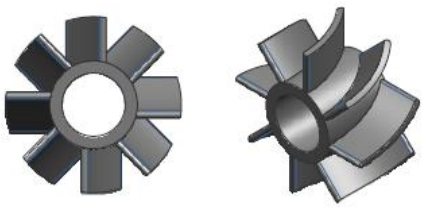

Figure 2.6. CAD rendering of the premixer's swirl vanes.

The modular premixer could also be assembled with a set of vanes that imparted zero turning to the flow. A CAD rendering of these vanes is shown in Figure 2.7. The purpose of these vanes was to simplify the flow field inside of the mixing chamber during dynamic testing of the fuel air mixing. This configuration was designed in an effort to ensure all acoustic waves remained planer in investigations of the mixing response. All tests performed with this premixer configuration will be classified as "No Swirl".

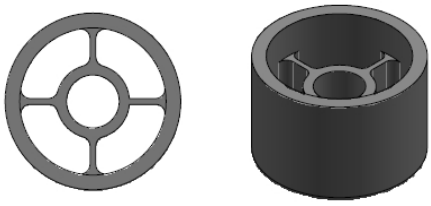

Figure 2.7. CAD rendering of the straight vane centerbody holder. This configuration will be referred to as "No Swirl".

Fuel Injection

The fuel was introduced into the mixing chamber using separate fuel injection blocks. Each block injected fuel through a single circumferential row of multiple high momentum fuel jets around the annulus at a single axial position. Each set of fuel jets were manifolded together, and supplied by a single 1/4" fuel line from a metered pressurized source. The fuel blocks could be interchanged with different designs, as well as be moved to different axial locations.

Three major design constraints were included into the design of the fuel injection strategy. First, the fuel must be injected in a manner to provide a uniform distribution of fuel in the shortest distance possible. The fuel must be evenly distributed in the radial and circumferential direction before reaching the exit of the premixer. Flow non-uniformities cause difficulties in the measurements of the mixing transfer function and promote an instability mechanism that would be uncontrollable using the current design approach. Second, the fuel source must be acoustically decoupled from disturbances created at the flame zone. Acoustic propagation into the fuel supply creates mass flow fluctuations that would not be separable from FAR fluctuations caused from the fuel/air mixing process. While this is not a necessary requirement if the appropriate measures are taken, the current investigation made no attempt to account for these

effects. Lastly, the injection of the fuel must not eliminate the swirl strength. This is a constraint that was self-imposed due to previous observations. For example, when using extremely high momentum fuel jets, the jets themselves act as flow barriers reducing the strength of the swirl. This reduction can lead to a decrease in mixing, which would then violate the first constraint.

Two generations of fuel injection strategies were developed during this project. The first generation had a major fault that required a re-design. This design produced no reportable results. Even though the second generation was far superior, it is important to mention the first generation to understand the shortcomings so that future designs can be further improved.

Generation 1 was based on a previous design by Farina [19]. The only modification was made to the spacing of the fuel jets due to an uneven distribution discovered as a result of previous work. Generation 1, shown in Figure 2.8 , used ten straight radial fuel jets. The diameter of each jet was 0.030" with even spacing between jets. This model is designated as '10-30S', where the '10' is the number of fuel jets, '30' is the diameter of the jets in thousandths, and 'S' refers to the orientation of the jets (either 'S' for Straight or 'T' for Tangential injection). The size and distribution of fuel jets was based on an optimized single side jet in a crossflow correlation provided by Holdeman [65]. The optimized mixing strategy resulted in a fuel injection design with relatively low velocity fuel jets. The fuel supply was decoupled by using a single 0.030" choked orifice at the entrance to the fuel manifold. However, as will be demonstrated later, the volume in the manifold was not decoupled, and it produced unwanted coupling effects for the reasons previously discussed.

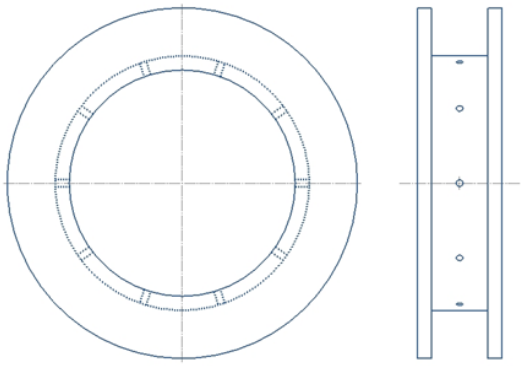

Figure 2.8. Generation 1 fuel injection block (10-30S).

Generation 2, as shown in Figure 2.9, used tangentially injected fuel jets. This design used small (0.018") diameter fuel jets, creating a much higher velocity and pressure drop across the holes than Generation 1. Eight and twelve jet models of this injection design were created for this project, and they are designated as '8-18T' and '12-18T' using the previously established nomenclature. The injection design produced a large pressure differential between the mixing chamber and fuel manifold, thus decoupling the fuel supply from acoustic disturbances in the air plenum. A comparative plot showing the pressure drop across the fuel manifold for Generations 1 and 2 is provided in Figure 2.10. For the majority of test conditions, the fuel jets were not choked. However, their acoustic impendence was measured to be sufficiently high to eliminate any fuel supply effects. This measurement will be presented in the following section. Also, the tangentially injected jets were directed with the swirling flow to increase the swirl instead of destroying it. The jets were also directed at the center of the annulus, so when injected, the fuel would penetrate into the circumferential direction of the annulus and spread in the radial direction, thus producing an extremely high level of mixing. This design was tested to be far superior to Generation 1 in every way.

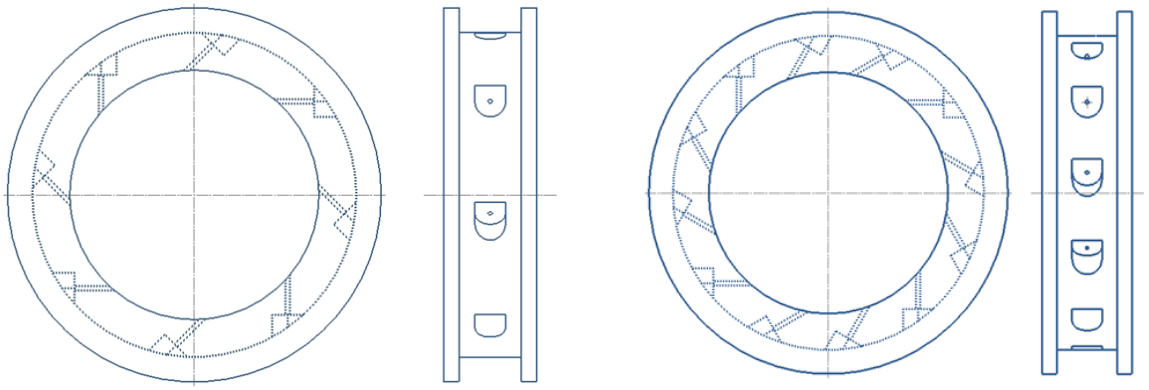

Figure 2.9. Generation 2 fuel injection blocks. (Left) 8-18T. (Right) 12-18T.

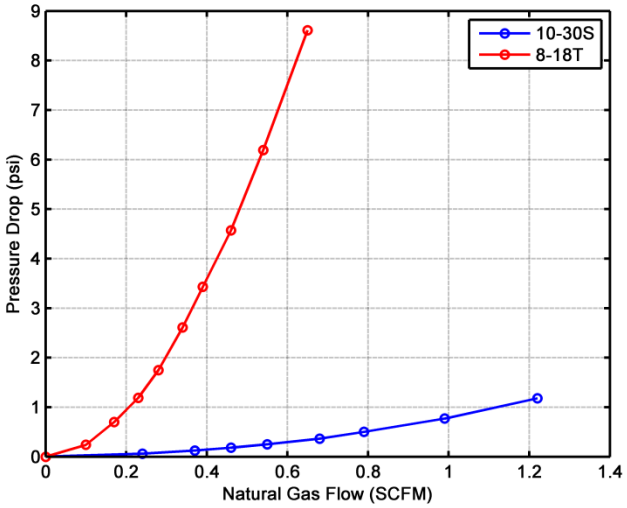

Figure 2.10. Experimental data comparing static pressure drop across the fuel manifold for Generation 1 (10-30S) and Generation 2 (8-18T).

The tangential fuel injection design provided a unique ability for the current research. In typical premixers, as already discussed, the swirl vanes are critical to operation. However, this project desired to investigate a premixer design with no swirl vanes, i.e. "No Swirl" premixer. Anchoring the flame, without swirl vanes, was only possible due to the momentum imparted to the core flow by the fuel jets creating a swirling flow. Unfortunately, the weak swirl was only found applicable for hydrogen combustion in the current design. While this did not create any limitations in the measurement of the mixing response, the flame zone produced by natural gas was too large to excite any unstable modes. This made this configuration unacceptable for the purposes of current research. However, this fuel injection strategy was found to be a viable technology to incorporate into premixer designs with simplified mixing chambers, which will be shown to be extremely beneficial to the proposed passive control technique.

Fuel Injection and Acoustic Decoupling

To obtain an accurate representation of the FAR fluctuation produced from the fuel/air mixing process, mass flow fluctuations in the fuel supply must be minimized. As already discussed, the fuel jets are not designed to be choked at every flow rate. Due to this limitation, the acoustic transmission loss was measured at a range of pressure drops across the manifold to find the minimum flow required to ensure that fuel supply effects could be neglected.

The acoustic transmission through the fuel manifold was measured by installing a dynamic pressure transducer in the fuel manifold and the air plenum. Acoustic excitation was supplied to the air side using the speaker. The excitation was varied between 75 and 500Hz, using a sine dwell technique (Section 2.2.6). The transmission loss (*TL*) through the manifold was calculated as the magnitude of the FRF between the air and fuel side pressure signals, eq. 2.3, where *p'* denotes acoustic pressure.

$$TL = 20 * log\left(\frac{p'_{fuel}}{p'_{air}}\right) \quad 2.3$$

For this experiment, the phase information between the signals is omitted because no plans were made to correct for the fuel supply effects.

The pressure drop across the manifold was varied by increasing the flow rate through the manifold. A zero flow excitation was performed first, as a baseline, because the air side microphone was not calibrated. The subsequent higher fuel pressure drop responses were then compared to this baseline, instead of determining the absolute transmission loss. The absolute transmission loss through the manifold encompasses resistive losses, due to the high velocity fuel jets, and the viscous dissipation losses in the extremely small diameter fuel passages without the presence of fuel. Transmission through the fuel manifold is shown in Figure 2.11 at three fuel jet Mach numbers (*Ma*). Mach number was used instead of pressure drop because it has more physical significance to acoustic transmission and is applicable to combustors operated at elevated pressures. Mach numbers of the fuel jets were estimated using the following compressible flow equation, shown in eq. 2.4, where p_0 is the total pressure in the fuel manifold, *p* is the downstream static pressure, and *k* is the specific heat ratio of the fuel [63].

$$Ma = \frac{2}{k-1}\left(\left(\frac{p_0}{p}\right)^{\frac{k-1}{k}} - 1\right)^{\frac{1}{2}} \quad 2.4$$

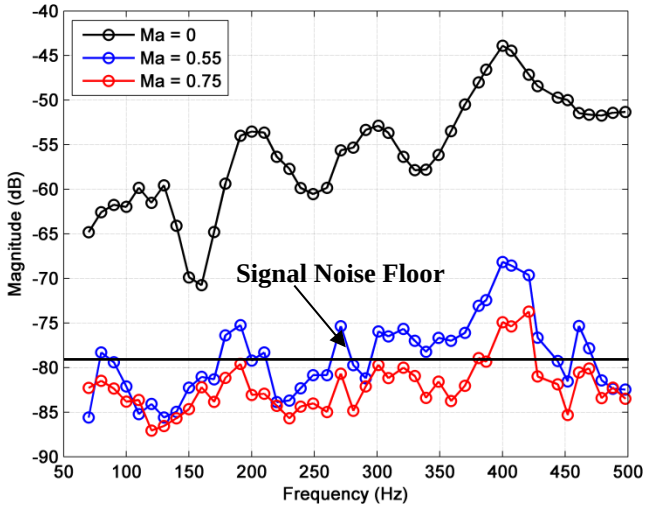

Figure 2.11. Experimental data showing the effect of fuel jet Mach number on transmission loss through the 8-18T fuel manifold.

A transmission loss of approximately 25 dB was measured across the frequency range for a fuel jet Mach number of 0.55. Only a slight improvement was observed at higher Mach numbers. This was attributed to the signal noise floor and loss of coherence between the signals, preventing an accurate estimation of the FRF. While the exact transmission loss could not be predicted, the loss of coherence between the pressure signals signified the communication between the fuel supply and air plenum was eliminated, or in other terms, decoupled. Two factors were considered in defining this decoupling criterion. First, because a portion of the transmission loss was due to the geometry of the fuel injection ports, without the presence of fuel, the result was geometry specific. That being said, all results reported hereafter used geometries with 0.018in diameter fuel jets (only the number of jets was varied between designs). However, designs with larger diameter fuel jets will incur lower losses and, therefore, caution should be taken caution in using the aforementioned criterion. Secondly, this criterion was tested and defined for acoustic disturbances that lie in the linear regime. Therefore, this criterion is only suitable for stable combustion experiments or open loop (forced excitation) mixing transfer function measurements. During strong unstable (non-linear) conditions, some degree of fuel feed system coupling will occur causing fuel mass flow fluctuations. However, because this project was interested in a passive control strategy that was based on a linear approach, no effort was made to quantify the amount of coupling that would occur under these conditions. In other words, the additional amplification of an already unstable system due to mass flow fluctuations

reveals no relevant information for the current research or the proposed passive control strategy. If an application requires zero fuel feed system coupling, the fuel jets should be choked (Ma = 1) throughout the entire operating range.

The corresponding flow rate requirement to achieve a Mach number of 0.55 is shown in Figure 2.12 for the 8-18T and the previous design. This data was gathered by measuring the pressure drop across the manifold for various flow rates and calculating the corresponding Mach number. This was performed using natural gas and hydrogen for all injection designs used for experimentation.

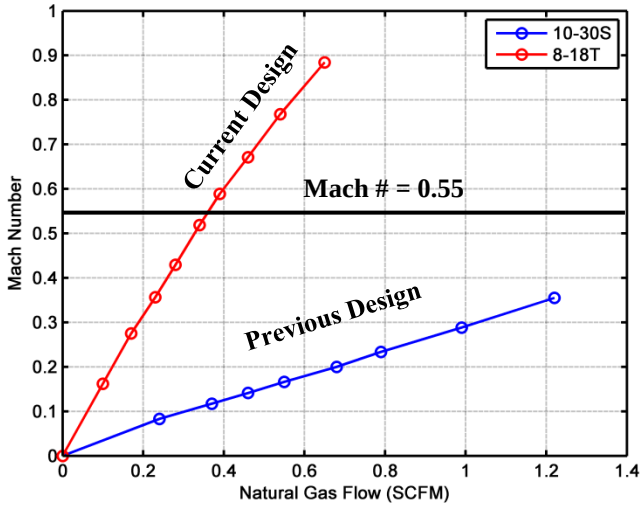

Figure 2.12. Experimental data of fuel jet Mach number plotted versus natural gas fuel flow rate, minimum fuel jet Mach number of 0.55 was required to decouple fuel supply from air plenum.

As can be seen, for the flow rates considered in this experiment, the previous design could not achieve a high enough Mach number to decouple the fuel supply. This was the primary reason for redesigning the fuel injection scheme. The minimum flow requirements for the 8-18T and 12-18T for both natural gas and hydrogen are provided in Table 2.1. These flows were maintained for all published results.

Table 2.1. Minimum fuel flow rate requirements to decouple fuel supply for 8-18T and 12-18T injection designs.

Injection	Natural Gas	Hydrogen
8-18T	0.36 SCFM	1.10 SCFM
12-18T	0.53 SCFM	1.65 SCFM

Manufacturing and Assembly of Modular Premixer

The premixer comprised an inlet, swirl body, swirler hub, two-piece centerbody, exit, spacer rings, fuel blocks, fuel manifold covers, and fuel lines. A labeled exploded view can be seen in Figure 2.13. The majority of the components required standard machining practices, so elaboration will not be included here. Emphasis will be placed on the process to manufacture the fuel injector blocks due to the difficulty encountered in machining these parts. This section will also include a brief overview of the process to assemble the premixer.

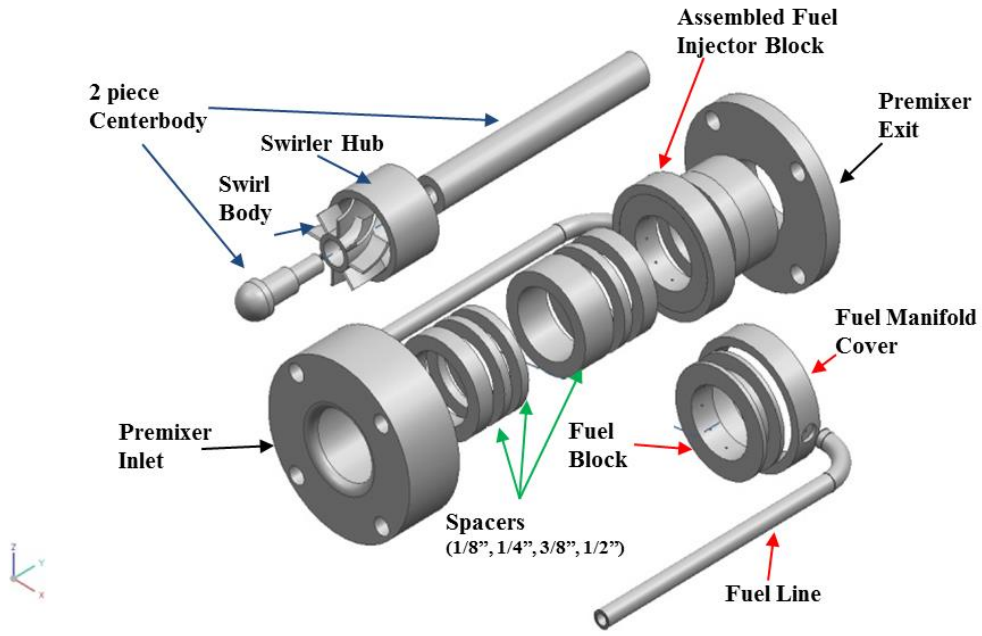

Figure 2.13. Labeled and exploded view of the modular premixer.

Each fuel injector block was fabricated out of three parts: the fuel block, fuel manifold cover, and fuel line. The fuel block was machined out of 303 SS, due to its better machinability than 304 or 316SS. The outer diameter and fuel manifold was first turned on a lathe. Then a 1/8" end mill was used to face each fuel jet location to provide a flat surface to drill. A CNC mill was

then used to bore the fuel jets. The CNC was required to provide a constant feed rate and pressure. The holes were bored deeper than required. Then the center hole was bored, exposing the fuel jets. This step was critical; otherwise the drill bit would break as it breached the curved surface. A finished fuel block is shown in Figure 2.14.

Figure 2.14. Machined fuel block (12-18T). Photo by author, 2012.

After machining, the fuel manifold cover was placed over the fuel block and welded into place. The manifold cover was machined out of 304 SS, which has superior weldability compared to 303SS. During welding, it is important to prevent the 303 from overheating because this will cause some of the alloying elements to vaporize and ruin the weld. After welding, the fuel block was faced on a lathe to create a flat mating surface. After facing, the fuel line (1/4" seamless 304SS tube) was bent and welded into place.

After all the components had been machined and fabricated, the premixer was assembled with the following procedure. The swirl body, which was CNC machined from 303SS, was pressed into the swirler hub and secured using an interference fit between the vanes and the hub. Then the upstream centerbody piece was slid through the swirler using a close sliding fit and threaded into the downstream centerbody, securing the assembly. The completed centerbody and swirler assembly was then slid into a recess in the Premixer Inlet using a close sliding fit. The recessed depth was identical to the wall thickness of the swirler hub, creating a seamless transition. The length of the hub was 0.002" longer than the premixer inlet. Therefore, when the premixer was fully assembled, compression on this lip, formed between the swirler hub and first spacer ring or fuel block, fixed this assembly in place. The rest of the assembly was completed with the aid of an alignment tool. The alignment tool was a 5" annular spoke that had a 0.502" outer diameter and 0.998" inner diameter. The tool was slid over the centerbody down to the swirler. Then the spacers, fuel injector block, and premixer exit were slid down the tool at the desired axial positions. The assembly was then secured, with the tool in place, using 4 (¼"-20) bolts that

extended throughout the assembly. The bolts were torqued in a two-step sequence, first at 5 in-lbs then 11 in-lbs. Lastly, the alignment tool was removed.

2.2 Measurement Techniques and Diagnostics

This section describes the diagnostic equipment and measurement techniques used to acquire the fuel concentration fluctuations, dynamic velocity and pressure, and heat release rate fluctuations.

2.2.1 Equivalence Ratio Measurement using Infrared Laser Absorption

Equivalence ratio oscillations were measured using an infrared laser absorption technique. Details on the theory of operation and previous applications of this measurement in lean premixed systems can be found in the following references [50, 66-68]. A schematic of the test set-up that was used in this experiment is shown in Figure 2.15

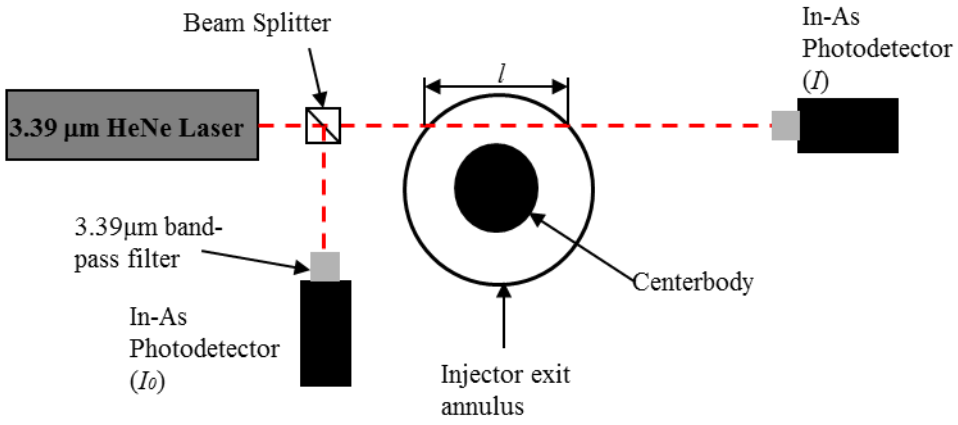

Figure 2.15. Schematic of the infrared laser absorption measurement technique.

A Helium-Neon Laser (Electro Optics LHIR-0100-339) was used to produce a 3.39µm wavelength laser beam, which was sent over the exit annulus of the injector and collected by an Indium-Arsenide photo detector (Electro-Optical Systems IA-010-H). To monitor the incident intensity, or power output of the laser, a fraction of the beam was diverted, using a beam splitter, and measured with a second detector before passing over the premixer exit. The remaining intensity passed through the fuel mixture, a fraction of which was absorbed by the fuel molecules. The ratio of transmitted (I_0) to incident (I) intensity is directly related to the fuel

concentration using Beer-Lambert's Law. This relation is shown in eq. 2.5, where l is the path length, c is the concentration of the fuel (mol/m^3), and ε is a molar absorption coefficient.

$$\frac{I}{I_0} = 10^{-\int_0^l \varepsilon c dx} \quad 2.5$$

The current set-up implemented an integrated line technique, such that the measured fuel concentration represents an average of the test volume. A 3.39μm wavelength laser was chosen because it corresponds to a strong energy level transition of the C-H bond [69], making this measurement suitable to all hydrocarbon fuels. Due to the strong absorptivity of this wavelength, the path length was kept to below 1 inch to maintain an adequate signal. The Indium-Arsenide detectors are specifically tuned to the wavelength of interest, and have a published bandwidth of 10 kHz, which is well beyond the frequency range of interest. Optical band pass filters were fitted to each of the detectors to minimize extraneous and uncorrelated light. The beam splitter used in this experiment was a simple microscope slide. The slide reflected roughly 10% of the incident light, which was then correlated to the output intensity of the laser so that fluctuations in the laser output power could be corrected. Selection of optic material is typically extremely important to achieve a high level of transmittance, especially for infrared wavelength. The exact transmission loss is a function of optic material and path length. The use of the microscope slide, which is not great for infrared wavelengths, created only minimal transmission loss due to the thickness (path length) of the slide.

The equivalence ratio measurement was calibrated by measuring the transmitted intensity through known fuel concentrations. The fuel concentrations were blended far upstream using calibrated mass flow meters and continuously flowed through the premixer. Mixing far upstream ensured that no spatial gradients of fuel concentration were present over the test volume, which was desired to enhance the accuracy of the calibration. The intensity of the transmitted laser was recorded and averaged over 15 seconds at each equivalence ratio. After all the points were recorded, a logarithmic fit was applied to the data. The accuracy of this technique was checked by plotting the data against predicted values from Beer-Lambert's Law using absorption coefficients found by Lee [66]. All measurements for this technique were performed with

natural gas. A calibration was performed every time the experiment was reconfigured. A sample calibration is provided in Figure 2.16 .

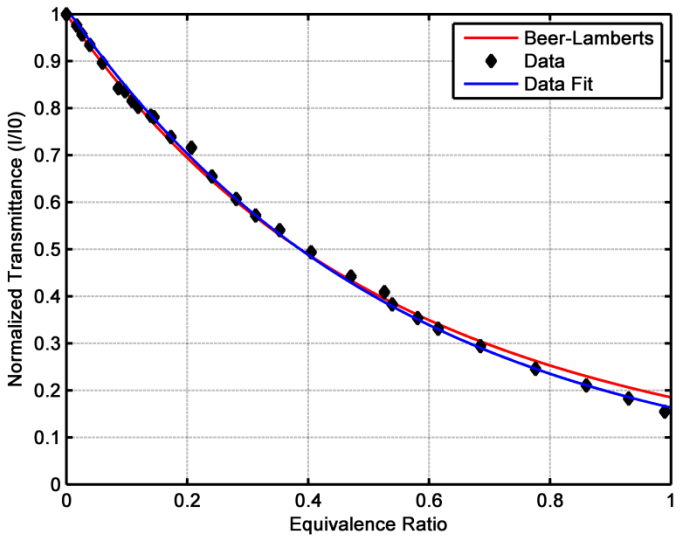

Figure 2.16. Sample calibration curve of equivalence ratio using an integrated line infrared laser absorption technique. Data are plotted with logarithmic best fit and theoretically predicted values.

2.2.2 Heat Release Rate Measurement using OH* Chemiluminescence

The unsteady heat release rate from the flame was measured using an OH* chemiluminescence technique. Measuring the chemiluminescence from excited species in the flame zone has been a common technique to indicate the heat or energy emitted during unsteady combustion, whether locally or globally. Lee and Santavicca [70] provide an excellent, detailed description of the theory of operation, along with measurement and analysis techniques. They also emphasize the great care that must be taken in interpreting and analyzing chemiluminescence signals to provide an accurate representation of heat release rate. Numerous parameters, such as unsteady strain, equivalence ratio fluctuations via fuel flow fluctuations, radiation losses, and chemiluminescence from other excited species, must be considered when using this technique. Because of the wealth of information that is provided by Lee and Santavicca, only a brief discussion of the theory of operation, along with the specifics of the technique that are unique to this experiment, are provided in this section.

During combustion, OH*, where the * signifies an excited species, quickly form and react, and in doing so, release energy in the form of photons. These photons are then collected using a Photo Multiplier Tube (PMT), which absorbs and amplifies the energy from the photons and produces a current. This current is then converted to voltage and read by the data acquisition. The PMT (Hamamatsu R955) was fitted with a band pass filter centered at 307nm (Andover Corporation P/N 307FS10-50 AM-45968 S/N:02) to isolate the wavelength of light emitted from OH*, as well as prevent the inclusion of wavelengths from other radicals or extraneous light. A schematic of the test set-up used in this experiment is shown in Figure 2.17.

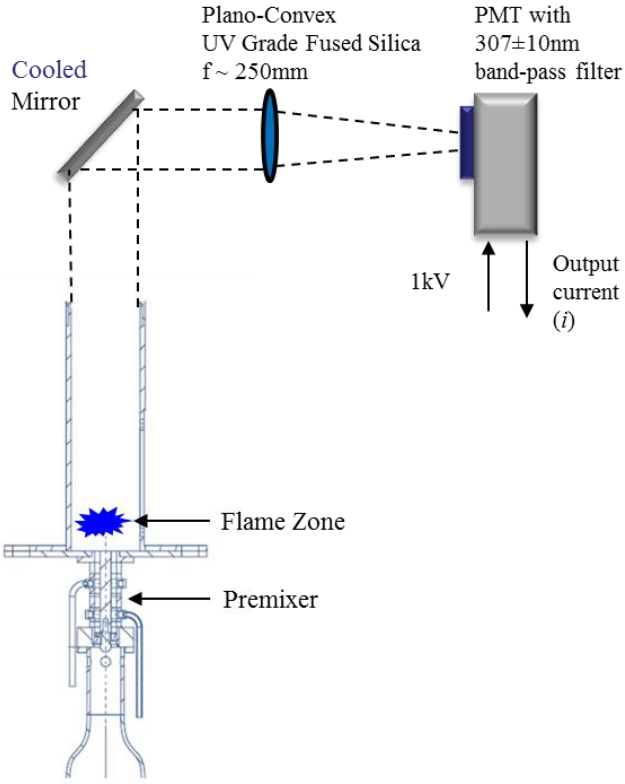

Figure 2.17. Schematic of the global heat release rate measurement using OH* chemiluminescence.

Due to the lack of optical access in the combustor, this project used a global heat release rate measurement. The nature of this measurement prevents any spatial information from being obtained. However, since the current research is aimed at suppressing the instability of the entire system, this measurement is acceptable. The only available optical access to the flame zone was the combustor exit. Because this area was in the hot gas path, the light emitted from the flame was redirected to a PMT using a front surface mirror that was actively cooled using an array of high velocity air jets. The reflected light was then focused using a 2" plano-convex UV grade

fused silica lens with a 250mm focal length. The light was focused down to approximately the aperture size of the PMT holder, while passing through the optical band-pass filter. It is important not to focus the beam to a single point. This can damage the sensor or produce an inconsistent measurement due to the saturation of internal elements. The PMT was powered with a 1000 V source (Pacific Instruments Model 204 High Voltage Power Supply). The output current of the PMT was converted to voltage using a current-to-voltage circuit with an adjustable gain. The gain was adjusted to utilize the maximum range of the input voltage of the data acquisition system (-5 to 5V), while leaving a conservative amount for dynamic fluctuations.

Heat release rate measurements can also be performed by collecting the light emitted from other chemical species, most commonly CH*. To adapt the current set-up, the optical filter would need to be changed to the one that is suited to the wavelength of the emitted light from CH*, which is 410nm. However, because this project requires the heat release rate measurement from hydrogen-air combustion, OH* chemiluminescence was the only suitable choice.

The linearity of the PMT was verified using a set of neutral density filters. A neutral density filter decreases the intensity of transmitted light by the following relation, eq. 2.6,

$$\frac{I}{I_0} = 10^{-ND} \tag{2.6}$$

where I and I_0 are the transmitted and incident intensities, and ND is the nondimensional neutral density filter number. The linearity of the PMT was verified by exposing the PMT to a constant intensity light source and interchanging seven neutral density filters (2, 1, 0.5, 0.4, 0.3, 0.2, 0.1 *ND*) over the aperture. The output voltage of the PMT was recorded with each ND filter installed. The results from this test are shown in Figure 2.18. Because a fixed ratio of light is transmitted through each neutral density filter, the intensity of the light source is not required to be known for this test.

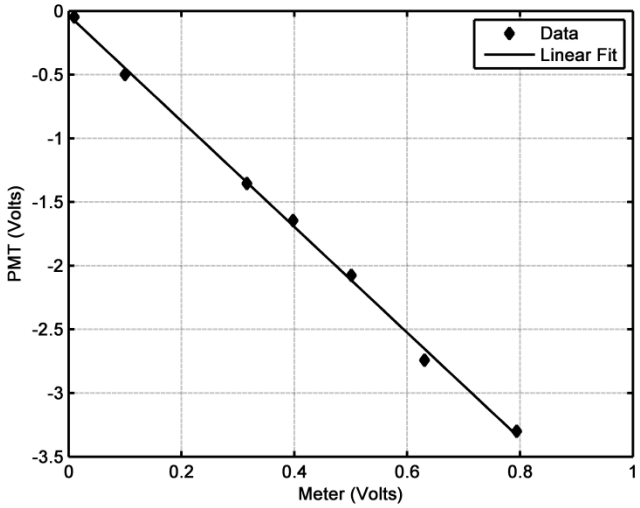

Figure 2.18. Experimental data verifying linearity of PMT.

The OH* chemiluminescence heat release rate measurement was calibrated by measuring the output voltage of the PMT exposed to both natural gas and hydrogen flames at different operating conditions. The intensity of light emitted from OH* is a function of both equivalence ratio and overall power. According to Lee and Santavicca [70], the intensity has a linear relationship with the overall power (maintaining a constant equivalence ratio) and an exponential relationship with the mean equivalence ratio. The exponential relationship comes from the fact that chemiluminescence intensity is more accurately a function of the temperature of the flame zone, which itself is an exponential function of equivalence ratio. Lee and Santavicca demonstrated this temperature dependence by measuring the intensity from a premixed flame while varying both the inlet temperature and the equivalence ratio. For this experiment, the overall power, or mean heat release rate, of the flame was estimated using the mass flow rate and Lower Heating Value (LHV) of the fuel, as shown in eq. 2.7.

$$\dot{Q} = \dot{m}_{fuel} LHV \qquad 2.7$$

To calibrate, the air flow was held constant, and the equivalence ratio was varied between 0.5 and 0.8 (for natural gas) and 0.2 and 0.4 (for hydrogen). The output voltage for each test condition was sampled and averaged for 20 seconds. Similar to the infrared absorption measurement, the air and fuel were premixed far upstream of the exit to supply a constant mixture to the flame zone. This process was then repeated at four different mean air flow rates

(13, 15, 17, 19 SCFM) for both natural gas and hydrogen. Results for natural gas are shown in Figure 2.19.

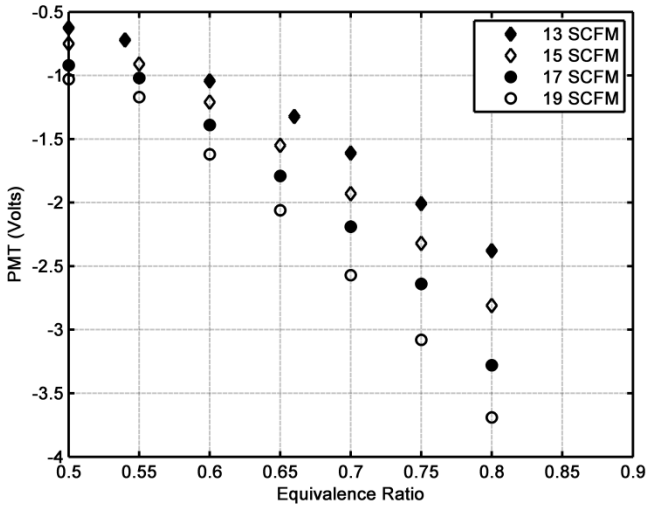

Figure 2.19. Experimental data showing effects of mean flow and equivalence ratio on heat release rate measurement using OH* chemiluminescence.

To correlate PMT output voltage with the heat release rated from the flame, the previously acquired results were normalized with the power (kilowatts) of the flame. This normalization is shown in Figure 2.20. The normalized heat release rate was linearly related to equivalence ratio. Since this project was only interested in dynamic heat release rate, the slope of this relation, along with mean equivalence ratio, was all that was required to properly scale the measured voltage to heat release rate fluctuations. During "partially premixed" operation, local variations in equivalence ratio exist inside the flame zone, which could produce a false signal. However, these local variations tend to be averaged out using the global measurement technique.

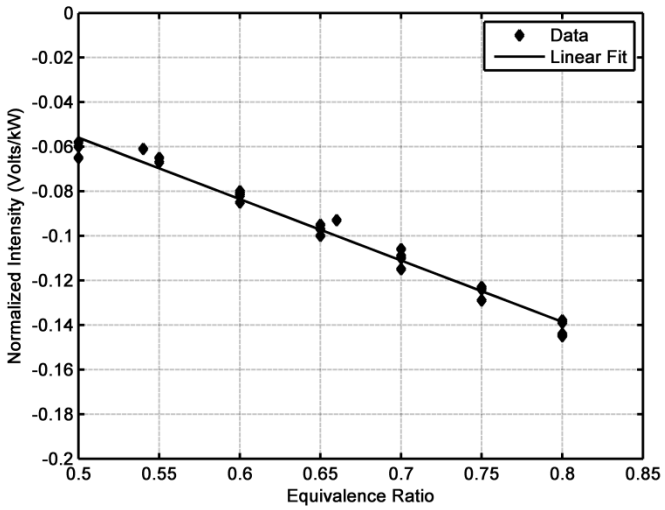

Figure 2.20. Experimental data of the normalized heat release rate measurement using OH* chemiluminescence.

It is important to note that, while a linear relationship was observed for the equivalence ratio range tested in this experiment, previous researchers have demonstrated that chemiluminescence intensity has an exponential relationship with equivalence ratio [70]. It would be expected that the normalized intensity would, in fact, demonstrate this behavior over a larger range of equivalence ratios. While this non-linear behavior is of no concern in the majority of testing conditions, it is, however, important to keep in mind during strong unstable events. Under these conditions, large equivalence ratio fluctuations that could lie outside of this linear regime are produced inside the mixing chamber. This would produce chemiluminescence intensities that no longer accurately describe the heat release rate of the flame.

2.2.3 Dynamic Velocity Measurement using a Hotwire Anemometer

The dynamic velocity was measured using a Constant Temperature hotwire Anemometer (CTA). A hotwire is a small diameter wire that is placed into a flow and is connected as a single leg of a Wheatstone bridge. The resistance of the hotwire is first recorded and nulled out by balancing the bridge. Once nulled, the resistance across the bridge is increased, causing current to flow through the hotwire, consequently heating it up. The supplied increase of resistance over the initial measurement is known as the overheat ratio. This ratio governs the operating temperature of the hotwire. As the fluid passes over the wire, heat is transferred away from the element,

which then causes the bridge to respond. The bridge balances by changing the current supplied to the hotwire element to maintain the preset temperature. The resulting change in current produces a corresponding voltage across the bridge that is measured and then correlated to the fluid velocity. The fluid velocity is related to the bridge voltage in accordance with King's Law, as shown in eq. 2.8 , where *E* is the bridge voltage, *U* is the fluid velocity, and *A* , *B*, and *n* are constants [63].

$$E^2 = A + BU^n \tag{2.8}$$

This type of device is capable of responses in the 10's of kHz due to the extremely fine wire size and the feedback circuit used to balance the bridge.

This project used a TSI-1201-T1.5 hotwire with a TSI 1150 probe support. The hotwire was used in conjunction with an AA Lab Systems (LTD AN-1003) Anemometer. The probe was connected to the anemometer using standard BNC connections and RG-58 cable. The overheat ratio was set to 1.1. The hotwire anemometer was calibrated by comparing the output voltage to the measured velocity using a Pitot-Static probe and a calibrated differential pressure transducer (Setra model 265 0-2.5" H_2O). The velocity is calculated from the measured differential pressure between the total and static ports on the Pitot-Static probe using the relation in eq. 2.9,

$$U = \sqrt{\frac{2\Delta p}{\rho}} \tag{2.9}$$

where *U* is velocity, Δp is the measured differential pressure, and ρ is the density calculated using the atmospheric pressure (from local airport reading) and measured air temperature. The hotwire and Pitot-Static probe were installed together in a calibration rig that produced a uniform velocity profile over a 1" diameter. The gain and offset of the anemometer were then adjusted to provide an output voltage that utilized the maximum range of the data acquisition (±5V). Care was taken to extend the calibration range to include excursions due to velocity fluctuations. A calibration was performed before every sequence of testing, but no more than twice a day. The data was fit using a third order regression, instead of a power fit as described by King's Law. This was observed to be a more accurate approximation for the flow conditions tested in this experiment. A sample calibration is shown in Figure 2.21.

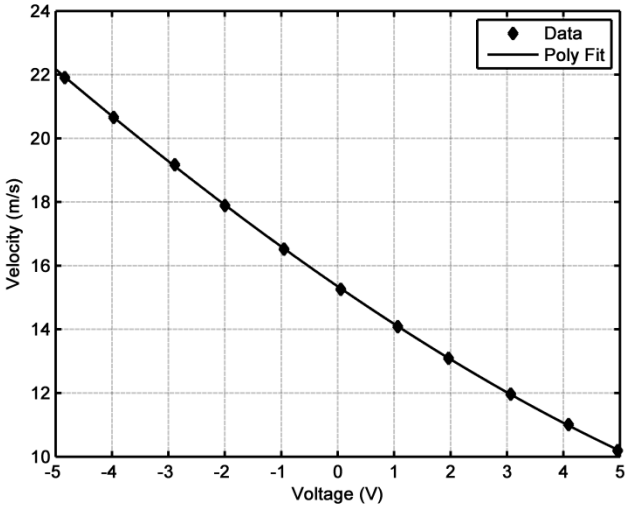

Figure 2.21. Sample hotwire anemometer calibration curve with a third order best fit.

2.2.4 Dynamic Pressure Measurement using a Microphone

Pressure fluctuations were measured using a Kulite (mic-152) dynamic pressure transducer, or microphone. This type of device is common for measuring pressure fluctuations in lean premixed combustion experiments [67]. This device is well suited for the current application due to its large dynamic range, sound pressure level (SPL) of 100-194dB, and low sensitivity to temperature change. It can withstand temperatures up to 250°F and static pressures up to 25 psig. This temperature range limits the device from being installed into the combustion chamber, so for this experiment the transducer was installed upstream of the premixer. The atmospheric combustor design presented no limitations to the static pressure range of the transducer. The microphone chosen has a published bandwidth of 125 kHz, which is well beyond the frequency range of interest for this experiment.

The dynamic pressure transducer was mounted into a modified 1/4" NPT plug fitting. This fitting could be installed into the experiment in one of the many tapped instrumentation ports available in the Premixer Inlet Section. The plug was threaded into a port so that the instrument was flush with the chamber wall. Excitation and signal conditioning were provided using a Strain Gage Conditioner (Vishay 2120). The excitation voltage for this device is 10Vdc, and the tunable gain was set to 100X to amplify the signal to a level more suited for the data acquisition

system (±5V). Again, care must be taken to prevent saturation of the signal during intense combustion instabilities.

The pressure transducer was calibrated using a sound level calibrator (GenRad 1562-A), which produces a constant 114 dB SPL at 125, 250, 500, 1000, and 2000Hz. The pressure transducer was mounted into the device and scanned through the above frequencies. Then a constant (digital) gain was applied to the output to match the known output of the calibrating device. The frequency spectrums, after the calibration, are shown in Figure 2.22.

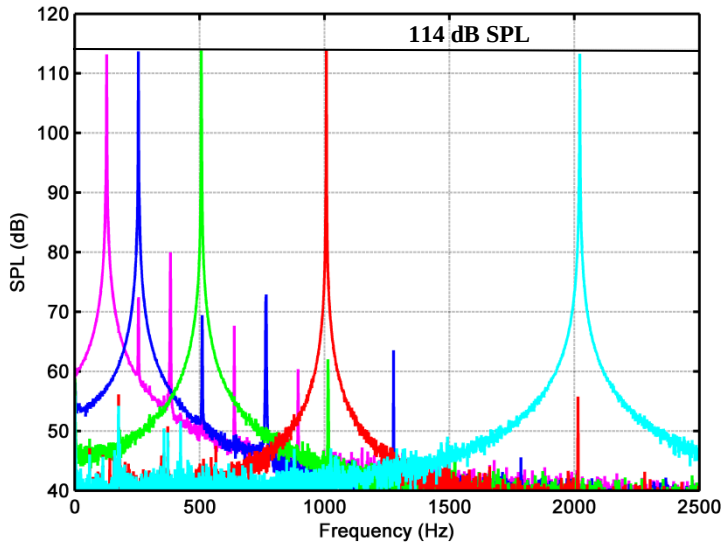

Figure 2.22. Measured responses verifying the calibration of Kulite mic-152 using a GenRad 1562-A Sound Level Calibrator. Calibrating device produced a constant 114dB SPL at 125, 250, 500, 1000, and 2000Hz.

2.2.5 Data Acquisition and Signal Processing

Data Acquisition

All signals produced by the various instruments were collected as voltages using a data acquisition system (DAQ) and National Instruments (NI) LabView software. The signals were sampled using an SCXI 1000 Chassis equipped with an SCXI-1141 8-channal data acquisition card. This card is equipped with an 8^{th} order Bessel filter and switchable gains for each channel. The gains were adjusted based on the voltages produced by the sensors. All instruments were connected to the DAQ using standard BNC connections. This was facilitated by a BNC connector block that was installed onto the card. The signals were sent to a controller card

(NIPCI-6143) using an SHC68-68 cable. The controller had a 16 bit Analog to Digital converter and communicated to the DAQ in parallel mode. This mode of operation acquires all 8 channels simultaneously, thus eliminating the need to correct the phase lag between channels. The digital signals were then recorded via a custom LabView program. The data was written and saved to the hard drive during operation. A solid state hard drive was used instead of a conventional hard disk to prevent crashing due to vibrations that were created from intense combustion instabilities.

Excitation signals were produced in a similar fashion. The only instrument that required excitation for this experiment was the acoustic driver. A digital sine wave was created in the LabView program and converted to an analog voltage using an NI PCI-M10-16XE-10 controller. The voltage was sent to the SCXI-1000 Chassis using an SCXI-1349 connector assembly. Then, external connectors sent the signal to the speaker amplifier and onto the speaker.

Signal Processing

Even though the signal processing techniques are not physically a part of the experimental rig, they are directly related to the data acquisition system. Techniques described hereafter are the general techniques that were used to process the data. This section is aimed at providing clarity for the various techniques and procedures used to average, window, and scale frequency spectrums. To keep this section as general as possible, a time domain signal will be labeled $x(t)$ or $y(t)$, with corresponding frequency spectrum $X(f)$ or $Y(f)$. The next paragraph details a frequency domain analysis on a single general time series, $x(t)$. This is followed by the procedure to determine the transfer function between an input, $X(f)$, and output, $Y(f)$.

A particular time signal, $x(t)$, was sampled and recorded at 8192Hz, which has a Nyquist frequency of 4096Hz. This frequency was chosen to well exceed the expected dynamics of the system, which, as previously discussed, is on the order of hundreds of Hz. An analog low pass filter was set to 3200Hz to prevent aliasing of higher frequencies. This filter setting was chosen based on the rule of thumb for 8^{th} order low pass filters. The data was recorded for various time lengths in one-second increments, depending on the specific test. The time data was then divided into one-second blocks and zero-meaned. A Hanning window was applied to each block to prevent peak broadening in the frequency spectrum. Each data block was transformed into a frequency spectrum using a Fast Fourier Transform (FFT). The resulting spectrums had 1 Hz

frequency resolution. The spectrums were then scaled to account for the window and the double sided spectrums produced by MATLAB. Then, component-wise averaging was applied to each frequency across all spectrums. This is referred to as vector averaging, resulting in X*(f)*. Averaging the spectrums minimizes the amplitudes of the incoherent signals, and thus, separates the true signal from the noise.

The auto spectrums (G_{XX} and G_{YY}) for each signal were calculated using the following expression,

$$G_{XX}(f) = X^*(f)X(f) \quad G_{YY}(f) = Y^*(f)Y(f), \tag{2.10}$$

where **(f)* represents the complex conjugate. The auto spectrums were then scaled, and amplitudes here will be presented using rms values. Cross spectrums were calculated using the following equations,

$$G_{XY}(f) = X^*(f)Y(f) \quad G_{YX}(f) = Y^*(f)X(f). \tag{2.11}$$

The auto and cross spectrums were then used to obtain the transfer function, also known as the Frequency Response Function (FRF). Because the experimental set-up had noise present in the input (*x*) and output (*y*) signals, an average transfer function was used to give the best representation of the data. H_1 is most suited for noise only in the output. H_2 is most suited for noise only in the input. The formulation of the average FRF is shown below.

$$H_1 = \frac{G_{XY}}{G_{XX}} \quad H_2 = \frac{G_{YY}}{G_{YX}} \quad FRF = \frac{(H_1 + H_2)}{2}. \tag{2.12}$$

The gain of the system is given by the magnitude of the FRF, and the phase between the input and output is the angle between the real and imaginary components. The coherence (γ^2) was calculated using eq. 2.13. Coherence describes the linear relationship between the input and output. The range of coherence is between 0 and 1, with 1 being perfectly related.

$$\gamma^2 = \frac{G_{XY}G_{YX}}{G_{XX}G_{YY}} \tag{2.13}$$

2.2.6 Sine Dwell Technique

Open loop transfer functions were measured using a sine dwell technique with acoustic excitation provided by the speaker installed into the air plenum. The frequency of excitation was scanned through the entire frequency range of interest at discrete intervals. The frequencies examined in this project ranged from 10 to 500 Hz, and they were incremented by either 10 or 25Hz. Larger frequency steps were typical for measuring the transfer functions for the majority of the tests, where the responses were fairly constant over the frequency range. However, smaller increments were used to measure the mixing transfer function for two injections to better capture the "notch" created by the interference of the waves. The amplitude of excitation was varied at each frequency by adjusting the power to the speaker until an excellent signal to noise ratio, typically greater than 15dB, was acquired on all desired signals. After establishing these amplitudes, the linearity at each frequency was ensured by measuring and checking the response at both half and double the set amplitude.

At each incremental frequency, the time signals of the input and output of the desired transfer function were recorded for 15 seconds. For all transfer functions, the signal used to drive the speaker was never used as the input to the system. The input was always a measured quantity, such as a velocity or pressure. The time domain data was transformed into the frequency domain using the techniques described in Section 2.2.5. A representative set of auto spectrums is provided in Figure 2.23. The responses shown are velocity (input) and equivalence ratio (output) excited at 100 Hz. These signals are specific to the mixing transfer function, but the process is general to any system. The amplitude of the excitation was set to ensure that an adequate signal to noise ratio was obtained on both signals. For each frequency tested, the amplitude was checked to ensure the responses were in the linear regime.

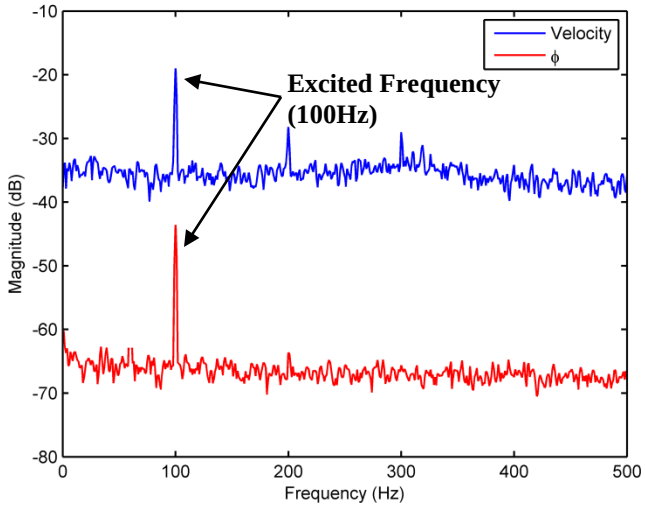

Figure 2.23. Plot of representative auto spectrums for velocity and equivalence ratio (φ) at 100Hz excitation during a sine dwell sweep.

The FRF was calculated to obtain the magnitude and phase of the transfer function at the excited frequency. An example of a 100Hz excitation is provided in Figure 2.24. The coherence between the signals, at the excited frequency, was maintained at 0.95 or higher for all tests. The magnitude, phase, and coherence were recorded at each excited frequency. All reported transfer functions using this technique are the results obtained from this sequence of testing.

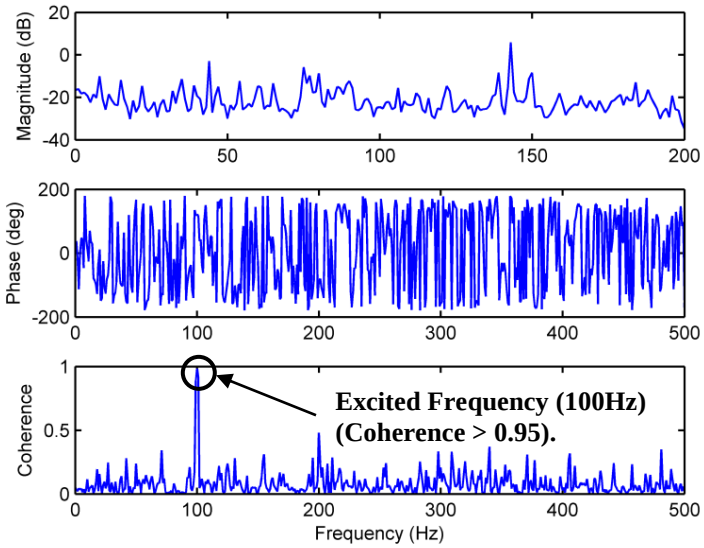

Figure 2.24. Plot of magnitude, phase, and coherence for an example transfer function excited at 100Hz during sine dwell sweep. Only coherent signal is at the excited frequency.

Chapter 3: Phase I: Cold Flow Mixing Response

The goal for the cold testing was to measure and characterize the mixing transfer function in a prototype lean premixed injector. Two important parameters are needed to accurately characterize the mixing response: Phase and Gain. Phase is the most critical parameter for the successful application of a multiple injection strategy. Relatively small errors in phase estimation have a strong influence on the location of FAR damping for multiple injections. Phase data will be presented as the slope of the phase/frequency correlation. Gain is the less critical parameter for applying a multiple injection strategy. The gain of the mixing transfer function represents the strength of the FAR fluctuations at the exit of the premixer created by velocity fluctuations at the fuel injection location. The magnitude of the mixing response is only of secondary importance. For example, gain is only critical if the magnitudes at each of the injection locations are different by a significant margin when operating at the same conditions.

This chapter begins with the characterization of the mixing response in the simplified "No Swirl" geometry and then proceeds to the full "Swirl" geometry premixer. Each configuration was tested at various operating conditions. The magnitude and phase delays were recorded at each condition and used to develop an experimental model that characterized the response for a single injection. Then, the mixing response was measured for two simultaneously fueled injection locations and compared with the equivalent response predicted using the single injection model.

3.1 Mixing Response of "No Swirl" Premixer

This section details the experimental techniques and findings obtained for the mixing transfer function for the "No Swirl" premixer. The first sub-section details the measurement technique used to obtain the mixing response for a single injection at various conditions. The second sub-section summarizes the phase delay and magnitude obtained at each condition. This section proceeds to develop the experimental model that best characterizes the system. The third sub-section details the measurement of the response from two simultaneous fuel injections and compares it with the response predicted from the single injection model. The final sub-section summarizes the findings obtained from this experiment.

3.1.1 Mixing Transfer Function Measurement for Single Injection

To accurately obtain the *MTF*'s, a two-step measurement technique was utilized. First, a transfer function was created between the velocity at the fuel injection plane (u_{inj}) and a reference pressure (p_{ref}), without the presence of fuel. This will be referred to as the velocity response or velocity transfer function. This was necessary because the high velocity fuel jets would corrupt the velocity measurement. Second, the fuel was introduced, and a transfer function between the equivalence ratio (φ') and the same reference pressure was measured. This will be referred to as the fuel response or fuel transfer function. Note this is not the mixing transfer function. The two transfer functions were then multiplied to yield the desired *MTF*, as shown in eq. 3.1.

$$MTF(f) = \frac{p'_{ref}(f)}{u'_{inj}(f)} * \frac{\varphi'(f)}{p'_{ref}(f)} = \frac{\varphi'(f)}{u'_{inj}(f)} \qquad 3.1$$

The combustor was first assembled with the "No Swirl" premixer and without the downstream variable length combustion chamber. This allowed the laser full optical access to the dump plane of the premixer. The reference pressure was measured using a microphone installed into one of the instrumentation ports directly upstream of the premixer. The velocity response at the injection plane was obtained by removing the fuel injection block and replacing it with a modified spacer ring designed to hold a hotwire. The hotwire was positioned at the exact plane of the fuel jets to accurately measure the velocity response at the fuel/air interface. When completed, the fuel injector was replaced, and the fuel response was measured using the infrared laser. A schematic of this setup is shown in Figure 3.1. The schematic shows the assembly with the fuel injection blocks installed, instead of the hotwire.

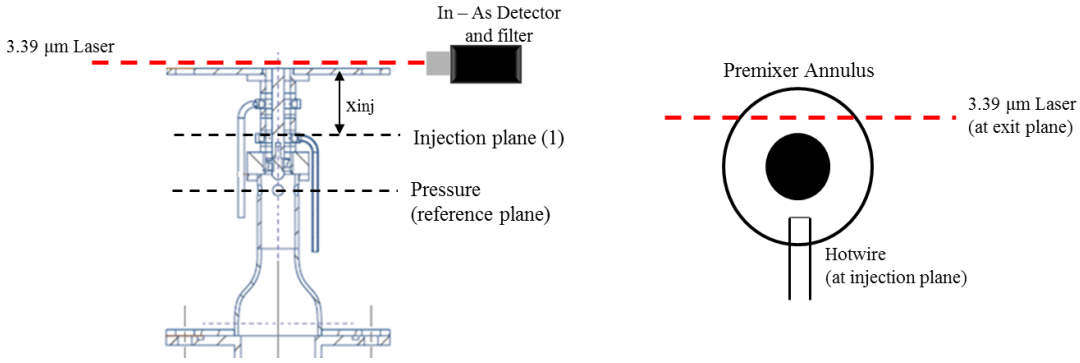

Figure 3.1. Schematic showing measurement locations used to obtain the mixing transfer function.

The velocity response was measured at all predetermined test conditions. Multiple measurements were made to check for mean flow or spatial effects that could be present in the mixing chamber of the premixer. Three injection locations (x_{inj} = 1.0625, 2.0625, and 3.0625") at three mean air flow rates (Q = 14.5, 15, and 19.5 SCFM) were tested. The data was collected between 10 and 550 Hz at 25 Hz increments using the aforementioned sine dwell technique. The results were then interpolated to provide a usable transfer function for tests measured at other frequency increments. A representative result is shown in Figure 3.2. No significant variations were observed in the transfer function for all tests performed. This makes the result shown applicable for any injection location or flow rate in the range tested. Higher flow rates would need to be tested to extend the applicability of the presented results. Phase differences would be expected as the mean flow Mach number increases.

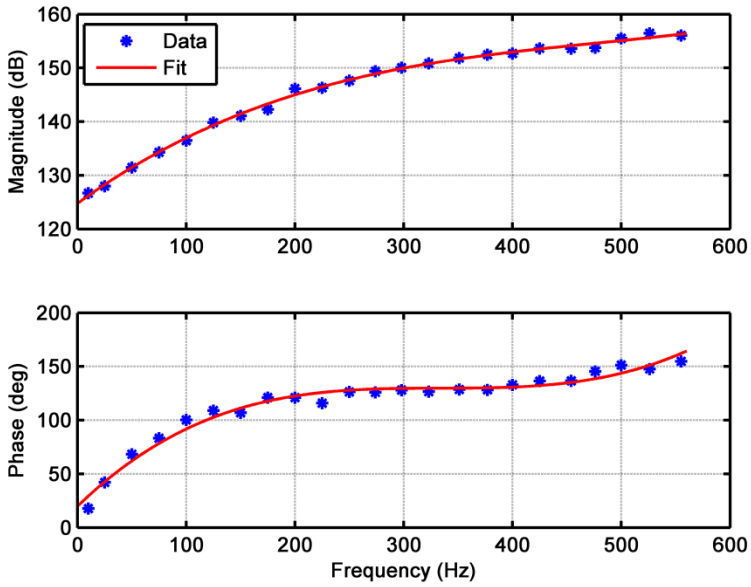

Figure 3.2. Measured transfer function between velocity, measured at the injection plane, and reference pressure in the "No Swirl" premixer.

The hotwire was removed and the fuel injection block was replaced to measure the fuel response. A full factorial test matrix, along with 13 random configurations, was tested with the following parameters:

- Injection distance, x_{inj} (1.0625in, 2.0625in, 3.0625in)
- Mean Equivalence Ratio (0.3, 0.5, 0.7)
- Air Mass Flow (14.5, 15, 19.5) SCFM

The results from these tests were then combined with the velocity response to produce the desired *MTF*. A typical result is shown in Figure 3.3. A "flat" magnitude response was observed in the frequency range of interest. This response allows for an average gain to accurately represent the response. No significant drop off was observed due to the theorized mixing effects. This observation will be discussed in more detail in the summary of this section. The linear phase delay, on the other hand, was exactly as expected. The linear phase delay was found to be in excellent agreement with the convective time delay model. Also, the 0 Hz phase crossing was observed to be 180 degrees, which, as previously developed, corresponds to the inverse relationship between the equivalence ratio and velocity. The phase delay, which is defined as the slope of the phase-frequency relation, was obtained by performing a linear regression on the selected data. R^2 values greater 0.98 were typical, demonstrating excellent correlation. For all tests, the coherence was maintained to be greater than 0.95, demonstrating great linearity between the acquired signals. The average gain and phase delay were recorded for each test condition and are presented in the next section.

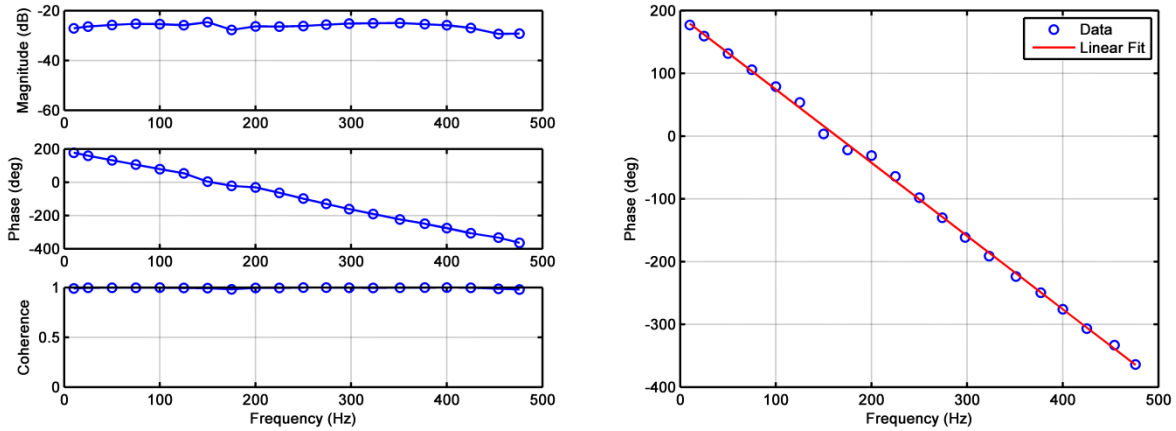

Figure 3.3. Measured mixing transfer function (Left) with an exploded view of phase and a linear fit (Right) for the No Swirl" premixer.

3.1.2 Results of Single Injection Tests

Phase Delay Results

The phase delay (deg/Hz) was recorded from each test condition and correlated against the convective delay (L/U), where L is the injection distance (x_{inj}) and U_{mix} is the average mixture velocity. The average mixture velocity was simply estimated assuming a uniform velocity

profile. This assumption was verified by traversing a pitot probe across the premixer annulus. From here on out, the convective delay will be referred to as (τ). The dominant variable was chosen due to the known relationship between phase delay and convective delay developed in the previously defined "Time Delay Model". The results of this correlation are shown in Figure 3.4, along with the 95% confidence intervals and the theoretically predicted values. The linear regression of the data had an adjusted R^2 of 0.965, thus producing an accurate characterization of phase delay for this system.

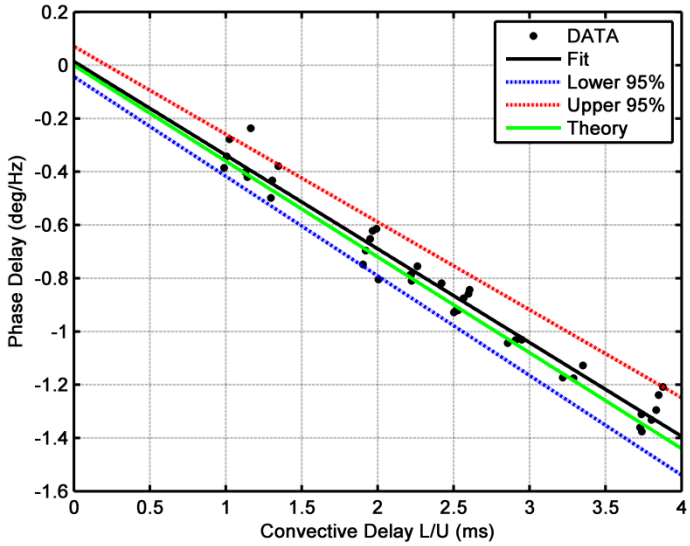

Figure 3.4. Experimental data showing effects of convective delay on phase delay for single injection configurations in the "No Swirl" premixer. Experimental data are plotted with a linear best fit, 95% confidence bounds, and theoretically predicted values.

Gain Results

The results obtained for the gain were more complicated to reduce into a characteristic model. Unlike phase delay, there was no prior knowledge about the dominant independent variables. To determine the most significant variables, a 2nd order multivariate regression analysis was conducted to investigate the relationship between the gain and equivalence ratio (φ), convective delay (τ), and mean velocity (U_{mix}). The significant variables were identified as $\varphi * \tau$ ($p < 0.00001$) and φ^2 ($p = 0.016$). The identification of these variables suggest that the mixing time along with the overall concentration are the most physically significant parameters, with secondary effects from the penetration distance and momentum ratio, as evidenced by the φ^2

parameter. Further regressions were performed with the single most significant variable, $\varphi^* \tau$, as well as with both significant variables, $\varphi^* \tau$ and φ^2. The higher order regression analysis produced a good correlation with the experimental data, which was evidenced by an adjusted R^2 value of 0.865. However, the bounds for the 95% confidence intervals produced unrealistic results making the correlation unacceptable to describe the gain of the system. When the system was only analyzed with the single most significant variable, it resulted in a lower R^2 of 0.636, but it had acceptable confidence bounds. The result from this analysis, along with the experimental data is shown in Figure 3.5.

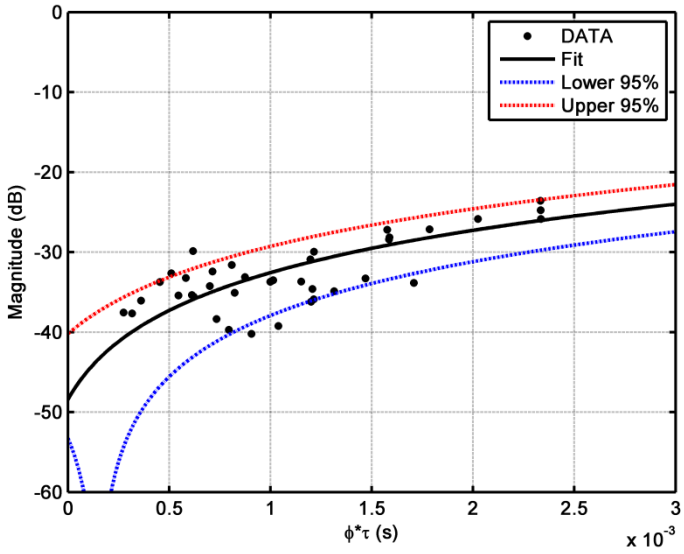

Figure 3.5. Experimental magnitudes of the mixing response for single injection configurations in the "No Swirl" premixer. Experimental data are plotted with a best fit and 95% confidence bounds.

3.1.3 Mixing Transfer Function Measurement for Multiple Injections

The measurement procedure for multiple injections was similar to the one for a single injection with two minor differences. First, the mixing response was measured for two injection blocks fueled at once with equal fuel flow rates, and second, the sine dwell frequency excitation was incremented at 10 Hz to better capture the physics.

A total of nine tests were conducted varying injection distance, separation distance between the injections, mean equivalence ratio, and mean air mass flow. All tests were performed with the 8-18T injection block fueled with natural gas. Tests were limited to configurations that would

produce FAR damping between 0-500Hz. The measured responses were then compared against the response of the addition of the two single injection locations (x_1 and x_2), predicted using the experimental models created in the previous section. The predicted response (MTF_{comb}) is shown in eq. 3.2. Two typical responses are shown in Figure 3.7 and Figure 3.7, where the center target frequencies are 285Hz and 420Hz, respectively.

$$MTF_{comb}(f) = MTF_{x1}(f) + MTF_{x2}(f) \qquad 3.2$$

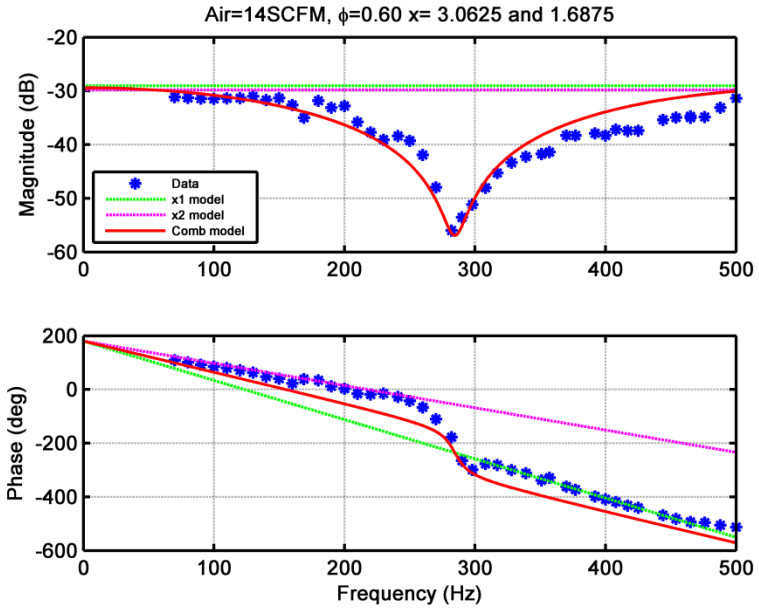

Figure 3.6. Measured mixing response showing evidence of FAR damping using two axial injections in the "No Swirl" premixer, target frequency of 285Hz. Data are compared with the predicted responses.

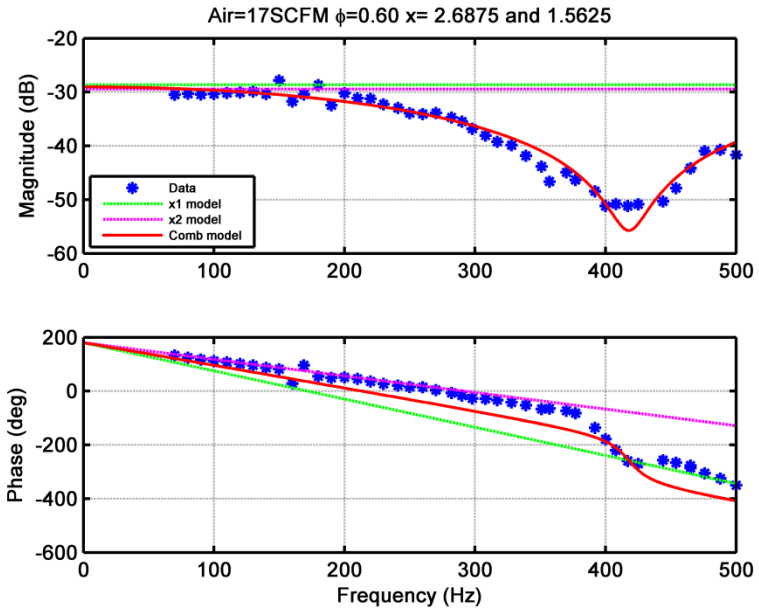

Figure 3.7. Measured mixing responses showing evidence of FAR damping using two axial injections in the "No Swirl" premixer, target frequency of 420Hz. Data are compared with the predicted responses.

In all tests performed, significant damping of FAR fluctuations was observed at select frequencies. The location of the damping was easily identifiable by a notch in the magnitude of the mixing response and a shift in phase, both centered at the target frequency. As predicted, the location of this target frequency was able to be manipulated by varying the convective delay between the axial injection locations. This is demonstrated in Figure 3.6 and Figure 3.7, where two different target frequencies are shown. One other useful observation was the direction of the phase shift. Depending on which injection location produced the stronger response, the phase would either shift up, for cases where the longer injection distance (steeper phase delay) dominated, or down, for cases where the shorter injection distance (shallower phase delay) dominated. Only the slightest difference in magnitude was required to swing the direction of the phase shift. This characteristic produced a metric to determine the dominant response, which, in turn, provides an avenue to adjust the responses to achieve higher FAR damping. Even though only 50/50 fuel splits were considered for these experiments, slight adjustments to the fuel flow could be used to more accurately match the magnitudes and create the maximum destructive interference between the two fuel waves.

In all cases tested, the response for two injections was accurately predicted using the previously developed single injection model. Overall, these tests validated the theory of using multiple injections to target and inhibit FAR oscillations at predetermined (target) frequencies.

3.1.4 Summary and Discussion of "No Swirl" Mixing

The mixing transfer function was measured for a total of 40 single injection configurations varying mean air flow, equivalence ratio, and injection distance. The linear phase delay was accurately captured and characterized using the convective time. The experimentally measured phase delay was shown to be in excellent agreement with the values predicted by the theoretical "Time Delay Model". The gain for each single injection response was approximated using a single average value. No significant damping was observed due to the theorized mixing effects in the frequency range tested. While this was originally a desired observation, it did not provide any limitation to the application of multiple injections. An experimental model for the gain was developed using the single most significant independent variable determined from a 2^{nd} order multivariate regression analysis. While there was a high degree of uncertainty in the gain measurement, the single variable model was ultimately proven to be adequate in describing the response of the system.

The mixing response was measured for two injection locations at nine different configurations. All responses showed significant damping of FAR fluctuations at select frequencies. The damped frequencies were shown to be a function of the convective delay between the injection locations, created by either changing the axial separation distance or mean velocity, and were easily identifiable by a significant drop in magnitude accompanied by a shift in phase. The direction of the phase shift, either positive or negative, was based on the relative strength of the response from each injection location. Additionally, these results were accurately predicted using the experimental single injection response model. These results confirmed that multiple injections are an effective technique to target and inhibit FAR fluctuations in a simple flow field.

3.2 Mixing Response of "Swirl" Premixer

Even though results obtained for the "No Swirl" geometry were successful in characterizing that system, it is not reasonable to assume those results also describe the swirl premixer. Because the goal of this project was to implement a multiple injection strategy in a swirl premixer, it was necessary to obtain the mixing response specific to this geometry. Therefore, results obtained from these measurements are more applicable to premixer designs that are currently in practice.

This section is aimed at measuring and characterizing the mixing response for the full geometry "Swirl" premixer. The experimental procedure and analysis follows the same steps as described in the previous section for "No Swirl". However, due to issues that were unique to the swirling flow field, adaptations were made to the experiment. These changes will be highlighted and expanded upon.

3.2.1 Mixing Transfer Function Measurement for Single Injection

The measurement of the *MTF* for the full geometry premixer follows the same procedure as outlined in the previous section for the "No Swirl" premixer. However, adaptions were required to the setup and measurement techniques to address specific issues that were encountered due to the incorporation of the swirl vanes. While this section aims at detailing the measurement process, selected results are presented to provide an explanation of the observations and to justify the techniques used to attempt to circumvent the difficulties caused by the swirling flow.

Unlike the "No Swirl" premixer, the flow field created by the swirl vanes creates a recirculation zone at the exit of the premixer. This flow field is illustrated for a general annular swirl flow in Figure 3.8, taken from Syred [45]. As previously discussed, this recirculation is designed to anchor and stabilize the flame zone during operation. However, this zone introduced problems due to placement of the infrared laser absorption measurement. As additional momentum was imparted to the flow from the tangential entry jets, this zone extended out into the annulus and eventually engulfed the measurement location. As the equivalence ratio (directly related to the momentum) was increased above 0.27, the rotation frequency of this zone was observed in the steady state concentration measurements, as shown in Figure 3.8. The frequency content

produced from the recirculation zone was in the frequency range of interest for the desired *MTF* and, therefore, had to be addressed. This phenomenon, which is typically referred to as a Precessing Vortex Core (PVC), has been extensively studied by previous researchers, most notably Syred [45], and is usually characterized by a non-dimensional Strouhal number (Str), eq. 3.3. The Strouhal number that was found to accurately describe the PVC for this geometry was 0.25 with a standard deviation of 0.01.

$$Str = \frac{D_{centerbody} * f}{U_{avg}} \qquad 3.3$$

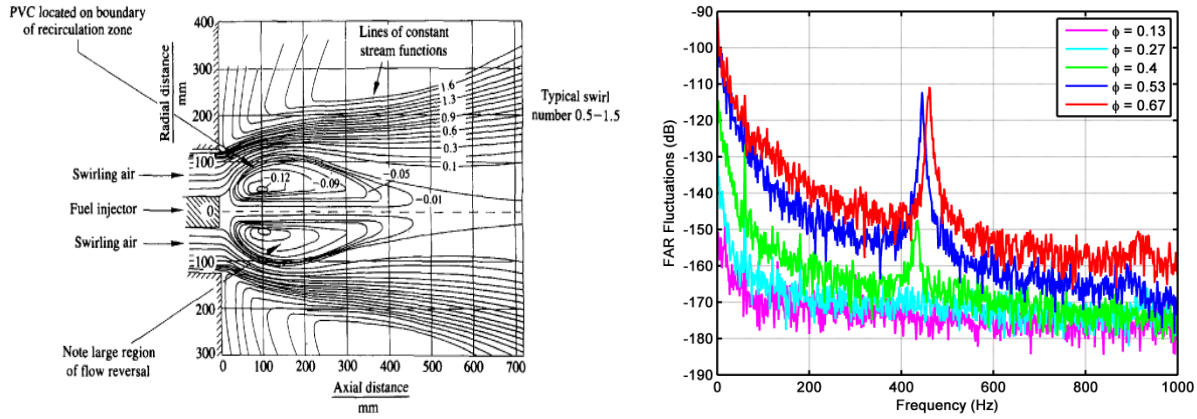

Figure 3.8. (Left) streamlines for a general swirl premixer illustrating the recirculation zone created at the end of the centerbody, taken from Syred [45]. (Right) measured FAR fluctuations caused by the recirculation zone as the swirl strength was increased by the high momentum tangential fuel jets.

To obtain an accurate *MTF*, measures were taken to eliminate this effect. Otherwise, FAR fluctuations produced as a result of the fuel/air mixing process would not be separable from the rotation of the recirculation zone. Clean (no recirculation zone effects) *MTF* measurements were achieved by extending the centerbody by two inches. This moved the recirculation zone away from the measurement plane without affecting the fuel/air mixing process. Comparing the results of the *MTF* before and after applying the centerbody extender verified that this technique did not affect the mixing process. This verification was performed in a configuration that was previously measured to have no effects from the recirculation zone, i.e. equivalence ratio of 0.27 or less. However, it is important to note that even though the FAR fluctuations produced from the recirculation zone were eliminated from the *MTF* measurements, they were not eliminated

for combustion tests. This observed behavior is a known instability mechanism [45] and was present in all combustion tests.

Other than the centerbody extender, the remaining test set-up was exactly the same as with "No Swirl", Figure 3.1. The procedure to obtain the mixing transfer function was also similar. The test utilized the same two stage transfer function approach to obtain the *MTF*. However, due to anomalies noticed in early velocity response measurements, a degree of freedom was added to the experiment. The hotwire holder and fuel injection blocks were indexed to include the theta component (θ) as a parameter in the test matrix. This allowed a more in-depth investigation of spatial effects that were suspected to explain some of the early observations. The revised experimental set-up is shown in Figure 3.9.

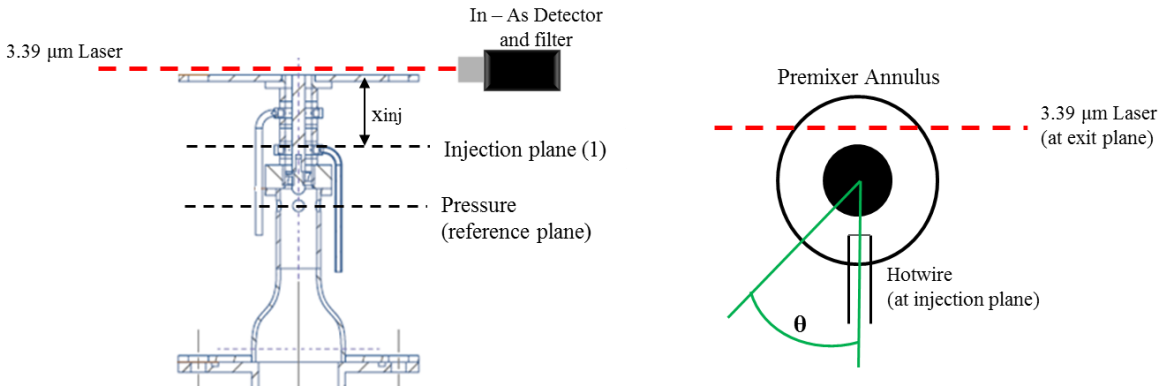

Figure 3.9. Schematic of the modified *MTF* measurement set up to include circumferential position (θ).

The velocity response was measured at three axial injection locations, three mean air flows, and six positions (θ) between 0 and 45 degrees. Circumferential measurements were limited to 45 degrees because the velocity field inside the premixer was assumed to be periodic about the eight swirl vanes. The test parameters for the velocity transfer function were:

- injection distance, x_{inj} (1.0625in, 2.0625in, 3.0625in)
- mean air flow (14.5, 17, 19.5) SCFM
- theta (0, 9, 18, 27, 36, 45) degrees

Unlike the "No Swirl" premixer, strong spatial discrepancies were observed in the various velocity response measurements. This effect is illustrated in Figure 3.10, where the velocity response was acquired at six theta positions at a single flow rate and axial position. This was a significant problem because one of the driving assumptions for this research was that the

acoustic disturbance was 1-D. At certain positions and frequencies, zero velocity fluctuations were observed, thus demonstrating strong localized spatial effects. At higher frequencies, deviations from the mean were as high as ±5dB. Similar results were also present in the phase measurement. Unfortunately, the rig was never designed to account for 2-D acoustic fields. In an attempt to retrieve useful data from this experiment, the velocity response for all six theta positions were averaged together to yield a single transfer function at each operating condition. This produced nine averaged velocity transfer functions. This was performed in an attempt to smooth out the spatial gradients, and to provide a better characterization of average velocity fluctuations over the entire injection plane. These averages were weighted by their corresponding coherence values to attempt to eliminate the inclusion of values that were a product of the signal noise. The result of this process can be seen in Figure 3.10, where the black line is the coherence weighted average for this operating condition.

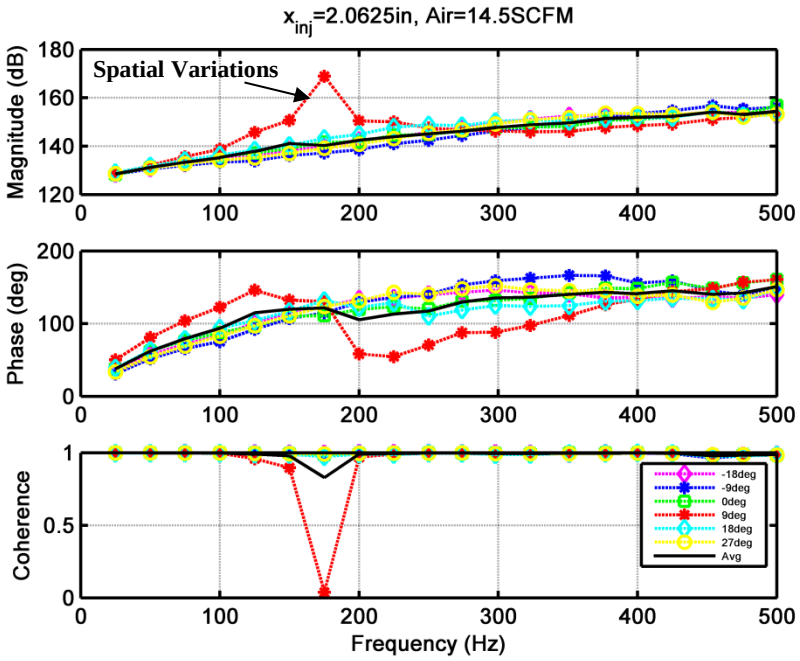

Figure 3.10. Measured velocity responses in the "Swirl" Premixer showing circumferential variations.

After the velocity responses were acquired at all of the predetermined test conditions, the fuel response was measured. The *MTF* was then produced by multiplying the two responses. However, unlike the "No Swirl" measurements, a single velocity transfer function, which was averaged over all theta positions, was insufficient in representing the response inside the

premixer. Therefore, each mixing response was obtained by multiplying the fuel transfer function by the velocity transfer function obtained for each specific axial location and mean velocity. The theta component was not considered in the velocity response because it was previously averaged out. This was required because the exact circumferential location of the fuel jets could not be described by a single point. The resulting test parameters for the fuel transfer functions were:

- injection distance, x_{inj} (1.0625in, 2.0625in, 3.0625in)
- mean air flow (14.5, 17, 19.5) SCFM
- theta (0, 9, 18, 27, 36, 45) degrees
- equivalence ratio (0.3, 0.5, 0.7)

These parameters were varied, and results were obtained at 107 test conditions. Similar to the observations previously obtained for the velocity response, as the orientation of the fuel block was rotated circumferentially, large variations were observed in the magnitude of the response. This is illustrated in Figure 3.11, where the *MTF* is plotted at six circumferential orientations. At higher frequencies, variations in the gain were measured to be as high as 10dB. These deviations prevented the gain of the system from being accurately described using a single value. Instead, the gain reported for this response was limited to the DC gain, which was defined as less than 125 Hz. Linear phase delay measurements were obtained for some of the tests. However, in some configurations the phase begins to deviate and can no longer be considered linear at higher frequencies, as seen in Figure 3.12. In general, the longer delay times demonstrated higher linearity than the shorter delay times. To provide the best approximation, the reported phase delay was limited to data collected below 250Hz.

It is important to note that the measurements maintained a high level of coherence. This ensured that the collected signals were linearly related and that there were no problems with the signal to noise ratio. This confirms that the responses measured were physical to the system, instead of a data acquisition error.

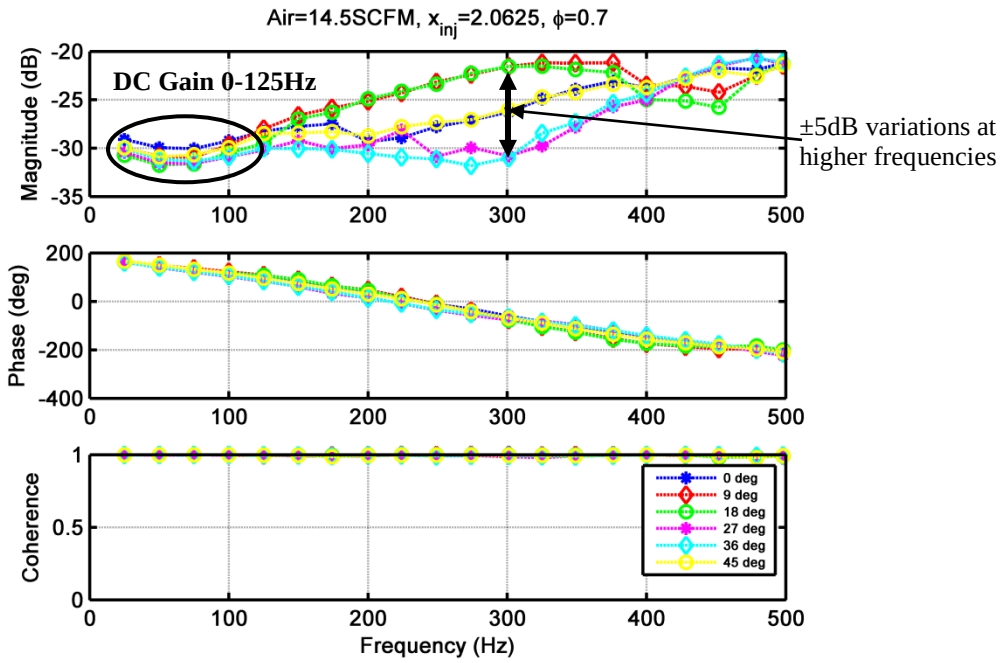

Figure 3.11. Measured mixing transfer function for the "Swirl" premixer showing a spatial dependence of injection location. The fuel injection block was rotated through 6 angles between 0 and 45 degrees.

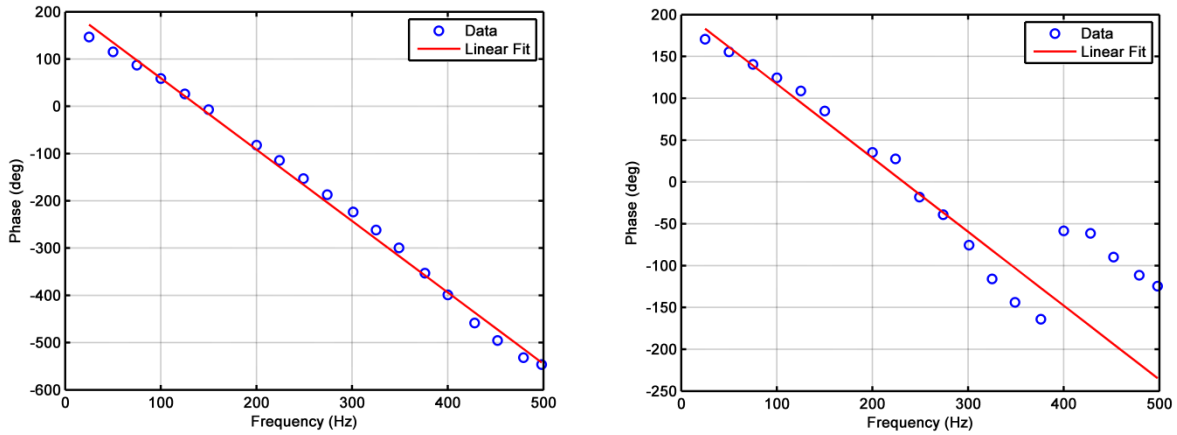

Figure 3.12. Phase delay measurements for the "Swirl" Premixer. (Left) representative phase response that remained linear. (Right) representative phase response that deviated from linear at higher frequencies.

Two adaptations to the experiment were made to attempt to remove the spatial effects from the *MTF* measurement. Both adaptations attempted to average the mixing response over a larger portion of the annulus to reduce the effect of acquiring localized extremes in the measurement test volume.

The first adaptation projected a laser sheet, created using a cylindrical lens, over approximately one-third of the exit annulus, as shown in Figure 3.13. The laser sheet was converged to a single point using a short focal length (f = 126mm) Bi-Convex lens. The detector was placed at the point of convergence and captured the entire transmitted signal. This measurement provided an average of the concentration over the covered area.

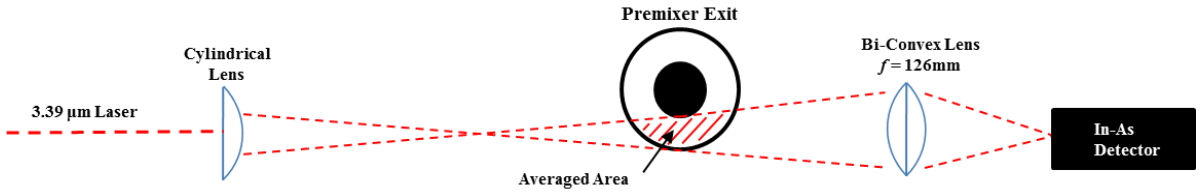

Figure 3.13. Schematic of the partial coverage laser sheet adaptation for concentration measurement.

The second modification to the measurement was similar to the first. The only difference was that the averaged area was approximately doubled by projecting the laser sheet over the entire annulus, as shown in Figure 3.14. The area shaded by the centerbody extender was the only area not accounted for in this measurement. The laser sheet was created using the same cylindrical lens, but it was collected and converged in a different manner. Instead of the previous approach, the laser was collected using a concave mirror. This mirror was slightly angled (not shown in schmematic) and projected the converging beam onto a front surface mirror. The beam was reflected off of the mirror and converged onto the infrared detector (beam was converging after the mirror, not shown). This method was necessary due to the lack of large diameter optics, suitable for infrared wavelengths, available to this experiment.

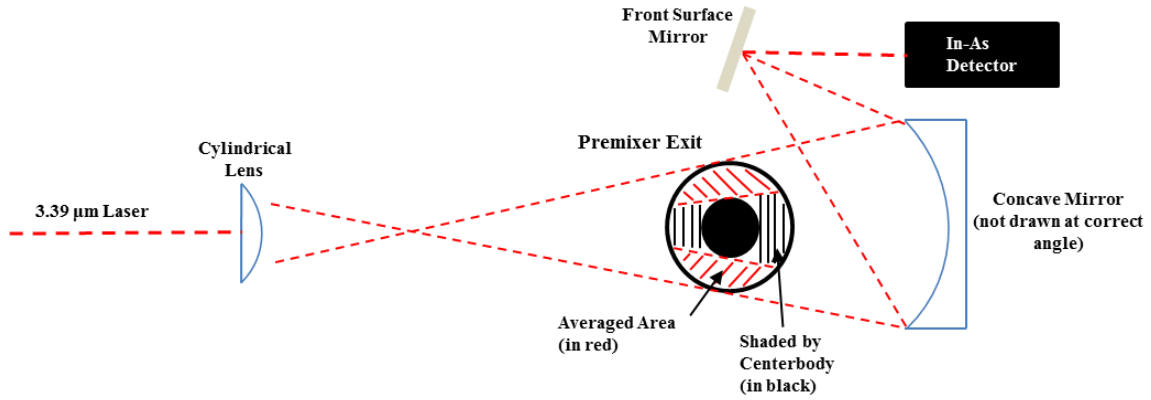

Figure 3.14. Schematic of the full coverage laser sheet adaptation for concentration measurement.

Both adaptations were tested at multiple conditions. However, the mixing response continued to demonstrate large variability, in both magnitdue and phase, as a function of the placement and orientation of the fuel injector block.

3.2.2 Results of Single Injection Tests

Phase Delay

The slope of the phase vs. frequency, or phase delay, was collected from the *MTF* for all test conditions. However, due to the deviations from linear observed in the majority of the responses collected, the phase delay results were limited to data collected below 250Hz.

The phase delay results were compared against the convective time delay. The results of this correlation are shown in Figure 3.15, along with the 95% confidence bounds and the theoretically predicted values. Similar to the "No Swirl" conditions, the measured phase delay was in excellent agreement with the values predicted from the "Time Delay Model". The data was highly correlated and had an R^2 value of 0.909. From this analysis, the low frequency phase delay was considered repeatable and predictable. However, no conclusions could be drawn from frequencies higher than 250Hz.

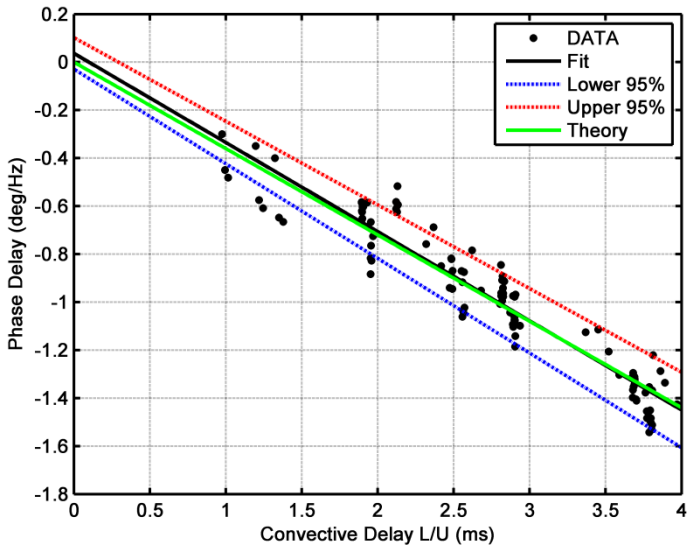

Figure 3.15. Experimental data showing effects of convective delay on phase delay for single injection locations in the "Swirl" premixer. Experimental data are plotted with a linear best fit, 95% confidence bounds, and theoretically predicted values. Results are limited to less than 250Hz.

Gain Results

The gain of the *MTF* was collected for each test condition. The reported gain was limited to 125Hz due to strong variations at higher frequencies. At these higher frequencies, a single gain value was inadequate at characterizing the response of the system. The characterization of the gain of the *MTF* for the "Swirl" premixer followed the same steps as outlined in the results section of the "No Swirl" premixer. Therefore, only the results and a brief discussion will be presented here.

The results from the 2nd order regression analysis yielded φ^2 as the only significant independent variable for the DC gain. The identification of this significant variable suggests that gain is predominantly concentration driven, with strong secondary effects from momentum ratio/jet penetration distance and mixing. For a fixed geometry and operating pressure, all of these secondary effects are related to φ^2. After identifying the significant variable, a correlation was created between this parameter and the gain. The experimental data are presented in Figure 3.16, along with the 95% confidence bounds. The correlation had an adjusted R^2 value of 0.81, with narrow confidence bands. It suggests that the DC gain of the mixing response was well characterized by this parameter. However, no characterization was possible for frequencies higher than 125Hz.

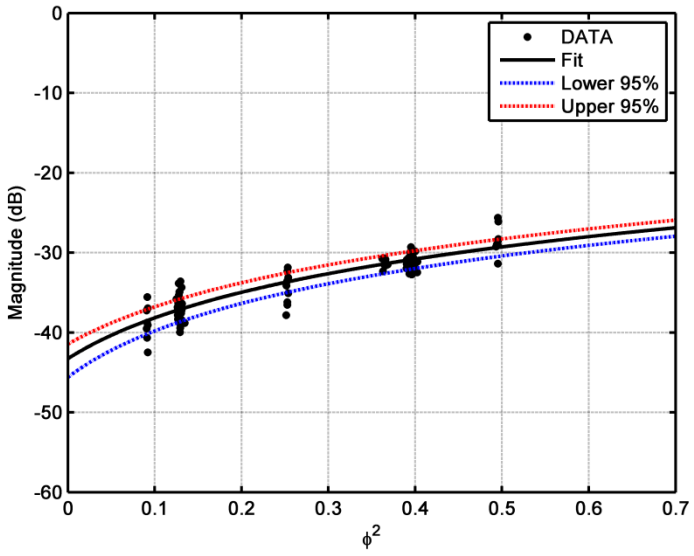

Figure 3.16. Experimental data of the gain of the mixing response in the "Swirl" premixer. Experimental data are plotted with a best fit and 95% confidence bounds. Results are limited to DC value (0-125Hz).

3.2.3 Mixing Transfer Function Measurement for Multiple Injections

The mixing response of two simultaneous fuel injections was measured to investigate the application of multiple injections as a technique to dampen FAR fluctuations. From the results previously obtained from the velocity and single injection mixing response, it was discovered that the spatial location of the fuels jets in the velocity field had a strong influence on the overall *MTF*. The following items address the limitations that were encountered from these spatial effects and how they affect the mixing response for two injections:

- One velocity transfer function, which was averaged in the circumferential direction, could not be used to accurately describe the velocity at the injection planes for both fuel injections simultaneously. In an attempt to produce the best representation of the velocity at both injection planes, all the velocity transfer functions that were measured were averaged over all the test conditions outlined in the previous section. Again, the experiment was not equipped to handle spatial variations in the velocity response, which led to this compromise.
- The phase delay was also observed to deviate from linear at higher frequencies. This limited the phase delay characterization to 250Hz. This uncertainly in phase makes the location of FAR damping extremely difficult to predict in a two injection system.
- The gain of the system had a strong dependence on the physical location of the fuel jets. As the jets penetrated into the variable velocity field, strong mixing gradients were created. This result was more prominent at frequencies above 125Hz, which produced deviations as high as 10dB. As a result, the characterization of the single injection mixing response magnitude was limited to the DC gain, which was defined as less than 125Hz. These variations produce conditions that would limit the amount of FAR damping achievable in a two injection system. For example, if one injection location has a high gain and the second injection has a low gain, the response from the first injection will dominate the system. While the responses do not have to be identical, they do need to be of the same order of magnitude to produce sufficient destructive interference between the two waves. The measured results suggest that this effect could be overcome by supplying unequal fuel flow rates to each injection location. However, this additional degree of freedom was not considered in the current investigation.

- The combination of the uncertainty in the phase and gain measurements severely handicapped the characterization of the mixing response above 125Hz. However, no test conditions were feasible to demonstrate FAR damping in this low frequency range. To lower the frequency of FAR damping, the convective delay between the fuel injection locations has to be increased. This was not possible for two reasons. First, the maximum separation distance could not be increased because it was limited by the physical size of the modular premixer. Second, the air and fuel flow rates could not be lowered enough to meet the minimum flow rate requirement to decouple the fuel supply, while maintaining lean equivalence ratios.
- To provide a best guess at the predicted response from two injections using the low frequency characterization, the models were extrapolated to 500Hz (see below). This was expected to be a poor approximation, but it was necessary due to the uncertainties in the data.

With all the limitations in mind, determining the response from two injections was performed at multiple test conditions. The number of operating conditions was limited due to the vast number of spatial combinations that were required to investigate a single condition. The first injection block, which is the longer injection distance, was fixed in place, and the second block was rotated through the five theta positions. The mixing responses for two representative test conditions are shown in Figure 3.17 and Figure 3.18.

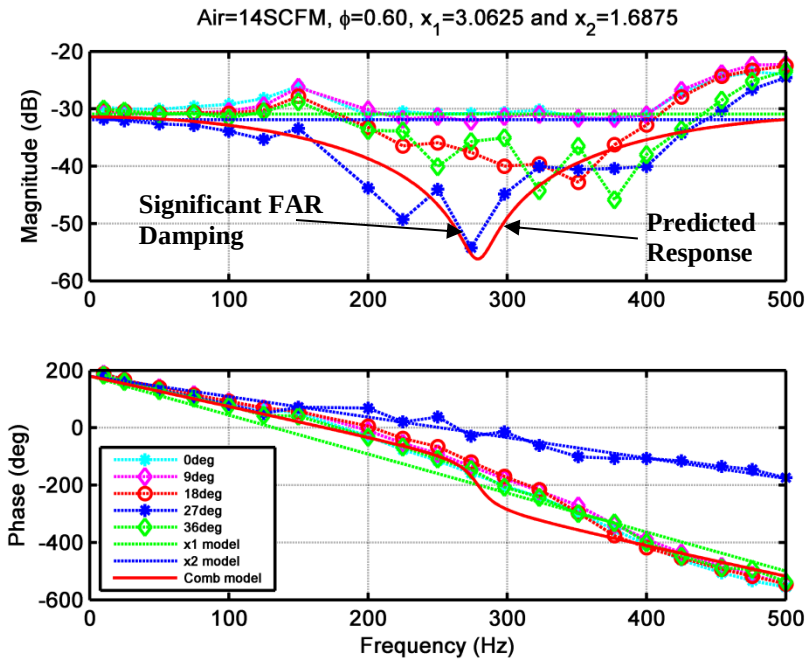

Figure 3.17. Measured mixing response for two injections in the "Swirl" premixer showing dependence of injection orientation. The second block was rotated through five orientations. One configuration demonstrated FAR damping.

Referring to Figure 3.17, the mixing response only demonstrated significant FAR damping in one orientation (27 degrees advanced). Interestingly, the location of the FAR damping was accurately predicted using the extrapolated phase delay. This suggests that this was the only orientation where the magnitudes were similarly matched. Two other responses (18 and 36 degrees advanced) demonstrated some decrease in amplitude, but it was unclear if this was attributed to the combined response from the two injection locations.

At a second operation condition, Figure 3.18, three orientations (0, 9, and 36 degrees advanced) demonstrated FAR damping. However, the location varied for each response and was not accurately predicted by the extrapolated phase delay. Two responses demonstrated no measureable decrease in the amplitude of the mixing response over the tested frequency range.

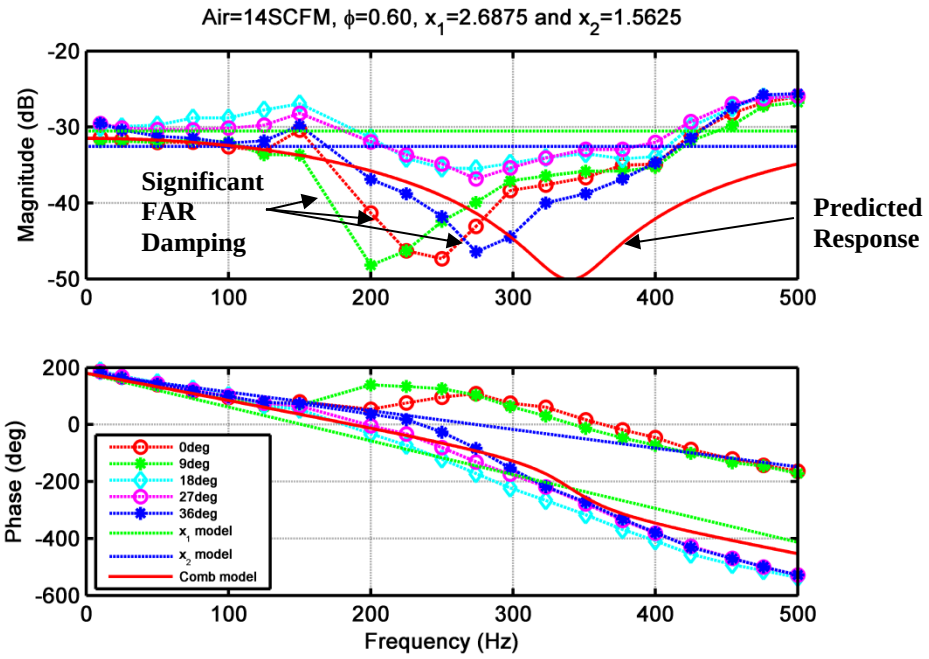

Figure 3.18. Measured mixing response at a second operating condition for two injections in the "Swirl" premixer showing dependence of injection orientation. The second injection block was rotated through five orientations. Three configurations demonstrated FAR damping.

3.2.4 Summary and Discussion of "Swirl" Mixing

The *MTF* for a single fuel injector was measured for a total of 107 tests varying mean flow rate, injection distance, theta position, and mean equivalence ratio. Strong unpredictable results were observed in both the phase and gain of the response as a function of theta position and mean flow. Due to these variations, the reported phase delay was limited to 250Hz, above which the phase could no longer be considered linear. Also, the reported gain was limited to only the DC gain, which was defined as less than 125Hz. Above this value, the gain could no longer be accurately described by a single value.

Examination of the velocity response inside of the premixer at multiple axial and circumferential positions indicated that the resulting velocity waves were not 1-D. Spatial discrepancies in this response signify that when the acoustic wave passed through the swirl vanes, a higher order response was produced. This higher order velocity response translates into the same phenomenon in the mixing response. As the fuel jets penetrate into the annulus, the jets cross

locations of localized extremes in the acoustic velocity field. This produces mixing responses that are spatially dependent on the placement of the fuel jet in relation to the resulting velocity field. Unfortunately, the experimental apparatus and diagnostics were not equipped to accurately measure the higher order velocity and concentration field. Using the reported values, a model was built for the single injection mixing response. However, the resulting model was only valid for low frequency.

In an attempt to average the mixing response over the entire premixer annulus, adaptations were made to the concentration measurement. A large portion of the annulus was covered by a laser sheet that was then converged back to the detector, thus averaging the concentration over the measurement volume. However, the mixing response continued to demonstrate the same spatial dependence. This suggests that the response of the system was not linear and could not be characterized by the mean. Similar averaging techniques were performed to the velocity transfer function. The velocity response was measured at 6 theta positions and coherence weighted averaged to provide the best approximation of the fuel/air interface. Again, due to the large spatial gradients, the velocity response was not well approximated by the mean.

Even though the mixing response could not be characterized for higher frequencies, the mixing response of two simultaneous fuel injections was measured to investigate the application of multiple injections as a technique to dampen FAR oscillations. The results were inconclusive. Some orientations produced FAR damping, while others did not. No pattern emerged during testing to indicate which configurations would produce FAR damping. This was expected due to the uncertainties measured during single injection tests.

The results for this series of testing indicate the possibility of successful implementation of a multiple injection technique for FAR damping in an annular swirl premixer. However, due to the lack of a model that could accurately characterize this system, the application of this technique is limited in a practical setting.

Chapter 4: Phase II: Hot Flow and Passive Control

This chapter is focused on the implementation and validation of using multiple injections to dampen FAR fluctuations and suppress the onset of combustion driven instabilities in a lean premixed combustor.

The first section details the procedures used to identify and characterize the natural resonant modes of the combustor. For the successful application of multiple injections, the frequencies of the driving instability must be known prior to the assembly of the premixer. This section first identifies the frequencies most likely to sustain an instability by measuring the acoustic transfer function, and then it covers measuring the resonant frequencies and amplitudes of the unstable combustor in numerous configurations. Tests were performed with both the "Swirl" and "No Swirl" premixer while varying fuel type, injection location, mean flow rate, and equivalence ratio. Each section concludes with a brief summary of the results along with a discussion of possible driving mechanisms.

The second section uses the results obtained in the first section to configure the premixer to "target" the known instability frequency. The term "target" will be used to refer to the premixer configuration that provides the maximum FAR damping at the dominant frequency in an attempt to suppress the instability by eliminating effects from FAR fluctuations. Due to the limited results in the *MTF* measurements, the primary investigation will focus on the implementation of this passive control technique in the "No Swirl" configuration. The results from these experiments are used to validate the application of a "targeted" two-point axial injection passive control strategy.

The final section will conclude the experimental research by commenting on the results obtained from the application of FAR damping in the "Swirl" premixer. Due to the unpredictable nature of the mixing response, these results could not be used to validate the current passive control strategy, yet they do provide promising evidence suggesting the possibly of successful implementation.

4.1 Combustor Characterization

This section details the procedures used to measure and characterize the resonant modes of the combustor. The characterization will examine the effects of fuel type, convective delay, and overall power level. The accurate prediction of the unstable frequencies is important for the application of FAR damping using two injections. With only two injections, the proposed method is only effective at a narrow range of frequencies. In terms of control, only the magnitude and frequency of the instability are important for this approach. No results will be presented regarding the phase relation between the pressure and heat release rate fluctuations.

The first sub-section details the measurement of the acoustic transfer function of the rig operating in a stable premixed mode. This provides a general acoustic signature of the rig, identifying the frequencies that are most likely to support a combustion driven instability. These frequencies are represented by an increase in gain between the acoustic pressure and the dynamic heat release rate, along with a phase change at the natural or resonant frequency. The measurement technique is then presented for identifying the dominant resonant frequencies and corresponding amplitudes of the pressure and heat release rate when operated with a single fuel injection.

The following sub-section presents the dominant resonant frequencies and corresponding amplitudes for the "Swirl" and "No Swirl" configurations. The "Swirl" premixer was studied extensively with natural gas and hydrogen. However, the "No Swirl" measurements were limited to hydrogen because an accurate characterization could not be performed with natural gas. Without the added flame anchoring and mixing benefits from the swirling flow, the natural gas flame zone was too large to be considered a compact source.

4.1.1 Acoustic Transfer Function Measurement and Resonant Modes

Acoustic Transfer Function Measurement

The acoustic transfer function of the combustor rig was measured using a similar procedure to the one outlined by Black [52]. The combustor was operated in a premixed mode of operation at a stable operating condition. The resulting premixed flame provided the excitation to the system.

The turbulent flame acted as a broad band energy source exciting the combustor. The power of the flame was increased to the maximum allowable level before the combustor demonstrated any nonlinear effects. This boundary was identifiable by a strong ringing sound, i.e. "singing" flame. Increasing the flame to this point provided the maximum measurable signal strength. The resulting dynamic pressure and heat release rate were measured using the previously described techniques. The signals were acquired for 25 seconds, and the vector averaged FRF was calculated between the signals. The FRF was normalized by the mean pressure and power level of the flame yielding the normalized acoustic transfer function ($\overline{ATF}$), shown in eq. 4.1. For this measurement, the pressure was used in lieu of the velocity for two reasons. First, the pressure was more convenient to measure because it was shielded from the flame zone, and only the frequencies of amplification were of interest. If this measurement was desired for modeling efforts, the dynamic velocity at the flame zone would be required to accurately measure the phase relationship.

$$\overline{ATF}(f) = \frac{p'(f)/\bar{p}}{q'(f)/\bar{q}} \tag{4.1}$$

The acoustic transfer function was measured for three combustor configurations. The "Swirl" premixer operated on natural gas and hydrogen, and the "No Swirl" premixer operated on hydrogen. The acoustic transfer for the "Swirl" combustor with natural gas is shown in Figure 4.1.

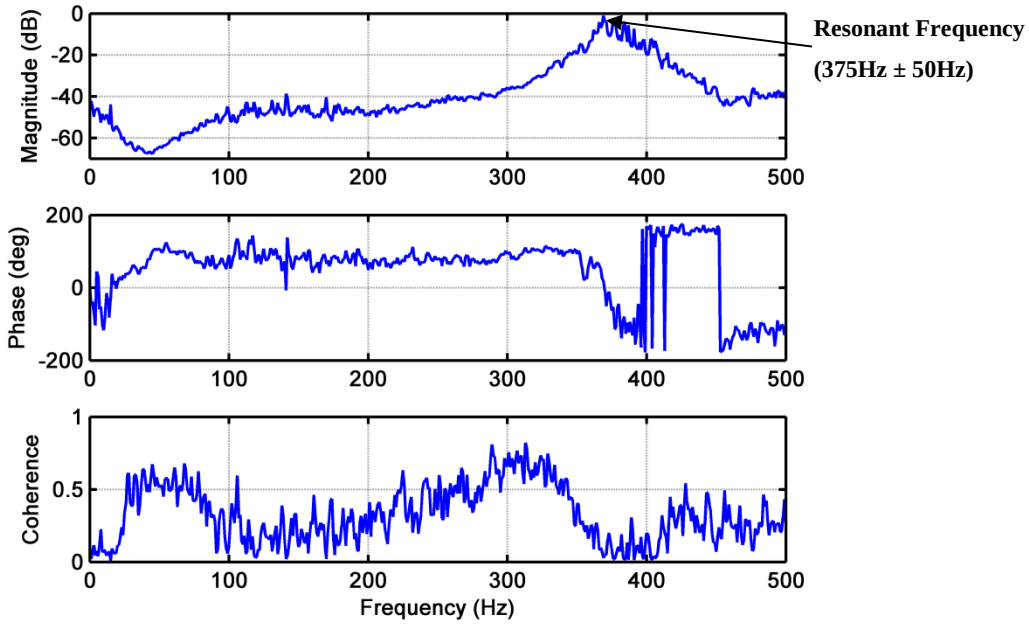

Figure 4.1. Measured acoustic transfer function for the premixed combustor operating on natural gas, normalized with mean conditions. Combustors demonstrated a 2nd order behavior.

All combustors demonstrated a 2nd order response. This characteristic was also observed by Ranalli [47] and Black [52]. The center or resonant frequency was identified for each combustor, along with the range of frequencies that demonstrated an increase in gain. The absolute magnitude of the response was not important, only the range of frequencies that would amplify the interaction between the acoustics and heat release rate of the flame. It is important to note that the coherence was prohibitively low to apply the measured responses to any modeling efforts. This was the result of inadequate signal strength across the frequency spectrum. Unfortunately, the system would become unstable before the flame energy was sufficient to produce a high signal to noise ratio. The center frequency, along with the upper and lower frequencies that had a significant increase in gain for each configuration are presented in Table 4.1.

Table 4.1. Resonant mode of combustors, measured from *ATF*.

Premixer	Fuel	Center (Hz)	Lower Limit (Hz)	Upper Limit (Hz)
Swirl	Natural Gas	375	325	425
Swirl	Hydrogen	350	325	410
No Swirl	Hydrogen	325	300	410

Resonant Mode Measurement

The resonant frequencies and peak amplitudes were measured for the "Swirl" and "No Swirl" combustor operating in multiple configurations. The results from these measurements were used to provide a characterization of the unstable behavior of the combustors. This section details the measurement set-up and procedure.

The combustor was assembled with one of two premixer configurations, and the operating parameters were set. The testing parameters were fuel type (natural gas or hydrogen), equivalence ratio, injection distance, mean flow rate, and fuel injector block (8-18T and 12-18T). The combustor was preheated until a steady state temperature was reached, typically around 15 minutes. The combustor was turned off and re-ignited after preheat to eliminate hysteresis effects. If the combustor was not extinguished between each test, a previously unstable condition could artificially drive the next test condition unstable. The dynamic pressure and heat release rate were recorded at each operating condition for 25 seconds. The data was vector averaged and the resulting frequency and amplitudes for each test condition were recorded. The rms amplitudes will typically be reported here as a percentage of their respective mean values. As before, the mean power level of the flame was estimated using a complete combustion model and the LHV of the fuel. The rms pressure was scaled using the mean combustor pressure, which was atmospheric for all tests in this study. The atmospheric pressure was obtained from the local airport reading, which is typically about 95kPa for Blacksburg, VA.

At unstable configurations, the combustor demonstrated large pressure and heat release rate fluctuations at a given frequency. This frequency is the dominant unstable mode of the combustor, and is commonly referred to as the resonant mode. The autospectrums of a typical unstable test condition are shown in Figure 4.2. Peak magnitudes with their corresponding frequency are reported for dynamic pressure and heat release rate.

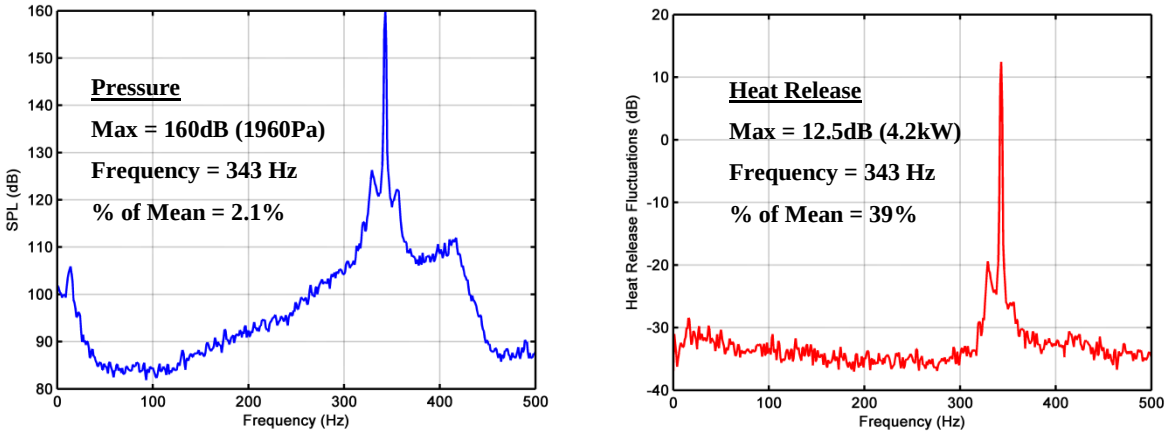

Figure 4.2. Pressure and heat release rate auto spectrums for an unstable test condition.

At stable configurations, little to no oscillations were observable in the pressure and heat release rate signals. The autospectrums of a typical stable condition are shown in Figure 4.3. The boundary between stable and unstable was defined as a pressure fluctuation greater than 0.5% of mean. This threshold was defined for two reasons. First, below this level, the resulting heat release rate fluctuations were typically less than 5%. The second reason was based on observations of the sound level of the combustor during operation. During operation, conditions below this level were generally observed to be quiet and steady with constant normal combustion noise. Above this level, the combustor would emit strong sound waves accompanied by noticeable vibrations in the experimental apparatus. This threshold will be used throughout the remainder of this project to define stability.

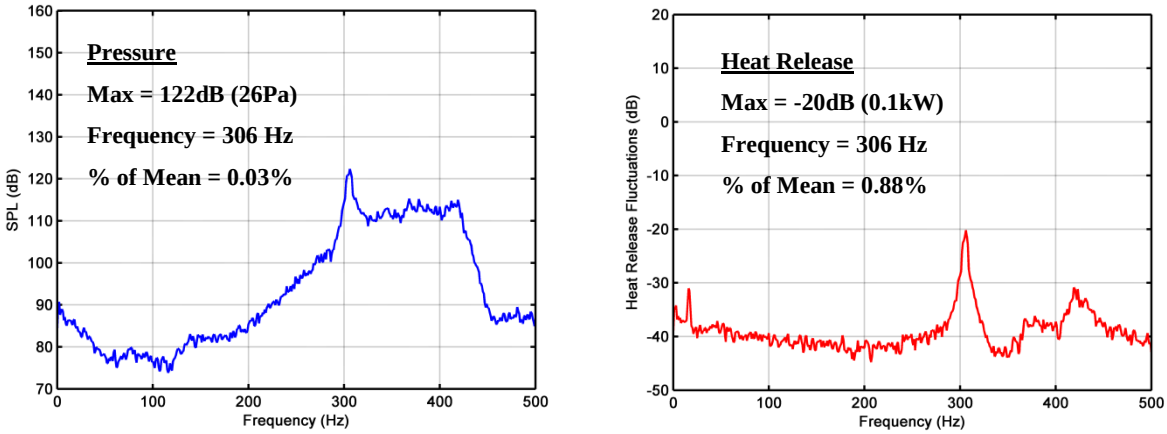

Figure 4.3. Pressure and heat release rate auto spectrums for a stable test condition.

4.1.2 Swirl Combustor Characterization

The peak amplitudes, along with the dominant unstable frequencies were recorded for the "Swirl" combustor operated at numerous configurations. This was performed to provide a characterization of the dominant resonant modes of the combustor and investigate the dependence on fuel type, mixing length (delay), power level, and fuel injector style. The test parameters for the natural gas and hydrogen tests are shown below. The test matrices are dissimilar because the dominant resonant mode for the hydrogen combustor demonstrated to be highly sensitive to equivalence ratio.

Table 4.2. Test parameters for natural gas operation.

Natural Gas	
Air Flow:	[13, 15, 17, 19] SCFM
Injection distance:	[1.1875, 1.8125, 2.4375, 3.0625, 1.4375, 2.5625] in
Fuel Injector:	12-18T and 8-18T
Equivalence Ratio:	0.6
Tests:	48

Table 4.3. Test parameters for hydrogen operation.

Hydrogen	
Air Flow:	[15, 19] SCFM
Injection distance:	[1.1875, 1.8125, 2.4375, 3.0625] in
Fuel Injector:	12-18T and 8-18T
Equivalence Ratio:	[0.25 0.28 0.31 0.34 0.37]
Tests:	80

Experimental results obtained from the natural gas and hydrogen tests are shown in Figure 4.4 and Figure 4.5, respectively. Both combustors demonstrated a frequency switching behavior, where the dominant frequency mode would jump between two different values. The combustor would lock to one or the other mode depending on the test configuration. The preferred frequency was extremely difficult to predict and was a function of all parameters tested. This behavior was also observed by Richards, et. al [48] in his experimental lean premixed combustor.

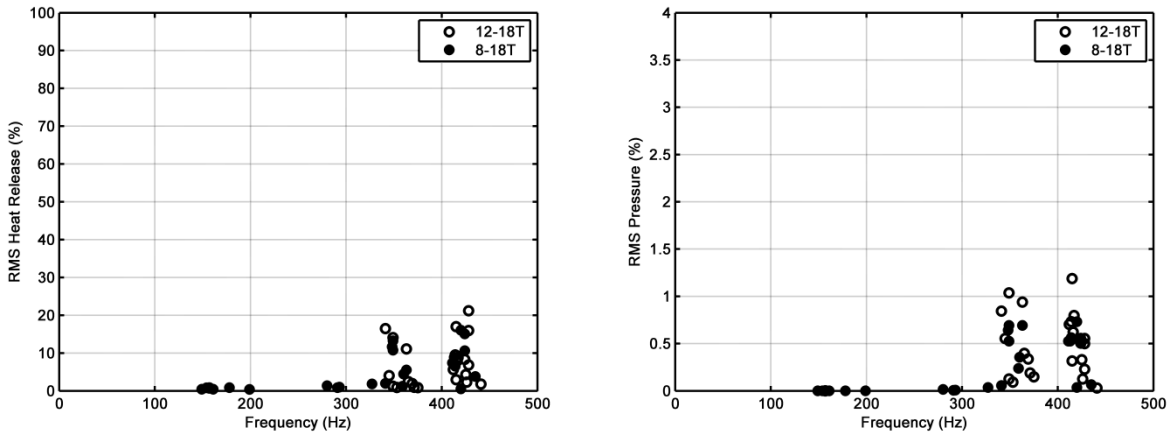

Figure 4.4 Plot of resonant frequencies and amplitudes of heat release rate (left) and pressure (right) fluctuations in a natural gas fueled "Swirl" combustor. Data shows the combustor had multiple unstable modes.

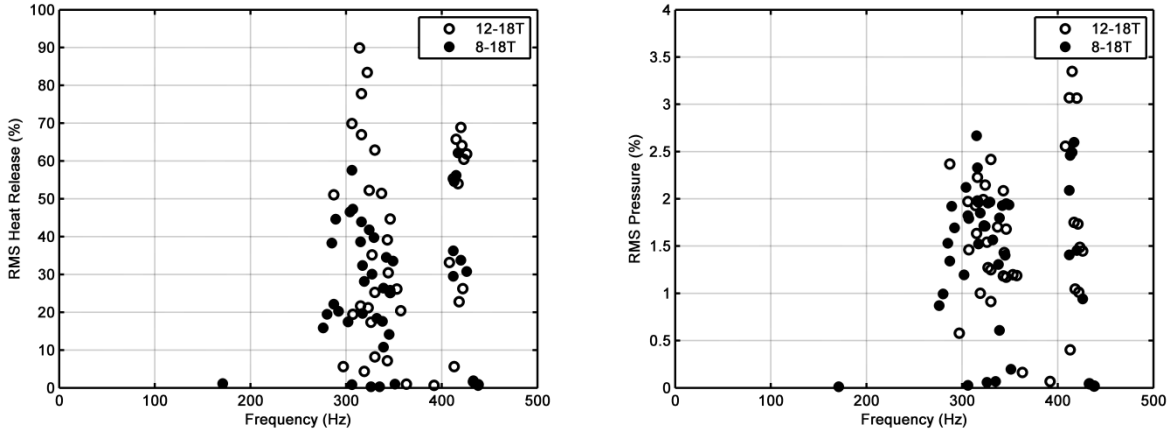

Figure 4.5. Plot of resonant frequencies and amplitudes of heat release rate (left) and pressure (right) fluctuations in a hydrogen fueled "Swirl" combustor. Data shows the combustor had multiple unstable modes

The two frequency modes were approximately 350 and 425Hz for natural gas and 325 and 415Hz for hydrogen. This switching behavior reiterates the difficulty in designing a stable single injection premixer. Using the time lag theory already developed, it is critical to know the phase between the fuel disturbance and the resulting pressure fluctuation to achieve stability. If stability was trying to be achieved by adjusting the phase, using the convective delay, a jump in frequency would create a new set of conditions that, instead of becoming stable, drive the system unstable at a different frequency. This was apparent in the hydrogen tests. Out of 80 conditions tested, where the convective delay was varied between 1ms and 4ms, only 9 conditions were

stable. It was also observed that much stronger instabilities were present in the hydrogen combustor. This makes hydrogen a stronger candidate for testing the proposed suppression technique.

It is important to draw attention to the magnitudes of rms heat release rate measured during highly unstable conditions during the hydrogen tests. As can been seen, rms values are estimated to be as high as 90% of the total energy available from the fuel input. These values correspond with peak to peak fluctuations that are higher than a total extinction and re-ignition of the flame. This is a physical impossibility. A couple of contributing factors are responsible for these excessive magnitudes. First, because the fuel manifold was not completely isolated from the acoustic disturbances, large pressure fluctuations produce small fuel mass flow fluctuations (refer to Section 2.1.3 for more detailed explanation), which according to Lee and Santavicca [70] artificially inflate chemiluminescence intensity. This increase in intensity, which was not accounted for by actively measuring equivalence ratio fluctuations, over-exaggerates heat release rate. Additionally, during these events, large equivalence ratio fluctuations are produced inside the mixing chamber that are no longer accurately characterized by the linear calibration used to describe heat release rate using OH* chemiluminescence (refer to Section 2.2.2). Fluctuations outside of this linear regime are known to follow an exponential increase in intensity, which are drastically under predicted using the linear approximation. These two dominate factors, along with other contributions from large unsteady strain on the flame and variations in radiation and heat transfer, yield heat release measurements that are no longer representative. It is important to emphasize that these errors only exist during very intense (non-linear) instabilities and, therefore, do not affect the heat release rate measurements at other conditions.

To investigate the dominant instability driving mechanism, the ratios of convective delays (τ) to acoustic periods ($T=1/f$), where f is the periodic frequency of the resonant interaction, were compared against the measured unstable amplitudes, commonly referred to as τf plots. The τ used to for this analysis was the mean convected delay between the fuel injection location and the dump plane of the premixer. As developed in the Section 1.2.4, if the dominant instability mechanism is mixing driven, the unstable modes should lie in τf bands. The τf plots for natural gas and hydrogen are shown in Figure 4.6 and Figure 4.7.

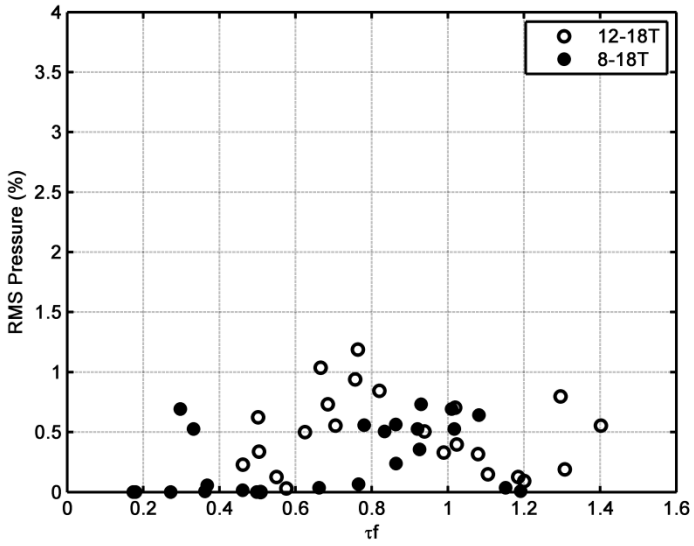

Figure 4.6. Experimental τf plot for the natural gas fueled "Swirl" combustor.

Typically, this analysis uses the convective delay from the fuel injection location to the center of heat release of the flame, which is measured using local chemiluminescence measurements. This was not available in this experiment, and therefore, a measurable parameter was chosen. This approach remains valid, even if the center of the flame is unknown, as long as the overall size of the flame remains fairly constant at all tested conditions. This was the observed behavior for the hydrogen flame. However, the size of the natural gas flame varied greatly depending on test condition (mean flow and equivalence ratio). This natural gas flame size variation produced a source of error in the current analysis and was kept in mind when attempting to draw conclusions.

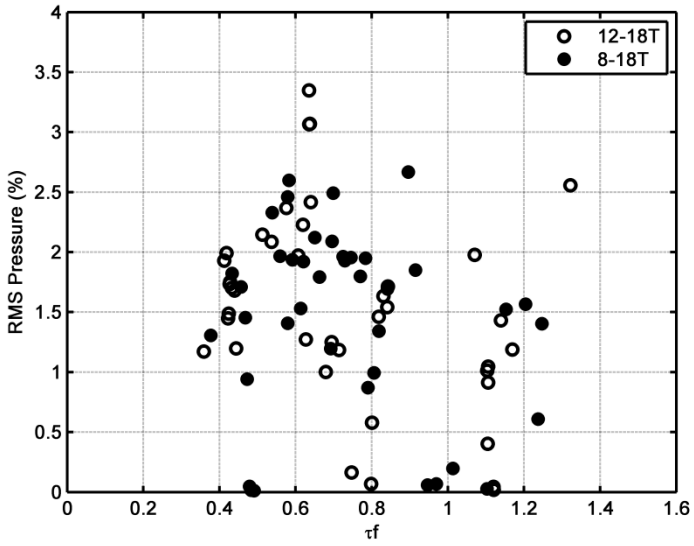

Figure 4.7. Experimental *τf* plot for the hydrogen fueled "Swirl" combustor.

It can be seen from the data that unstable modes exist over the entire range of *τf*'s tested. This was observed in both the natural gas (variable flame size) and hydrogen (constant flame size) combustion experiments. This suggests that other instability mechanisms are present. This is not an unexpected result for practical combustors, where it is typical to have multiple driving mechanisms present. Even so, this result does not negate the current passive suppression technique. As mentioned in the background, the elimination of FAR oscillations can decrease or prevent a resonant mode that is predominantly driven by another mechanism.

4.1.3 No Swirl Combustor Characterization

An investigation of the resonant modes of combustion was also performed with the combustor configured with the "No Swirl" premixer. This configuration was only tested with hydrogen as the fuel. Without the increase in flame anchoring and mixing produced by the swirling flow, the resulting natural gas flame could not be considered a compact source, i.e. the flame length was much less than the acoustic wave length. Additionally, due to the large flame zone, no conditions tested supported an unstable resonant interaction. With no unstable modes present, the application of the proposed passive control technique was unnecessary and required no investigation.

The “No Swirl” configuration was tested at a range of convective time delays, mean flow rates, and mean equivalence ratios. The experimental results are shown in Figure 4.8. This configuration only demonstrated one dominant frequency mode, centered at approximately 310Hz. One outlier was measured at 410Hz. This suggests that a higher unstable mode was present but was difficult to excite with this configuration.

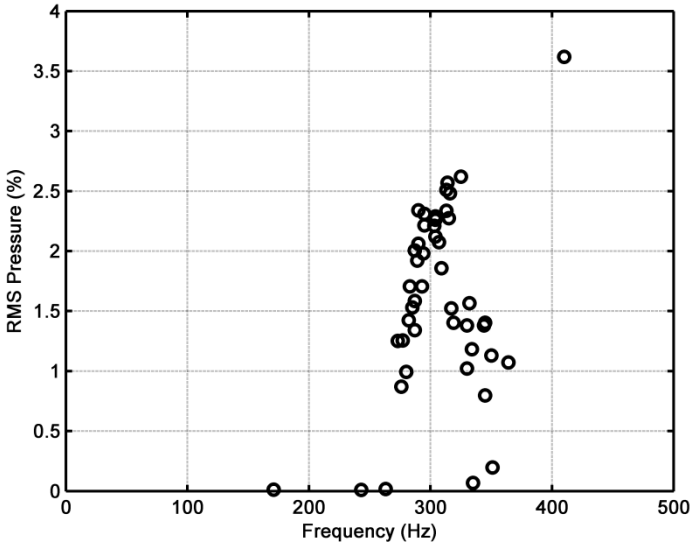

Figure 4.8. Experimental data showing resonant frequencies and amplitudes of pressure fluctuations for the hydrogen fueled "No Swirl" combustor.

Of the 46 conditions tested, only 5 were stable. This was a similar percentage to the previously tested “Swirl” combustor. Again, this demonstrates the difficulty in finding stable operating conditions for a single fuel injection location. However, the high percentage of unstable conditions is favorable to the implementation of the proposed passive control strategy.

The resulting τf plot for the “No Swirl” combustor is shown in Figure 4.9. Unlike the “Swirl” combustor, the unstable modes lie in two distinct τf bands. This suggests that FAR fluctuations are the dominant driving mechanism for this configuration. The experimentally determined stability boundaries were found to be $0.4 < \tau f < 0.75$ and $0.95 < \tau f < 1.15$. Interestingly, the range of the first τf band was almost identical to the range measured by Richards et. al.[48], which was approximately $0.45 < \tau f < 0.8$ for his experimental set-up. There was no reason to expect this result, but it may be explained by a similarity in acoustic boundary conditions between the experiments.

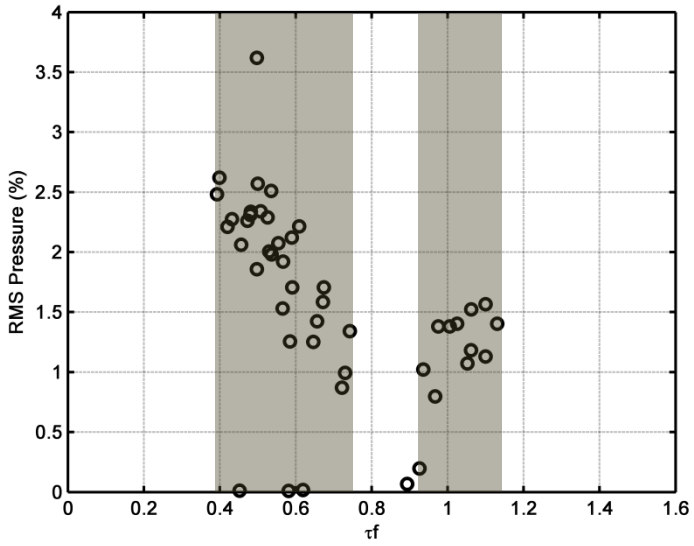

Figure 4.9. Experimental *τf* plot for the hydrogen fueled "No Swirl" combustor showing the measured stability boundaries.

4.1.4 Summary of Characterizations

Swirl Combustor

The combustor configured with the "Swirl" premixer was tested at a large range of operating conditions with hydrogen and natural gas. Two distinct dominant resonant modes were found in each combustor. Depending on the conditions, the combustor would jump between the two different frequencies. The preferred mode was extremely difficult to predict and appeared to be a function of every parameter tested. The existence of two dominant unstable modes complicates the application of the proposed passive control technique due to the limited range of frequencies that are controllable using only two injections.

Examination of the resonant modes against their *τf* values suggested that more than one dominant instability mechanism was present in the combustor. Multiple mechanisms are common in practical combustor systems and do not negate the current approach. However, with multiple mechanisms available to drive the system, validating the current control technique is more difficult.

For the two reasons listed above, and the uncertainty in the *MTF* measurements, the "Swirl" combustor will not be used to validate the passive control technique. While this configuration will not be used to validate the theory, it was investigated to evaluate the effectiveness of the passive control technique in a realistic premixer design.

No Swirl Combustor

The combustor configured with the "No Swirl" premixer was tested at a large range of operating conditions with hydrogen. Hydrogen was the only fuel tested because it provided a compact flame zone without the presence of swirl. The combustor was found to have a single dominant unstable mode at approximately 310 ±30Hz and experienced no frequency switching behavior.

Examination of the τf plot revealed that all unstable modes lied in two distinct τf bands ($0.4 < \tau f < 0.75$ and $0.95 < \tau f < 1.15$). This suggests that the combustion instabilities are predominantly mixing driven, thus making this configuration an excellent candidate for validating the proposed passive control technique.

4.2 Multiple Injection Implementation and Validation

This section details the application of a two-axial-point injection scheme to passively suppress combustion driven instabilities using FAR damping. The results obtained from these experiments are intended to validate the proposed control technique. The validation experiment was performed with the "No Swirl" premixer using hydrogen as the fuel.

The "No Swirl" configuration was chosen for the following reasons:

- This configuration produced predictable and repeatable *MTF's* that were validated to accurately predict FAR damping using two injections.
- The combustor demonstrated only one dominant unstable mode, approximately 310Hz.
- The dominant instability mechanism was identified to be mixing driven.

These reasons are all extremely important to confidently prove or disprove the proposed control technique as a method to dampen FAR fluctuations and suppress the onset of an unstable event by using two axial injections.

Hydrogen was the preferred testing fuel for the following reasons:

- Hydrogen combustion produced a small compact flame zone, even in the "No Swirl" combustor. This was required to satisfy the "compact source" and plane wave assumption. Furthermore, natural gas combustion in this configuration was unable to excite any unstable modes due to the extended flame zone. This result made it impossible to validate a passive control strategy in this configuration.
- Hydrogen's smaller flame zone, even at atmospheric conditions, better represents the flame zones produced in high temperature and pressure gas turbine combustors.
- In all cases tested, hydrogen produced more unstable operating conditions. This aids in the validation of this technique.
- Even though it has not been expressed in detail, the stable operation of a lean premixed hydrogen combustor was the ultimate goal of the project.

The first sub-section outlines the implementation procedure to apply the proposed technique. It steps through the process of identifying and measuring the amplitudes of the instability and configuring the premixer. This is done in two parts. The first part details how to configure the premixer to provide the maximum FAR damping at the measured unstable modes of the combustor. The goal of this "targeted" configuration is to suppress the dominant instability mechanism (which is mixing driven in the "No Swirl" combustor) to produce a stable combustor. The second part intentionally configures the premixer incorrectly, which is referred to as "un-targeted". These tests were performed to demonstrate the importance of accurately predicting the *MTF*. Select examples are shown throughout to illustrate each process.

The second sub-section presents the results from applying the proposed control strategy in the "No Swirl" lean premixed combustor. The amplitudes of the instability are given before and after implementation, along with tables summarizing the number of stable tests. These experiments provide a measure of effectiveness of the passive control strategy.

The two-point axial injection strategy was also applied to the "Swirl" premixer. This was done to investigate the application of the proposed technique in the full geometry. However, due to

the large uncertainties obtained in each prior phase of testing, this configuration could not be used to validate the proposed control strategy. The results from these tests will be briefly discussed at the end of this section.

4.2.1 Application Methodology (Targeted and Un-Targeted)

Targeted

Prior to configuring the modular premixer, operating conditions were set. In a practical application, the operating conditions would be known to the combustion engineer before designing the premixer. However, for testing purposes these conditions were systematically varied. An example is provided to illustrate the process of targeting an instability. The example used the following configuration:

- "No Swirl" Premixer
- Hydrogen Fuel
- 8-18T Fuel Injector
- Standard temperature and pressure (293K and 95kPa)
- Air Flow = 17 SCFM
- Equivalence Ratio = 0.28

This yielded an average mixture velocity of approximately 26 m/s in the annulus of the premixer.

The required axial location of the two injection blocks was then determined. Knowledge of the dominant unstable modes is critical to this step. From the previous combustor characterization, the primary unstable frequency for this configuration was known to be approximately 310 ± 30Hz. Using the *MTF* characterization, the convective delay between the injection locations was set to provide maximum FAR damping at the center frequency, i.e. the two locations produced FAR waves 180 degrees out of phase. Note that only the difference in delay needs to be known between each fuel injection location, not the absolute convective delay. This is extremely beneficial because, as already discussed, the exact time delay is extremely difficult to predict due to the distributed reaction zone. The relation between the target frequency and the convective delay between the injection locations ($\Delta\tau$) is provided in eq. 4.2. To better illustrate this relation,

the equation is left in a raw form, without cancelling terms, and uses nomenclature consistent with the rest of the document, namely 180 degrees instead of π.

$$Target\ Frequency = \frac{-180deg}{-2\pi\Delta\tau} \quad 4.2$$

This equation uses the theoretical phase delay (-2πτ), which is close to the experimentally determine phase delay, to demonstrate the application strategy. However, the targeted tests presented hereafter used the experimental phase delay (Section 3.1.2), instead of the theoretical.

For the example combustor configuration, a 1.8ms difference in delay was required to target unstable modes around 310Hz. The two axial injection locations selected for this example were $x_1 = 2.9375"$ (3.2ms delay) and $x_2 = 1.4375"$ (1.4ms delay). Recall, the smallest increment available to position the fuel injector was 0.125". This limits the accuracy of targeting a single frequency. However, it was generally observed that targeting a range of frequencies was adequate to provide a significant amount of FAR damping at the unstable modes of each injection location.

After configuration, each injection location was tested individually. To be considered for a "targeted" test, the following criteria had to be met:

1.) The combustor had to be unstable when operated with each injection location, independently. If one location produced a stable condition, the results were discarded. This was to ensure any positive results obtained were only the product of FAR damping.
2.) The measured unstable modes had to lie in the previously assumed "targeted" range. If a frequency was measured beyond the range of FAR damping, the combustor was reconfigured, and the test was repeated.

After meeting these criteria, the peak amplitudes were recorded for each injection. The combustor was operated using a similar procedure as outlined previously. The combustor was preheated, extinguished, and re-ignited before reporting any results. The sound pressure levels (SPL) for each individual injection location are shown in Figure 4.10. Both locations met the aforementioned criteria.

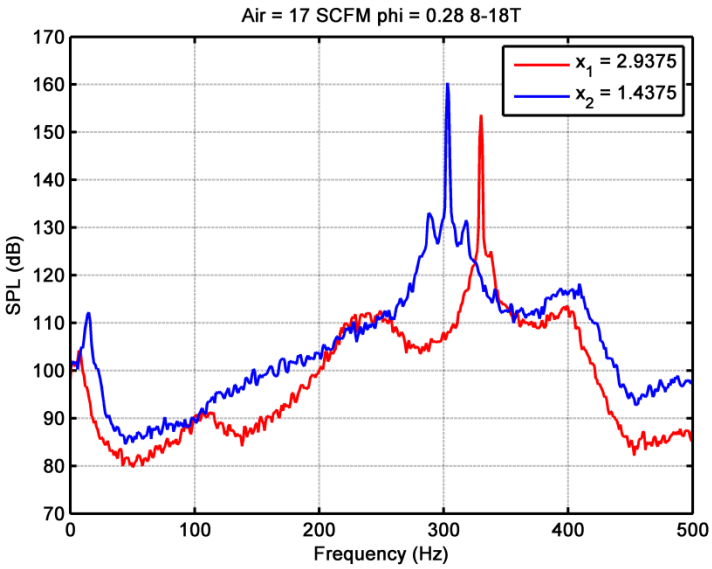

Figure 4.10. Measured sound pressure levels for two injection locations before application of passive control.

The dominant resonant modes for x_1 and x_2 were 303Hz and 330Hz, respectively. The predicted *MTF* for the two injections is shown in Figure 4.11. As designed, the response predicts a significant amount of FAR damping at the two measured unstable modes.

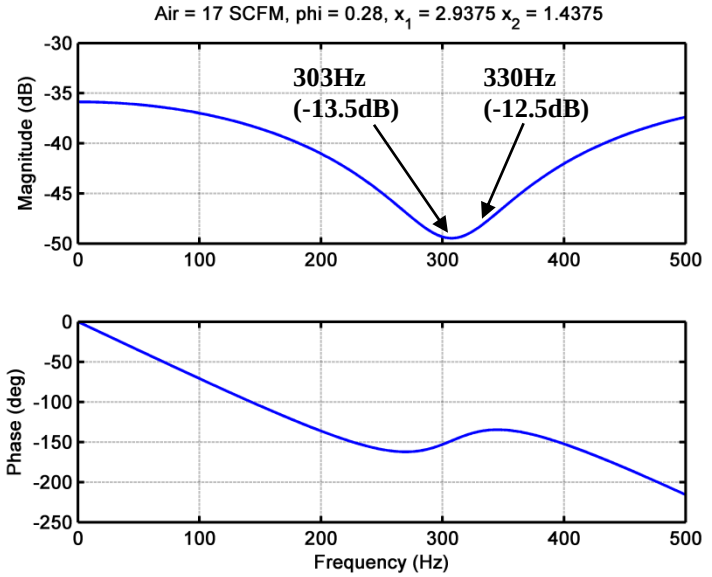

Figure 4.11. Predicted *MTF* for simultaneous fuel injection from the two locations. The amount of FAR damping is indicated at each previously measured unstable mode.

The combustor was then operated with both injection locations fueled simultaneously. The results from this example are shown in Figure 4.12, and they are tabulated in Table 4.4. This test

was successful at demonstrating the application of two "targeted" fuel injections to passively suppress the previously unstable combustor.

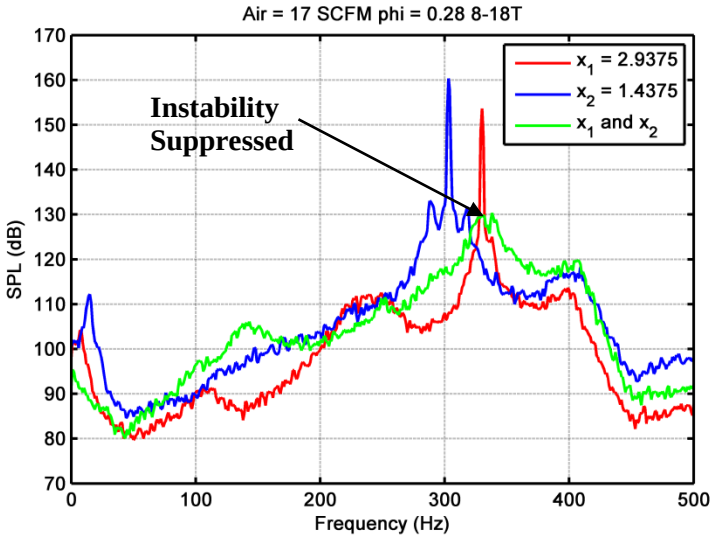

Figure 4.12. Measured sound pressure levels before and after implementation of passive control. Application of two "targeted" injections successfully suppressed the instability.

Table 4.4. Peak pressure amplitudes and corresponding frequencies for single and combined injection configurations. Application of two "targeted" injections successfully suppressed the instability.

x_{inj} (in)	Freq (Hz)	SPL (dB)	RMS Pressure (Pa)	RMS Pressure (%)
2.9375	330	154.6	960	1.01
1.4375	303	160.3	2080	2.19
Combined	**338**	**130.3**	**65**	**0.07**

The results from these experiments will be presented hereafter as either stable or unstable. While the amplitudes are reported as a measure of stability, the current technique is aimed at suppressing the onset of the instability, not decreasing the amplitude. During an instability, the amplitude is only a function of the non-linear viscous losses in the system, which is commonly defined as the limit cycle. Once a resonant interaction initiates, there is nothing stopping the system from reaching this amplitude. The current technique aims at eliminating the mechanism responsible for exciting, or initiating, this resonant interaction. Therefore, if the FAR fluctuations are sufficiently damped, the combustor should remain stable. However, if a resonant interaction is permitted, the predicted amount of FAR damping has no impact on the amplitude

of the resulting combustor. Recall, all measured and predicted mixing responses are based on a linear analysis and are therefore not valid if the combustor becomes unstable.

Un-targeted

To confirm the validity of the proposed passive control technique, tests were performed with two axial injection locations that were purposely configured to provide minimal FAR damping at the dominant resonant modes. These tests were also performed to demonstrate the importance of accurately predicting the mixing response of multiple injections. The testing procedure for this technique was similar to the one previously outlined. However, the distance between injection locations was selected so that the difference in time delay did **not** coincide with the unstable modes of the combustor. The following example is used to illustrate an "un-targeted" test:

- "No Swirl" Premixer
- Hydrogen Fuel
- 8-18T Fuel Injector
- Standard temperature and pressure (293K and 95kPa)
- Dominant unstable mode = 310 ± 30Hz (from combustor characterization)
- Air Flow = 17 SCFM
- Equivalence Ratio = 0.31
- U_{mix} = 27 m/s (average mixture velocity in annulus)
- x_1 = 2.1875in (2.1ms delay) , x_2 = 1.6875in (1.6ms delay)
- Center frequency for maximum FAR damping (925Hz)

Again, the combustor was first operated with each selected injection location indivdually. Both injection locations demonstrated a strong unstable mode, one at 283 Hz and the other at 309Hz. The combustor was then operated using both injections. As expected, the instablity remained in the combustor. The pressure spectrums and "un-targeted" *MTF* are shown in Figure 4.12 and Figure 4.13, respectively. The amplitudes and frequencies of the instabilty, before and after implementation, are given in Table 4.5.

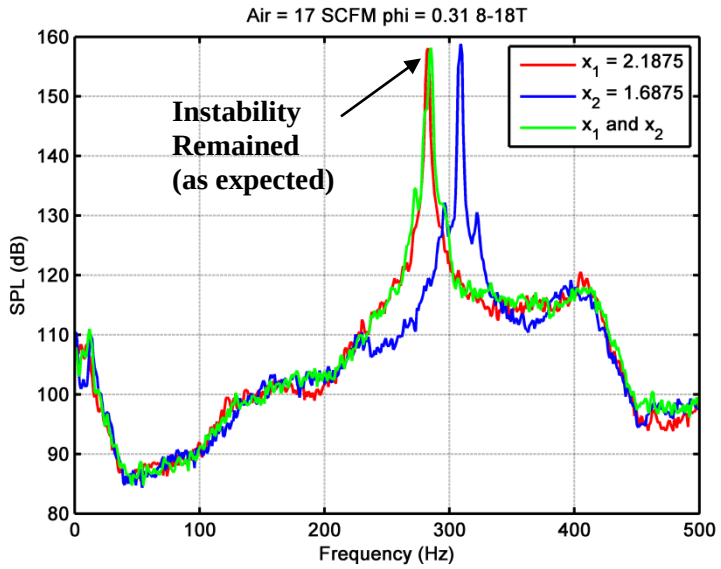

Figure 4.13. Measured sound pressure levels before and after implementation of two "un-targeted" injections. The instability remained present in the combustor as expected.

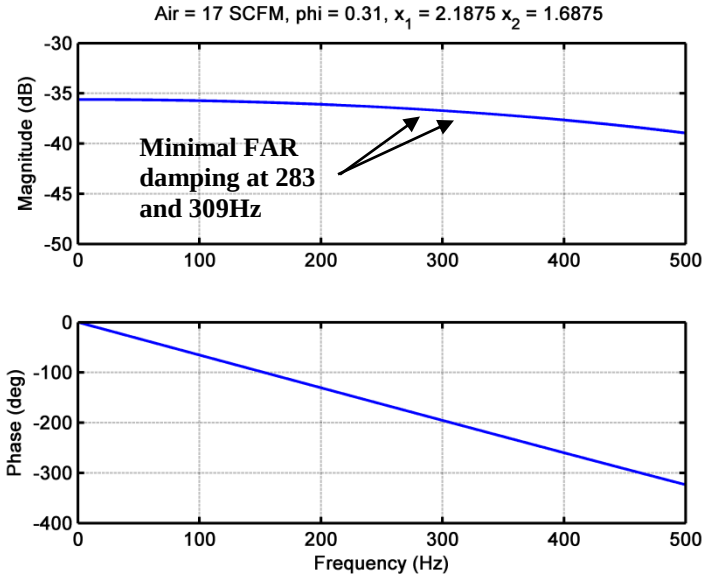

Figure 4.14. Predicted MTF for "un-targeted" two injection configuration. Minimal FAR damping at measured unstable modes.

Table 4.5. Measured pressure amplitudes and frequencies before and after "un-targeted" application.

x_{inj} (in)	Freq (Hz)	SPL (dB)	RMS Pressure (Pa)	RMS Pressure (%)
2.1875	283	158.1	1605	1.69
1.6875	309	158.8	1745	1.84
Combined	**285**	**158.2**	**1625**	**1.71**

4.2.2 Implementation and Validation of Passive Control

The proposed two-point axial fuel injection passive control technique was tested in the "No Swirl" premixer using hydrogen as the fuel. Multiple "targeted" tests were performed varying axial injection separation distance (difference in convective delay), absolute axial position (absolute delay), mean flow rate, and equivalence ratio. The variations in mean flow rate and axial separation allow the application of this technique to be applied to the single dominant mode of the combustor using only the convective delay between the axial locations.

Results from the implementation of the two-point axial injection passive control technique are shown in Figure 4.15. A total of 19 test results are presented. While more conditions were tested, the only results shown are configurations that met the two previously defined criteria for "targeted" tests. Therefore, the results shown are a measure of stability against configurations that were 100% unstable. The experiments showed that when the convective delay between the two fuel injections were correctly matched to the dominant unstable mode of the combustor, i.e. targeted, the instability in the combustor was suppressed for every test configuration when the equivalence ratio was held below 0.34, except for one. The one test configuration that remained unstable demonstrated a unique behavior that prevented the successful implementation of the current technique. This behavior was identified as "chugging" and will be elaborated on later. All test conditions operated at an equivalence ratio of 0.34 remained unstable. This was also observed in equivalence ratios above 0.34, but due to the lack of unique information, those tests are not reported here. The number of stable tests for each equivalence ratio is summarized in Table 4.6.

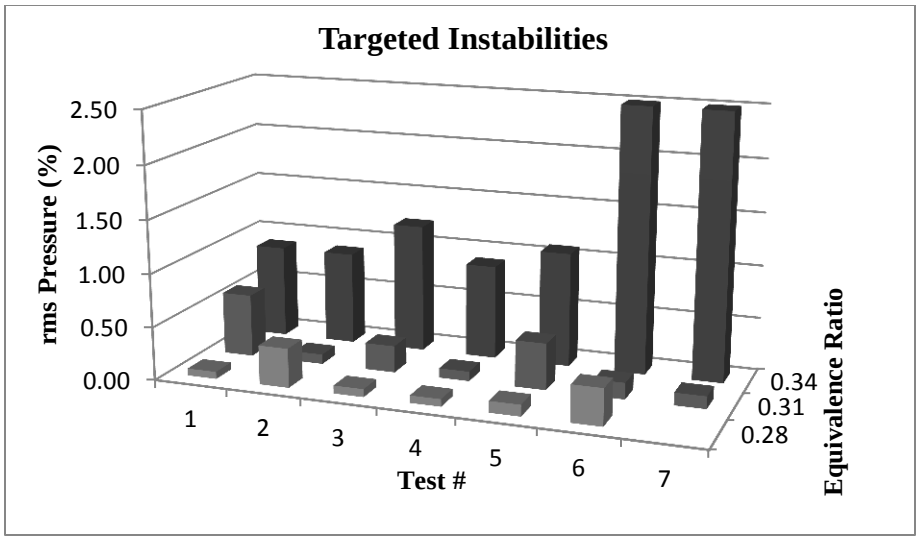

Figure 4.15. Experimental data showing peak amplitudes from the application of two "targeted" axial fuel injections. Passive control technique was effective at lean operating conditions.

Table 4.6. Experimental results showing the number of stable tests from the implementation of two-point axial injection passive control (targeted). *Combustor demonstrated different unstable behavior (chugging).

Targeted Tests			
EQ ratio	**# Tests**	**# Unstable**	**% Stable**
0.28	6	0	100
0.31	7	1*	86
0.34	6	6	0

The single test that remained unstable after implementation demonstrated a low frequency "chugging" phenomenon. This low frequency oscillation produced large fluctuations in the bulk flow velocity. This low frequency oscillation can be seen in the time trace and frequency spectrum of the pressure signal inside of the combustor, Figure 4.16. The two injection passive control strategy cannot compensate for changes in bulk flow velocity, which creates changes in the time delay of each injection. This produces conditions that are no longer optimized for the dominant resonant mode and, therefore, allows the instability to set-up. As a result, the dominant higher frequency mode of the combustor becomes superimposed on the lower frequency wave.

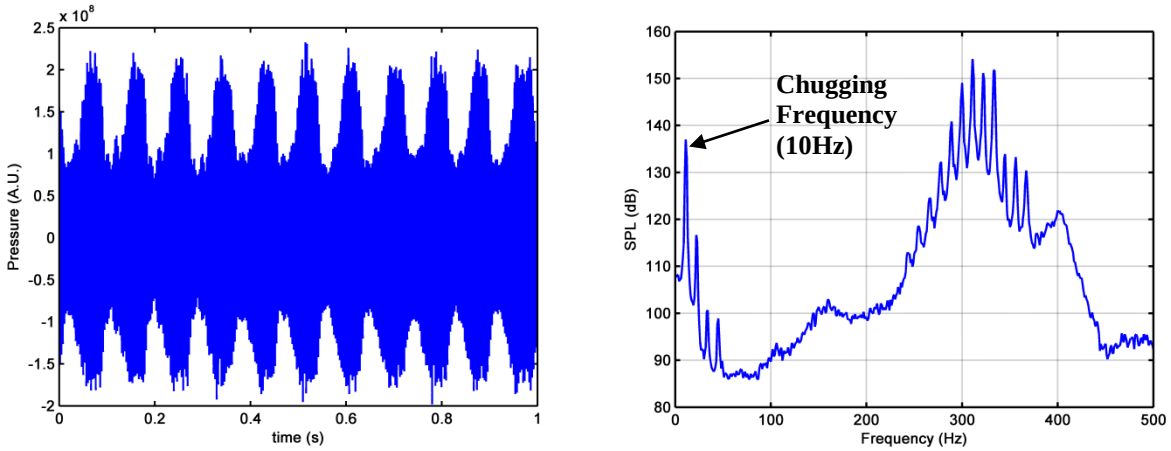

Figure 4.16. Measured combustor pressure exhibiting "chugging" behavior. (Left) Combustor pressure time trace, and (Right) combustor pressure spectrum demonstrating a 10Hz chugging frequency.

To confirm the validity of the previous results, a series of "un-targeted" tests were performed. The results from 8 test configurations are presented in Figure 4.17. Again, more configurations were tested but were discarded because they failed to meet the criteria that required both single injections to be unstable before implementation. Even with the limited number of tests, all two-point "un-targeted" tests remained unstable after implementation, shown in Table 4.7.

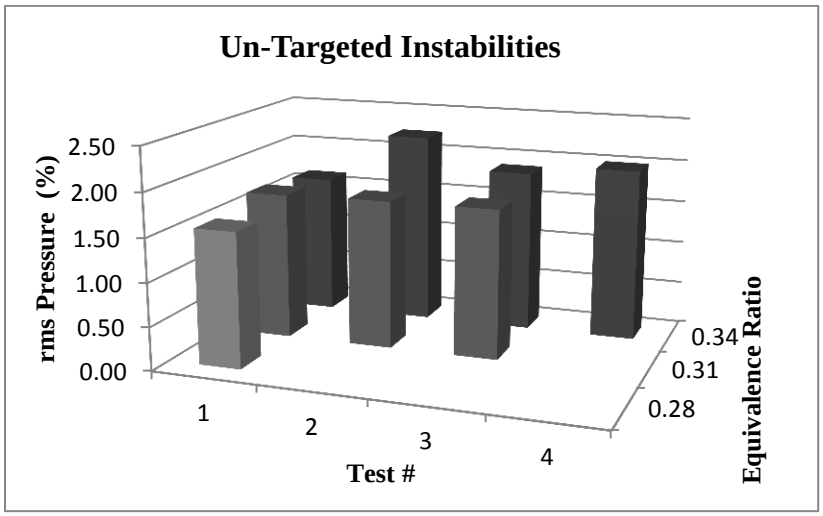

Figure 4.17. Experimental data showing peak amplitude from two-point "un-targeted" axial fuel injections. No stable conditions were found when the convective delay between axial injection locations was misaligned with the dominant unstable mode.

Table 4.7. Experimental results showing the number of stable test configurations for two-point "un-targeted" axial fuel injections.

Un-Targeted Tests			
EQ ratio	**# Tests**	**# Unstable**	**% Stable**
0.28	1	1	0
0.31	3	3	0
0.34	4	4	0

This series of testing validated the application of using two “targeted” axial fuel injections to suppress the onset of a resonant thermo-acoustic interaction in a simplified lean premixed hydrogen combustor. These experiments produced binary type results: the combustor was either stable or unstable. At leaner equivalence ratios, the passive control strategy was extremely effective in suppressing the onset of an unstable event. Of the 13 tests performed, only one configuration remained unstable, which was determined to be the result of a chugging behavior in the combustor. However, as the equivalence ratio increased, the passive control technique failed to be effective. This suggests that the total energy available in the flame zone is an important parameter in determining the effectiveness of this strategy. As previously discussed, at higher equivalence ratios, more energy is available to drive an instability. Therefore, small fluctuations in the flame zone could easily drive the system unstable or non-linear. If resulting velocity oscillations in the mixing chamber were driven non-linear, the current technique and characterizations are no longer applicable. This could explain why no conditions were stable at higher equivalence ratios in any tests performed, whether the combustor was fueled by a single, two-point “targeted”, or two-point “un-targeted” injection scheme.

The “un-targeted” tests confirmed the validity of the “targeted” experiments. When the premixer was configured with two axial injection locations that were incorrectly positioned to target the dominant unstable mode, all configurations remained unstable. The results from these experiments simultaneously confirmed two major aspects of this research. First, stability was achieved in the unstable combustor due to damping of FAR oscillations produced in the mixing chamber. Additionally, the characterization of the *MTF* was accurate at predicting the response, specifically the frequency of maximum FAR damping from two axial injection locations in a simplified lean premixed combustor.

4.2.3 Comments on application in a "Swirl" Premixer

The original goal of this research was to develop a lean premixed injector that could implement a multi-port fuel injection passive control strategy in a practical combustor. In most practical premixer designs, the mixing chamber utilizes some type of swirl to increase the mixing effectiveness and strengthen the recirculation zone to anchor the flame. However, due to the strong spatial effects that were observed in the *MTF* measurements of the "Swirl" premixer, the application of multiple injections to dampen FAR oscillations could never be validated. This limited the current research to focus on the simplified geometry, which turned out to be highly successful. Due to these successes and understanding of the limitations, the current approach was applied to the full "Swirl" geometry in hopes of gaining knowledge for future research efforts to make this passive control strategy applicable to practical systems.

The "Swirl" combustor was operated using two "targeted" axial fuel injection locations. Here "targeted" refers to the best guess from the extrapolated *MTF* characterizations. Recall, the characterization was limited to low frequencies due to the spatial discrepancies and non-linearities. Only two configurations are presented here to demonstrate the results that were commonly observed. In some configurations the instability was effectively eliminated using two "targeted" injections, and an example is shown in Figure 4.18.

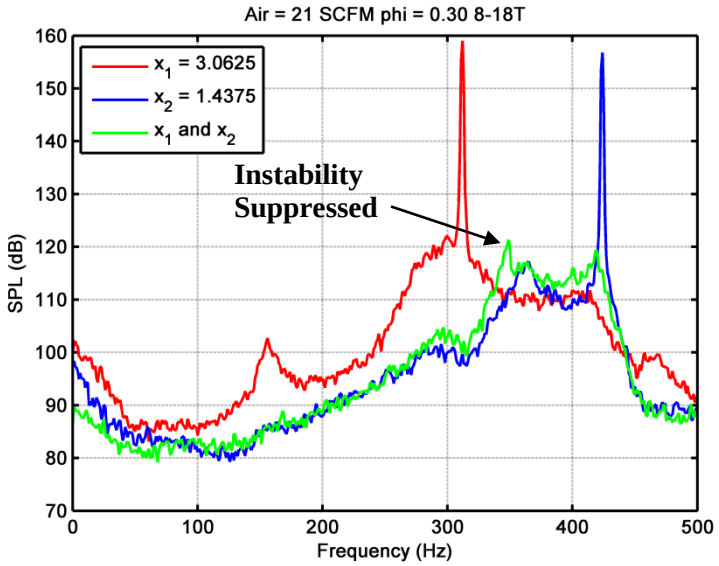

Figure 4.18. Measured responses demonstrating prevention of the instability after implementation of passive control in the combustor configured with the hydrogen fueled "Swirl" premixer.

However, in other "targeted" configurations the instability remained, an example is shown in Figure 4.19.

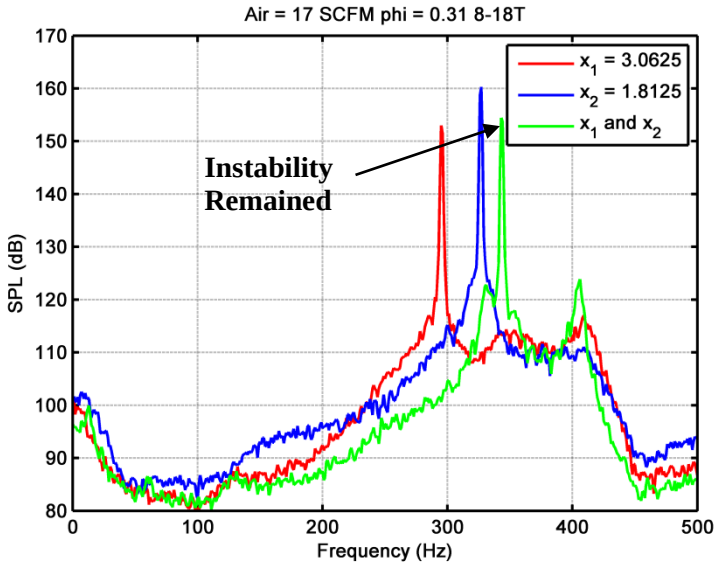

Figure 4.19. Measured responses showing the instability remaining in the combustor after implementation of passive control in the combustor configured with the hydrogen fueled "Swirl" premixer.

The results obtained from these experiments, along with the conclusive evidence for FAR damping as an effective control strategy found in the "No Swirl" tests, suggest that the configurations that successfully suppressed the instability were the result of FAR damping. Recall that during cold testing, certain configurations did in fact produce significant FAR damping. However, two major factors made it impossible to confirm this hypothesis. First, no model of the *MTF* was ever produced that could accurately predict which conditions would create the desired response. Additionally, the fuel concentration could not be measured during a combustion experiment. No optical access was designed into the combustion chamber or the premixer's annulus. Instead, the combustion chamber had to be removed to allow for these measurements, thus preventing acquisition of the fuel concentration during operation. These two factors eliminated the possibly of confirming that the instability was suppressed due to FAR damping.

Overall, the results from these tests were highly unpredictable. No definitive conclusions could be drawn from the use of multiple injections to suppress an unstable event in the "Swirl"

combustor test. However, because stable operation could be obtained in certain configurations, it was possible to see the potential of using this passive control strategy in practical lean premixed combustors.

Chapter 5: Conclusions and Recommendations

This chapter summarizes the approach and major findings from each phase of this research and presents the conclusions that were drawn. The chapter proceeds to address the shortcomings that were observed and list future recommendations that could be used to further the application of the proposed passive control technique.

5.1 Summary

This research investigated and applied a multi-port axial fuel injection strategy to passively suppress the onset of resonant thermo-acoustic interactions in lean premixed combustors. It utilized a unique modular premixer that was designed to target and eliminate FAR fluctuations from entering the flame zone by using multiple staged axial fuel injection locations. The position, or more accurately, the convective delay between the injection locations was specifically chosen to coincide with the dominant resonant mode of the combustor to inhibit a positive coupling between FAR fluctuations and the heat release rate of the flame. Specifically, this project utilized a "targeted" two-point axial fuel injection passive control strategy. To successfully implement this strategy, it was necessary to have an accurate model of the mixing response, along with a complete characterization of the unstable modes of the combustor. The goal of this work was to successfully demonstrate this passive control measure in a prototype combustor and provide an application methodology that could be applied to similar premixed systems with two or more injection locations.

Phase I

This phase focused on the measurement and characterization of the mixing response of the premixer in an un-reacting flow. The mixing response was first investigated in a simplified premixer design that utilized a straight annular mixing chamber, i.e. no swirl. The typical response demonstrated a constant or "flat" magnitude and a decreasing linear delay. The magnitude across the frequency range tested (0-500Hz) was accurately approximated by a single value. Over this range, no significant decrease in amplitude was observed due to the theorized mixing effects. While mixing effects are believed to be present in the system, the experimental apparatus, which was designed around a practical premixer, could not provide the level of

accuracy needed to capture these physics. However, this finding did not hinder the application of the current approach in any way. The phase delay of the response was accurately described by the slope of the phase versus frequency relation and was found to be in excellent agreement with the previously developed "Time Delay Model". To develop a full characterization of the system, mixing responses were measured for a multitude of single injection locations varying the convective delay, using both axial position of the fuel jets and the mean flow rate, and mean equivalence ratio. The project then proceeded to measure the response from two simultaneously fueled injection locations. This was performed to investigate the application of using multiple injections to target and eliminate temporal FAR fluctuations at specific frequencies. The results from these tests provided both conclusive and repeatable evidence of damping FAR fluctuations at select frequencies. Additionally, in all cases tested, the response for two injections was accurately predicted using the previously developed single injection model, therefore confirming the ability to target and eliminate FAR fluctuations at predetermined frequencies in a simple flow field.

A similar parameterized study of the mixing response was then performed on a premixer design that incorporated a set of swirl vanes in the mixing chamber. This geometry is more representative of premixer designs that are currently in practice. Unfortunately, the introduction of these vanes was found to create effects that limited the proposed control technique. Strong deviations were measured in both the magnitude and phase delay of the mixing response as a function of both axial and circumferential position of the fuel injector. After further examination, it was discovered that these deviations were the result of the fuel jet interaction with a complex, higher order flow field produced from the transmission of acoustic waves through the swirler passages. Unfortunately, the experimental apparatus was not able to accurately account for the spatial distribution of the velocity and fuel concentration resulting from the exact placement and orientation of the fuel jets. This prevented the mixing response from being accurately characterized over the necessary frequency range. Even though a model could not be produced to accurately characterize the single injection mixing response, two injection responses were still investigated. The results were, as expected, unpredictable. In some configurations, effective damping was observed, and in other configurations, it was not. While it was not possible to model the system, it was found that the desired response could be

obtained by iteratively manipulating the placement of the fuel jets. These findings suggest the possibility of using a multiple injection strategy to suppress FAR fluctuations in a more complex flow field. However, without further investigation, the application of the current technique is limited in a practical setting.

Phase II

The second phase of this research was divided into two sections. The first section focused on the measurement and characterization the resonant modes of the combustor. An investigation was also performed to identify the dominant driving instability mechanisms present in the combustor configurations. The second section focused on the implementation and validation of the proposed passive control technique.

The acoustic transfer function of the combustor was first measured to provide a general acoustic signature of the rig. This was used to identify the range of frequencies that would amplify and promote an unstable event. All combustor configurations demonstrated a 2^{nd} order behavior with a peak amplitude located at the dominant natural frequency. The natural frequencies of the different combustor configurations varied between 325 and 375Hz with significant amplification occurring at approximately ±50Hz. These measurements ensured that the previous mixing response characterizations were applicable to dampen FAR fluctuations in this range.

The resonant modes of the combustor were then measured and characterized at various operating conditions using the swirl geometry premixer. The conditions were varied to examine the effects of fuel type, convective delay, and mean flow rate. Two distinct dominant unstable modes were observed. The combustor demonstrated a frequency switching behavior, in which the combustor would randomly jump and lock to one of the two modes. The preferred unstable mode was difficult to predict and appeared to be a function of every parameter tested. The results from these experiments were also used to attempt to reveal the instability driving mechanism by examining the relation between the unstable mode and convective delay of the fuel, i.e. τf plots as shown in Figure 4.6 and Figure 4.7. Unfortunately, it was discovered that multiple driving mechanisms were present in this combustor geometry.

A similar investigation was then performed on the combustor using the simplified premixer geometry, i.e. No Swirl. Hydrogen was the only fuel tested in this configuration because it was able to produce a compact flame zone without the presence of swirl, whereas the natural gas could not. The combustor was found to have a single dominant unstable mode at approximately 310 ±30Hz and experienced no frequency switching behavior. Examination of the τf plot revealed that all unstable modes lie in two distinct τf bands ($0.4 < \tau f < 0.75$ and $0.95 < \tau f < 1.15$). This suggests that the combustion instabilities are predominantly mixing driven. These two findings made this configuration an excellent candidate for validating the proposed passive control technique.

The passive control strategy was implemented and tested in the combustor with the simplified geometry premixer, i.e. No Swirl. The two staged axial injection locations were configured in two different manners. In the first configuration, classified as "targeted", the convective delay between the injection locations was set to eliminate FAR fluctuations at the predetermined unstable modes. In the second configuration, classified as "un-targeted", the convective delay between the injection locations was not set to coincide with the predetermined modes. When targeted, the passive control strategy was extremely effective at suppressing the instability when operated at lean equivalence ratios (0.28 and 0.31). Of the 13 tests performed, only one configuration remained unstable, determined to be the result of a low frequency chugging phenomenon. However, as the equivalence ratio increased (0.34 and above), the passive control technique failed to be effective. This suggests that the total energy available in the flame zone is an important parameter in determining the effectiveness of this strategy. Furthermore, it was found that when the instability was incorrectly targeted, the combustor always remained unstable. This finding simultaneously confirmed two aspects of the current approach. First, the successful suppressions of the instabilities in the targeted tests were the result of damping of FAR fluctuations. Second, the convective delay between injections could be correctly set to target the unstable frequencies using the previously developed mixing response model in a simplified geometry premixer.

The proposed passive control technique was also investigated in the combustor operated with the swirl geometry premixer. The results from these tests were highly inconclusive. In some

configurations, the instability was prevented, and in others, the instability remained. This type of unpredictability was identical to what was observed in the measured cold flow swirl geometry mixing response. The results obtained from these experiments, along with the conclusive evidence for FAR damping as an effective control strategy found in the "No Swirl" tests, suggest that the configurations that successfully suppressed the instability were the result of inhibiting FAR fluctuations. However, because this could neither be measured nor predicted, this hypothesis could never be validated. Even so, it is possible to see the potential of using this passive control strategy in practical, complex lean premixed combustors.

5.2 Conclusions

The use of multiple staged axial injection locations was found to be an effective technique to suppress the onset of a resonant thermo-acoustic interaction in lean premixed combustors. Stable combustion was achieved by varying the convective delay between the injection locations in accordance with a linear time delay model to inhibit FAR fluctuations at the dominant unstable mode of the combustor. This passive control strategy was found to be applicable to lean premixed combustor designs if the following criteria could be met:

- The dominant instability mechanism is mixing driven.
- Acoustic waves in the mixing chamber are 1-D (typically observed in straight flow ducts). Swirl passages produce higher order flow fields.
- The fuel source is decoupled from acoustic disturbances.
- Extremely lean operating conditions. Energy dense flames zone produced at higher equivalence ratios can readily drive the system unstable.

While this research only investigated a "targeted" two injection approach, this technique can be expanded to inhibit FAR fluctuations across a broad range of frequencies by using three or more axial injection locations. However, because many premixer designs incorporate complex geometries, such as swirl vanes, the control strategy is limited in its current form. Spatial gradients formed in the dynamic velocity field yield mixing responses that are no longer a function of only the convective delay. Exact placement and orientation of the fuel jets in relation to the velocity field must be considered, and accurately accounted for, to successfully eliminate FAR fluctuations from propagating into the flame zone. Results from experiments performed

with complex mixing chambers and multiple instability mechanisms suggest that the elimination of FAR fluctuations using multiple injections is a possible control strategy, but further research is required to make the current approach more applicable.

5.3 Recommendations for Future Work

To successfully apply the current passive control strategy in complex flow fields, such as those developed by swirl vanes, additional measures should be taken. The root of this problem was discovered to be strong spatial gradients produced by higher order velocity fields created inside the mixing chamber. These effects make the placement and orientation of the fuel injection a critical design parameter that was unfortunately not implemented in the current research. However, the successful demonstration of the proposed passive control technique in the simplified geometry, as well as some of the full "Swirl" geometry configurations, offers motivation to explore and enhance the current application of this work. Based on the findings of this research, the following recommendations are offered.

- To successfully apply a multiple injection passive control technique in complex geometry premixer designs, the mixing response must be well known. The locations of the fuel jets must be placed in configurations where the phase and magnitude are correctly matched to eliminate temporal fuel concentration fluctuations. This could be accomplished using an experiment similar to the one used for this research, but it should be equipped with more degrees of freedom. An intensive parameterized study could be performed to fully characterize the mixing response. Exact placement and orientation of the fuel jets would need to be taken into account, instead of the averaging approach that limited the current research. The study should also investigate the use of unequal fuel flow rates to find suitable configurations. This would be an extremely difficult task, although it would be achievable and undoubtedly informative. Once the mixing response is well characterized, the multiple injection strategy could be implemented.

- A more elegant, and possibly more informative approach would be to utilize diagnostic techniques capable of making either 2-D or 3-D mixing response measurements. Phase

locked PLIF (Planar Laser Induced Fluorescence) measurement is one possible approach that could be used to obtain the 2-D concentration profiles. If the design of the mixing chamber allowed for optical access, these measurements could be obtained at various axial positions. Also, techniques such as PIV (Particle Image Velocimetry) could be similarly applied to measure the dynamic velocity field. These measurements could possibly shed light on the physics driving the mixing responses observed in the current research.

- Another possible avenue of research would be to investigate the propagation of acoustic waves through a complex, axisymmetric annular mixing channel. Even without the presence of fuel jets, the understanding of the mode shapes and resulting dynamic velocity field would provide critical information required to accurately apply the current passive fuel control strategy.

- To define the effective range of this passive control strategy, an array of premixed combustion tests varying fuel type, energy density, and mean flow conditions should be performed. These results, accompanied by a stability analysis, could be used to predict the applicability of the proposed strategy in other systems. The current investigation indicates that the strategy is limited to low energy density flame zones. If proven correct, techniques, such as nitrogen dilution or exhaust gas recirculation, could be used to broaden the stability envelope.

- To reduce the current knowledge into practice, the following design suggestions are provided. Expand the use of tangential injection to provide all momentum necessary for achieving a sufficient swirl number to effectively mix and anchor the flame zone. This eliminates the need for swirl vanes and allows for the use of a simplified mixing chamber to be directly implemented into the premixer design. Also, decrease the diameter of the fuel injection ports, if machining permits. This provides two possible advantages. One, it could be used to increase the momentum imparted by the fuel jets by increasing the velocity at a given mass flow. Two, smaller diameter ports allow for more axial injection locations to be used to achieve broad band suppression of FAR fluctuations. Keep in mind, however, that the pressure drop across the fuel manifold should be maintained to achieve a high fuel jet Mach number to successfully decouple the fuel supply.

REFERENCES

[1] P. Chiesa, G. Lozza, and L. Mazzocchi, "Using hydrogen as gas turbine fuel," *Journal of Engineering for Gas Turbines and Power-Transactions of the Asme,* vol. 127, pp. 73-80, 1, Jan 2005.

[2] S. R. Turns, *An introduction to combustion : concepts and applications*, 2nd ed. Boston: WCB/McGraw-Hill, 2000.

[3] I. Glassman, *Combustion*, 3rd ed. San Diego, Calif.: Academic Press, 1996.

[4] T. Lieuwen, "Modeling premixed combustion-acoustic wave interactions: A review," *Journal of Propulsion and Power,* vol. 19, pp. 765-781, 5, Sep-Oct 2003.

[5] K. R. Mcmanus, T. Poinsot, and S. M. Candel, "A Review of Active Control of Combustion Instabilities," *Progress in Energy and Combustion Science,* vol. 19, pp. 1-29, 1, 1993.

[6] J. M. Cohen and A. Banaszuk, "Factors Affecting the Control of Unstable Combustors," in *Combustion Instabilities in Gas Turbine Engines: Operation Experience, Fundamental Mechanisms and Modeling*, ed Reston, VA: American Institute of Aeronautics and Astronautics, 2005.

[7] J. M. Cohen, W. Proscia, and J. DeLaat, "Characterization and Control of Aeroengine Combustion Instability: Pratt & Whitney and NASA Experience," in *Combustion Instabilities in Gas Turbine Engines: Operation Experience, Fundamental Mechanisms and Modeling*, ed Reston, VA: American Institute of Aeronautics and Astronautics, 2005.

[8] G. A. Richards, D. L. Straub, and E. H. Robey, "Passive control of combustion dynamics in stationary gas turbines," *Journal of Propulsion and Power,* vol. 19, pp. 795-810, 5, Sep-Oct 2003.

[9] E. Laudien, R. Pongratz, R. Pierro, and D. Preclik, "Experimental Procedures Aiding the Desing of Acoustic Cavities," in *Liquid Rocket Engine Combustion Instability*. vol. 169, ed Washington, DC: Progress in Astronautics and Aeronautics, 1995, pp. 377-399.

[10] T. Scarinci, C. Freeman, and I. Day, "Passive Control of Combustion Instability in a Low Emissions Aeroderivative Gas Turbine," *American Society of Mechanical Engineers,* ASME Paper GT2004-53767, 2004.

[11] A. F. Ghoniem, A. Annaswamy, S. Park, and Z. C. Sobhani, "Stability and emissions control using air injection and H-2 addition in premixed combustion," *Proceedings of the Combustion Institute,* vol. 30, pp. 1765-1773, 2005.

[12] G. S. Jackson, R. Sai, J. M. Plaia, C. M. Boggs, and K. T. Kiger, "Influence of H-2 on the response of lean premixed CH4 flames to high strained flows," *Combustion and Flame,* vol. 132, pp. 503-511, 3, Feb 2003.

[13] G. L. Juste, "Hydrogen injection as additional fuel in gas turbine combustor. Evaluation of effects," *International Journal of Hydrogen Energy,* vol. 31, pp. 2112-2121, 14, Nov 2006.

[14] O. Tuncer, S. Acharya, and J. H. Uhm, "Dynamics, NOx and flashback characteristics of confined premixed hydrogen-enriched methane flames," *International Journal of Hydrogen Energy,* vol. 34, pp. 496-506, 1, Jan 2009.

[15] R. W. Schefer, "Hydrogen enrichment for improved lean flame stability," *International Journal of Hydrogen Energy,* vol. 28, pp. 1131-1141, 10, Oct 2003.

[16] H. S. Guo, G. J. Smallwood, F. S. Liu, Y. G. Ju, and O. L. Gulder, "The effect of hydrogen addition on flammability limit and NOx emission in ultra-lean counterflow CH4/air premixed flames," *Proceedings of the Combustion Institute,* vol. 30, pp. 303-311, 2005.

[17] W. Krebs, S. Bethke, J. Lepers, P. Flohr, B. Prade, C. Johnson, and S. Sattinger, "Thermoacoustic Design Tools and Passive Control: Siemens Power Generation Approaches," in *Combustion Instabilities in Gas Turbine Engines: Operation Experience, Fundamental Mechanisms and Modeling,* ed Reston, VA: American Institute of Aeronautics and Astronautics, 2005.

[18] R. C. Steele, L. H. Cowell, S. M. Cannon, and C. E. Smith, "Passive control of combustion instability in lean premixed combustors," *Journal of Engineering for Gas Turbines and Power-Transactions of the Asme,* vol. 122, pp. 412-419, 3, Jul 2000.

[19] J. T. Farina, "Conversion of a Gas Turbine Engine to Operate on Lean-Premixed Hydrogen-Air: Design and Characterization," Masters Thesis, Mechanical Engineering, Virginia Polytechnic Institute and State University, Blacksburg, VA, 2010.

[20] J. T. Farina, M. V. Perry, S. D. LePera, U. Vandsburger, and W. F. O'Brien, "Design of a Lean Premixed Hydrogen Combustor for a Gas Turbine Engine," in *45th AIAA/ASME/SAE/ASEE Joint Propulsion Conference & Exhibit*, Denver, Colorado, 2009.

[21] M. V. Perry, J. T. Farina, S. D. LePera, W. F. O'Brien, and U. Vandsburger, "Instrumentation, Modeling, and Testing of a Gas Turbine Engine Using Lean Premixed Hydrogen Combustion," in *45th AIAA/ASME/SAE/ASEE Joint Propulsion Conference & Exhibit*, Denver, Colorado, 2009.

[22] G. W. Koroll, R. K. Kumar, and E. M. Bowles, "Burning Velocities of Hydrogen-Air Mixtures," *Combustion and Flame,* vol. 94, pp. 330-340, 3, Aug 1993.

[23] K. K. Kuo, *Principles of combustion*, 2nd ed. Hoboken, NJ: John Wiley, 2005.

[24] A. H. Lefebvre and D. R. Ballal, *Gas turbine combustion : alternative fuels and emissions*, 3rd ed. Boca Raton: Taylor & Francis, 2010.

[25] B. D. Mugridge, "Combustion Driven Oscillations," *Journal of Sound and Vibration*, vol. 70, pp. 437-452, 3, 1980.

[26] J. Fritz, M. Kroner, and T. Sattelmayer, "Flashback in a swirl burner with cylindrical premixing zone," *Journal of Engineering for Gas Turbines and Power-Transactions of the Asme*, vol. 126, pp. 276-283, 2, Apr 2004.

[27] J. O. Keller, L. Vaneveld, D. Korschelt, G. L. Hubbard, A. F. Ghoniem, J. W. Daily, and A. K. Oppenheim, "Mechanism of Instabilities in Turbulent Combustion Leading to Flashback," *Aiaa Journal*, vol. 20, pp. 254-262, 2, 1982.

[28] V. Bellucci, D. Nowak, W. Q. Geng, and C. Steinbach, "On the use of thermoacoustic analysis for robust burner design," *Journal of Engineering for Gas Turbines and Power-Transactions of the Asme*, vol. 130, 3, May 2008.

[29] H. C. Mongia, T. J. Held, G. C. Hsiao, and R. P. Pandalai, "Incorporation of combustion Instability Issues into Design Process: GE Aeroderivative and Aero Engines Experience," in *Combustion Instabilities in Gas Turbine Engines: Operation Experience, Fundamental Mechanisms and Modeling*, ed Reston, VA: American Institute of Aeronautics and Astronautics, 2005.

[30] C. O. Paschereit, B. Schuermans, V. Bellucci, and P. Flohr, "Implementation of Instability Prediction in Design: ALSTOM Approaches," in *Combustion Instabilities in Gas Turbine Engines: Operation Experience, Fundamental Mechanisms and Modeling*, ed Reston, VA: American Institute of Aeronautics and Astronautics, 2005.

[31] A. H. Lefebvre, *Gas turbine combustion*, 2nd ed. Philadelphia: Taylor & Francis, 1999.

[32] G. A. Richards and M. C. Janus, "Characterization of oscillations during premix gas turbine combustion," *Journal of Engineering for Gas Turbines and Power-Transactions of the Asme*, vol. 120, pp. 294-302, 2, Apr 1998.

[33] Y. Huang and V. Yang, "Dynamics and stability of lean-premixed swirl-stabilized combustion," *Progress in Energy and Combustion Science*, vol. 35, pp. 293-364, 4, Aug 2009.

[34] J. J. Keller, "Thermoacoustic Oscillations in Combustion-Chambers of Gas-Turbines," *Aiaa Journal*, vol. 33, pp. 2280-2287, 12, Dec 1995.

[35] T. Scarinci and J. L. Halpin, "Industrial trent combustor-combustion noise characteristics," *Journal of Engineering for Gas Turbines and Power-Transactions of the Asme*, vol. 122, pp. 280-286, 2, Apr 2000.

[36] M. C. Janus, G. A. Richards, M. J. Yip, and E. H. Robey, "Effects of Ambient Conditions and Fuel Composition on Combustion Stability," *American Society of Mechanical Engineers*, ASME Paper 97-GT-266, 1997.

[37] P. G. Hill and C. R. Peterson, *Mechanics and thermodynamics of propulsion*, 2nd ed. Reading, Mass.: Addison-Wesley, 1992.

[38] G. P. Sutton and O. Biblarz, *Rocket propulsion elements*, 7th ed. New York: John Wiley & Sons, 2001.

[39] V. Yang and W. E. Anderson, *Liquid Rocket Engine Combustion Instability*: Amer Inst of Aeronautics &, 1995.

[40] A. A. Putnam, *Combustion-driven oscillations in industry*. New York,: American Elsevier Pub. Co., 1971.

[41] J. W. S. Rayleigh and R. B. Lindsay, *The theory of sound*, 2d ed. New York,: Dover publications, 1945.

[42] B. T. Chu, "On the Generation of Pressure Waves at a Plane Flame Front," *Fourth Symposium (International) on Combustion, The Combustion Institute*, pp. 761-769, 1953.

[43] D. Durox, T. Schuller, and S. Candel, "Combustion dynamics of inverted conical flames," *Proceedings of the Combustion Institute*, vol. 30, pp. 1717-1724, 2005.

[44] E. D. Gonzalez-Juez, J. G. Lee, and D. A. Santavicca, "A Study of Combustion Instabilities Driven by Flame-Vortex Interactions," in *41st AIAA/ASME/SAE/ASEE Joint Propulsion Conference & Exhibit*, Tucson, Arizona, 2005.

[45] N. Syred, "A review of oscillation mechanisms and the role of the precessing vortex core (PVC) in swirl combustion systems," *Progress in Energy and Combustion Science*, vol. 32, pp. 93-161, 2, 2006.

[46] H. M. Altay, R. L. Speth, D. E. Hudgins, and A. F. Ghoniem, "The impact of equivalence ratio oscillations on combustion dynamics in a backward-facing step combustor," *Combustion and Flame*, vol. 156, pp. 2106-2116, 11, Nov 2009.

[47] J. A. Ranalli, "Spatially Resolved Analysis of Flame Dynamics for the Prediction of Thermoacoustic Combustion Instabilities," PhD Dissertation, Mechanical Engineering, Virginia Polytechnic Institute and State University, Blacksburg, VA, 2009.

[48] G. A. Richards, D. L. Straub, and E. H. Robey, "Passive Control of Combustion Instabilities in Stationary Gas Turbines," in *Combustion Instabilities in Gas Turbine Engines: Operation Experience, Fundamental Mechanisms and Modeling*, ed Reston, VA: American Institute of Aeronautics and Astronautics, 2005.

[49] H. J. Merk, "An Analysis of Unstable Combustion of Premixed Gases," *Sixth Symposium (International) on Combustion, The Combustion Institute*, pp. 500-512, 1956.

[50] J. A. Ranalli, C. R. Martin, P. R. Black, and U. Vandsburger, "Measurement of Flame Transfer Functions in Swirl-Stabilized, Lean-Premixed Combustion," *Journal of Propulsion and Power,* vol. 25, pp. 1350-1354, 2009.

[51] J. A. Ranalli, C. R. Martin, and U. Vandsburger, "Measurements of ensemble averaged flame dynamics using spatially resolved analysis," *Experimental Thermal and Fluid Science,* vol. 35, pp. 1409-1417, 7, Oct 2011.

[52] P. R. Black, "Acoustic transfer functions derived from finite element modeling for thermoacoustic stability predictions of gas turbine engines," Masters Thesis, VPI & SU Mechanical Engineering M S 2007, Virginia Polytechnic Institute and State University, Blacksburg, VA, 2007.

[53] T. Lieuwen and B. T. Zinn, "The Role of Equivalence Ratio Oscillations in Driving Combustion Instabilities in Low NO_x Gas Turbines," *Twenty-Seventh Symposium (International) on Combustion, The Combustion Institute*, pp. 1809-1816, 1998.

[54] T. X. Yi and D. A. Santavicca, "Determination of the Instantaneous Fuel Flow Rate Out of a Fuel Nozzle," *Journal of Engineering for Gas Turbines and Power-Transactions of the Asme*, vol. 132, 2, Feb 2010.

[55] Q. V. Nguyen, "Measurements of Equivalence Ratio Fluctuations in a Lean Premixed Prevaporized (LPP) Combustor and its Correlation to Combustion Instability," in *ASME Turbo Expo*, Amsterdam, The Netherlands, 2002.

[56] R. K. Mongia, R. W. Dribble, and J. A. Lovett, "Measurement of Air-Fuel Ratio Fluctuations Caused by Combustor Driven Oscillations," *American Society of Mechanical Engineers,* ASME paper 98-GT-304, 1998.

[57] C. Martin, "Systematic Prediction and Parametric Characterization of Thermoacoustic Instabilities in Premixed Gas Turbine Combustors," Master Thesis, Mechanical Engineering, Virginia Polytechnic and State Unviersity, Blacksburg, VA, 2006.

[58] T. Scarinci and C. Freeman, "The Propagation of a Fuel-Air Ratio Disturbance in a Simple Premixer and its Influence on Presure Wave Amplification," *American Society of Mechanical Engineers,* ASME Paper 2000-GT-0106, 2000.

[59] S. B. Pope, *Turbulent flows*. Cambridge ; New York: Cambridge University Press, 2000.

[60] J. B. Kelman, D. A. Greenhalgh, and M. Whiteman, "Micro-jets in confined turbulent cross flow," *Experimental Thermal and Fluid Science,* vol. 30, pp. 297-305, 4, Mar 2006.

[61] J. A. Lovett and K. T. Uznanski, "Prediction of Combustion Dynamics in a Staged Premixed Combustor," *American Society of Mechanical Engineers,* ASME Paper GT-2002-30646, 2002.

[62] C. Fannin, W. T. Bauman, W. R. Saunders, G. A. Richards, and D. L. Straub, "Thermoacoustic Stability Analysis for Multi-Port Fuel Injection in a Lean Premixed Combustor," in *Aerospace Sciences Meeting,* Reno, Nevada, 2000.

[63] F. M. White, *Fluid mechanics,* 5th ed. Boston: McGraw-Hill, 2003.

[64] T. Schuller, D. Durox, P. Palies, and S. Candel, "Acoustic decoupling of longitudinal modes in generic combustion systems," *Combustion and Flame,* vol. 159, pp. 1921-1931, 5, May 2012.

[65] J. D. Holdeman, "Mixing of Multiple Jets with a Confined Subsonic Cross-Flow," *Progress in Energy and Combustion Science,* vol. 19, pp. 31-70, 1, 1993.

[66] J. G. Lee, K. Kim, and D. A. Santavicca, "Measurement of equivalence ratio fluctuation and its effect on heat release during unstable combustion," *Proceedings of the Combustion Institute,* vol. 28, pp. 415-421, 2000.

[67] J. G. Lee and D. A. Santavicca, "Experimental Diagnostics of Combustion Instabilities," in *Combustion Instabilities in Gas Turbine Engines: Operation Experience, Fundamental Mechanisms and Modeling,* ed Reston, VA: American Institute of Aeronautics and Astronautics, 2005.

[68] R. K. Mongia, E. Tomita, F. K. Hsu, L. Talbot, and R. W. Dibble, "Use of an Optical Probe for Time-Resolved *In Situ* Measurement of Local Air-To-Fuel Ratio and Extent of Fuel Mixing with Applications to Low NO_x Emissions in Premixed Gas Turbines," *Twenty-Sixth Symposium (International) on Combustion, The Combustion Institute,* pp. 2749-2755, 1996.

[69] S. Yoshiyama, Y. Hamamoto, E. Tornita, and K. Minami, "Measurement of Hydrocarbon Fuel Concentration by Means of Infrared Absorption Technique with 3.39 μm He-Ne Laser," *JASE Review,* vol. 14, No. 4, pp. 339-345, 1996.

[70] J. G. Lee and D. A. Santavicca, "Experimental Diagnostics for the Study of Combustion Instabilities in Lean Premixed Combustors," *Journal of Propulsion and Power,* vol. 19, pp. 735-750, No. 5, 2003.